Research Paper

GEOSPHERE

GEOSPHERE; v. 18, no. 2

https://doi.org/10.1130/GES02199.1

11 figures; 6 tables

CORRESPONDENCE: manuel.martin.m3@gmail.com

CITATION: Martín-Martín, M., Guerrera, F., Maaté, A., Hlila, R., Serrano, F., Cañaveras, J.C., Paton, D., Alcalá, F.J., Maaté, S., Tramontana, M., and Martín-Pérez, J.A., 2022, The Cenozoic evolution of the Intrarif (Rif, Morocco): Geosphere, v. 18, no. 2, p. 850–884, https://doi.org/10.1130/GES02199.1.

Science Editor: David E. Fastovsky
Associate Editor: Roberto Stanley Molina-Garza

Received 12 September 2019
Revision received 30 August 2021
Accepted 27 September 2021

First published online 8 February 2022

The Cenozoic evolution of the Intrarif (Rif, Morocco)

Manuel Martín-Martín[1], Francesco Guerrera[2], Alí Maaté[3], Rachid Hlila[3], Francisco Serrano[4], Juan C. Cañaveras[1], Douglas Paton[5], Francisco J. Alcalá[6,7], Soufian Maaté[8], Mario Tramontana[2], and José A. Martín-Pérez[4]

[1]Departamento de Ciencias de la Tierra y Medio Ambiente, University of Alicante, AP 99, 03080 Alicante, Spain
[2]Dipartimento di Scienze Pure e Applicate (DiSPeA), Università degli Studi di Urbino Carlo Bo, Campus Scientifico E. Mattei, 61029 Urbino, Italy
[3]Université Abdelmalek Essaâdi, Laboratoire de Géologie de l'Environnement et Ressources Naturelles, Département de Géologie, 93002 Tétouan, Maroc
[4]Departamento de Ecología y Geología, University of Málaga, 28071 Málaga, Spain
[5]School of Earth and Environment, University of Leeds, Leeds LS2 9JT, UK
[6]Departamento de Desertificación y Geo-Ecología, Estación Experimental de Zonas Áridas (EEZA-CSIC), 04120 Almería, Spain
[7]Instituto de Ciencias Químicas Aplicadas, Facultad de Ingeniería, Universidad Autónoma de Chile, 7500138 Santiago, Chile
[8]Université Moulay Ismaïl, Laboratoire de Géologie Appliquée, Faculté des Sciences et Techniques, BP. 509, Boutalamine, 52000 Errachidia, Maroc

ABSTRACT

This paper provides an understanding of the sedimentary-tectonic evolution of the Cenozoic strata of the El Habt and Ouezzane Tectonic Units (Intrarif, External Rif) in Morocco. New data provide information about the depositional architecture and enable a correlation of the evolution of the External Rif in Morocco with that of the Betic Cordillera in Spain and the Tunisian Tell, which provides new insights for hydrocarbon exploration in the region regarding possible source, reservoir, and seal rocks. The reconstructed Cenozoic succession was bio-chronologically defined, and the major unconformities and stratigraphic gaps were identified. The presence of these unconformities allowed three main stratigraphic sequences to be defined by age: Danian *p.p.*, early Ypresian–early Bartonian *p.p.*, and the early Rupelian–early Serravallian *p.p.* Three secondary stratigraphic sequences in the former upper main sequence were also defined by age: early Rupelian–late Chattian *p.p.*, Burdigalian *p.p.*, and the Langhian–Serravallian *p.p.* The depositional setting evolved from deep basin during the Late Cretaceous–Paleocene to external platform-slope during the Eocene–Miocene. The Cenozoic sandstones contain metamorphic and sedimentary rock fragments derived from a recycled orogen source area. The clay mineralogy in the Cenozoic strata consists of associations of Ill+(I–S) ± Sme, Ill+(I–S) ± Sme+Kln and Ill+(I–S) ± Sme+-Kln+Chl. These associations indicate an initial unroofing in the Paleogene period, then in the Cretaceous period, and finally in the Late Jurassic period during the Eocene–Oligocene. This detritus was followed by variable amounts of a sedimentary mix of Paleogene to Late Jurassic terrains due to several phases of erosion and deposition partly related to syn-sedimentary tectonics during the Miocene. Equivalent features (similar types of sediments, tectofacies, gaps, and unroofing) were also recognized along the Betic Cordillera in Spain and Maghrebian Chain (Morocco and Tunisia) and interpreted as related to a pre-nappe tectonic activity of soft basement folding, which occurred during the Paleogene after the generalized tectonic inversion (from extension to compression) occurred in the Late Cretaceous. The Upper Cretaceous is considered to be the hydrocarbon source rock, while the fractured Eocene and the porous Oligo-Miocene suites are proposed as possible hydrocarbon reservoirs. The Cenozoic stratigraphic architecture and the nappe structure of the region could provide the necessary trap structures.

Manuel Martín-Martín https://orcid.org/0000-0002-5797-9892

INTRODUCTION

As summarized by Michard et al. (2008), Morocco includes the following four main structural belts: (1) the Neoproterozoic Pan-African belt that outcrops in the Anti Atlas, which is an anticlinorium with a core of Precambrian and lower Paleozoic rocks that surrounds the northern portion of the Paleoproterozoic West African Craton; (2) the Variscan Moroccan Mesetas (western and eastern), which consists of Paleozoic to Cenozoic rocks; (3) the Alpine Middle and High Atlas Mountains, which consist of Paleozoic to Paleogene rocks; and (4) the Alpine Rif Chain, which consists of Paleozoic to Miocene rocks and records the effects of Miocene-Quaternary deformation associated with Maghrebian or Atlas orogeny. This tectonic framework is overprinted by the following Cenozoic basins: Gharb, Oujda, Souss, Ouarzazate, Boudenib, Tarfaya, and Tindouf.

The Rif Chain constitutes the western branch of the Maghrebian Chain in North Africa, and with the Betic Cordillera of southern Spain, forms the Gibraltar Arc (Fig. 1). These chains are part of the peri-Mediterranean Alpine Orogenic Belt (Fig. 1). In the Rif Chain, there are three main tectonic zones, which consist of strata derived from the deformation of the Internal (continental margin), Maghrebian Flysch Basin (located in an intermediate zone), and External (Africa margin) domains (Fig. 2).

(1) The Internal Rif Zone consists of greatly deformed Hercynian basement (crystalline nappes) with a cover of Mesozoic carbonates that is thrusted over the adjacent outermost units. According to many authors (e.g., Doglioni, 1992; Guerrera et al., 1993, 2005, 2021; Doglioni et al., 1998, 1999; Guerrera and Martín-Martín, 2014; Critelli et al., 2017; Martín-Martín

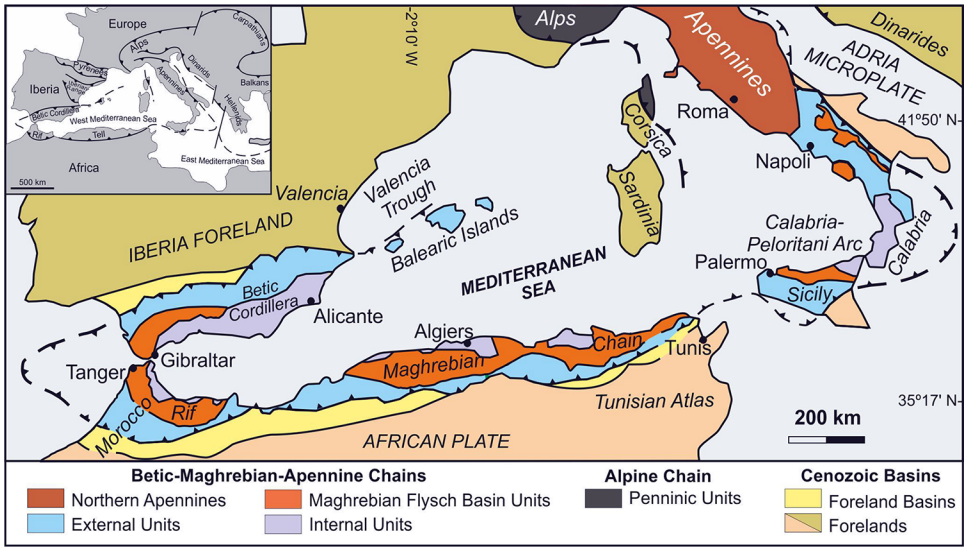

Figure 1. Geological sketch map showing the Betic-Maghrebian-Apennine Chains. Modified from Guerrera and Martín-Martín (2014).

et al., 2018, 2020a, 2020b, 2020c), the Internal Rif Zone was derived from an intervening microplate located between the European and African Plates.

(2) The Flysch Zone consists of tectonic units characterized by Cretaceous–Miocene siliciclastic strata derived from the Maghrebian Flysch Basin. In this basin, sedimentation took place on a deep oceanic to continental thinned crust (Guerrera et al., 1993, 2005; Durand Delga et al., 2000, among others). Maghrebian Flysch Basin units were mainly thrusted over a variety of external units. The Maghrebian Flysch Basin also extends laterally into the Betic Cordillera in southern Spain and into the southern Apennines in Italy (Fig. 1).

(3) The External Rif Zone consists of structural and stratigraphically complex nappes of Mesozoic–Cenozoic strata that accumulated on the continental African Margin. These units were thrusted over the Atlas Foreland with a SW-vergence (Fig. 2). On the basis of stratigraphic age and the structural position, Suter (1980a, 1980b) subdivided these units into Intrarif (mainly Cretaceous strata), Mesorif (predominant Jurassic carbonate to deep water turbidite deposits), and Prerif (consisting of Cenozoic olistostromes with fragments of ultrabasic rocks from a marine basement, Jurassic carbonate platform deposits, and Triassic basic subvolcanic rocks in a Miocene marly matrix; Fig. 2). Nevertheless, there is no agreement in the current literature for either the definition of the main units or for their constituent formations and units. Moreover, in the western Rif, Suter (1980a, 1980b) presented the following division for the Intrarif: (1) the Intrarifian Zone, which is composed of the internal Tanger Unit, the external Ketama-Tanger Unit, and the Loukkos Unit; and (2) the allochthonous units of "Intrarifian origin" that form the El Habt and Ouezzane Nappes, which are described in detail in this paper. These latter tectonic units are allochthonous and unrooted units that overthrust the Mesorif and Prerif Units. These units are mainly formed by Cretaceous–Cenozoic succession with an Intrarifian affinity.

This paper presents a well-defined and consistent stratigraphic and tectonic framework of the western Intrarif on the basis of new stratigraphic data and revised paleogeographic and paleotectonic interpretative models. In this paper, the Intrarif is considered to be a unit of the External Rif Zone and is subdivided into internal and external subdomains according to their structural positions.

The aims of this paper are to improve the definition of the Cenozoic stratigraphic record of the western Intrarif and to provide petrographic and mineralogic characterization of these strata. In particular, this paper presents new data on the Upper Cretaceous–Miocene strata of the western Intrarif to improve characterization of the El Habt and Ouezzane structural units of the Intrarif. In addition, this paper provides an improved framework for understanding hydrocarbon exploration of Morocco in terms of hydrocarbon source, traps, and seal rocks.

GEOLOGICAL SETTING

Within the Gibraltar Arc, two different external zones are distinguished: the Betic and the Rifian. The two zones are interpreted as having formed as a

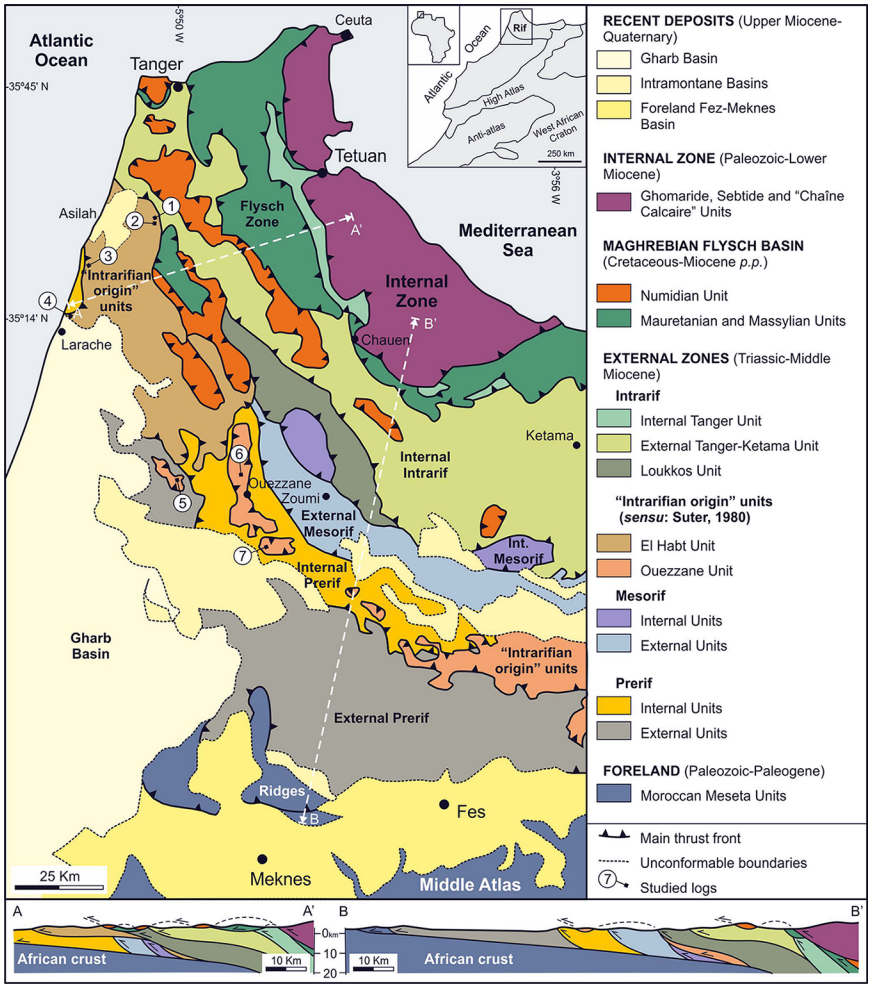

Figure 2. Geological map shows the External Zone (including the Intrarif, the units of intrarifian origin, and the locations of logs). Modified from Maaté et al. (2017).

consequence of the two distinct paleo-margins belonging to the Iberian and African Plates, respectively.

The External Rif (Fig. 2) is part of the Alpine Rif Chain and represents the northern African continental crust and the passive paleo-margin of the southern Maghrebian Tethyan Ocean (Chalouan and Michard, 2004; Frizon de Lamotte et al., 2017; Michard et al., 2017; Leprêtre et al., 2018, among others). This margin has undergone different stages of subsidence (mainly during the Cretaceous) and progressive Miocene–Pliocene deformation. In some basins of this paleo-margin, the earliest sediments to have accumulated are Triassic evaporitic deposits (Germanic facies) overlain by Lower Jurassic carbonates, Upper Jurassic siliciclastic strata, and thick Cretaceous–Paleogene-Miocene siliciclastic strata. However, the strata are characterized by marked lateral variations in thickness and lithofacies with the frequent presence of olistostromes (e.g., Lespinasse, 1977; Asebriy et al., 1987; Asebriy and Cherkaoui, 1995; Tejera de Leon and Duée, 2003; Zaghloul et al., 2005; Frizon de Lamotte et al., 2017; Maaté, 2017; Maaté et al., 2017, among others). In the northern portion of the External Rif Zone, the main orogenic deformation is thought to have taken place during the early–middle Miocene, propagating southwestward during the late Miocene to the Quaternary and being overprinted during the Neogene by strike-slip faults (Azdimousa et al., 2007, and references therein).

The Intrarif comprises a variety of tectonic and stratigraphic units of Triassic to Miocene age (e.g., Chalouan et al., 2008). Suter (1980a, 1980b) proposed a modern geological framework of the Rif Chain. Later, different reconstructions of the Intrarif were proposed (Asebriy et al., 1987; Azdimousa et al., 1998, 2007; El Mrihi et al., 2004; Tejera de Leon and Duée, 2003; Bargach et al., 2004; Zaghloul et al., 2005; Chalouan et al., 2008; Vázquez et al., 2013; Jabaloy-Sánchez et al., 2015; Maaté et al., 2017, 2018, among others, and references therein) addressing a range of topics within the External Rif Zone.

Many authors highlighted the tectonic complexity of the Intrarif, pointing out a nappe structure consisting of units detached from their original paleogeographic locations and overriding more external units (Lespinasse, 1977; Suter, 1980a, 1980b; Chalouan et al., 2008; Vázquez et al., 2013; Jabaloy-Sánchez et al., 2015). The original stratigraphic successions were completely deformed and translated, so published paleogeographic and geodynamic reconstructions should be considered hypothetical.

Suter (1980a, 1980b) subdivided the External Rif Zone into the Intrarif, Mesorif, and Prerif, but different interpretations and unrelated terminologies have subsequently been introduced (e.g., Chalouan et al., 2008). Suter (1980a, 1980b), in turn, divided the Intrarifian units in the Central and Western Rif belt into: (1) the Intrarifian origin nappes and (2) the Intrarifian Zone comprising, from external (south) to internal (north), the following three tectonic units (Fig. 2): Loukkos, External Tanger-Ketama, and Internal Tanger. However, this approach creates some confusion in correlating the stratigraphic record reconstructed in different areas of the tectonic units and in defining other tectonic units such as the El Habt and Ouezzane Nappes in the western Intrarif and the Tsoul and Aknoul Nappes (among others) in the eastern Intrarif (out of the study area). Therefore, we will follow the next scheme for the Intrarifian tectonic units: (1) the External Tanger-Ketama Unit is characterized by rocks affected by diagenesis and anchizone conditions and deformed by recumbent folds, (2) the Internal Tanger Unit partially detached from the latter unit, (3) the Loukkos Unit completely detached from the Tanger-Ketama Unit and is also made of Upper Cretaceous to Cenozoic rocks, and (4) the El Habt, Ouezzane, and Tsoul Nappes contain Cenozoic rocks. The successions of these latter units are the focus of this work. Two major E-NE– to NE–trending strike-slip faults (Jebha and Fahies Faults) in the Eastern Rif provide evidence for the obliquity of the movement of the Internal Rif Zone relative to the rest of Africa (Fig. 2).

Zaghloul et al. (2005) subdivided the Intrarif into the following three zones or units (Fig. 2): the Intrarifian Zones; the Intrarifian Nappes, and the Oligocene–Miocene Asilah-Larache Sandstones. These sandstones belong to the Oligocene–Miocene strata of the Intrarifian-origin nappes (*sensu* Suter 1980a, 1980b) as follows: the Asilah Sandstones (Critelli, 1985/1986; Cazzola and Critelli, 1986) belong to the Habt Tectonic Unit (*sensu* Suter and Fiechter, 1966), whereas the Larache Sandstones (Didon and Hoyez, 1978) are a part of the Ouezzane Tectonic Unit (Fig. 2). The El Habt and Ouezzane Tectonic Units are completely detached from their Cretaceous substratum and were transported ~100 km to the SW where they appear as tectonic klippen over the Mesorif (Hottinger and Suter, 1962; Durand Delga, 1972; Lespinasse, 1977; Ben Yaïch et al., 1991; Frizon de Lamotte et al., 1991; Tejera de Leon et al., 1995; Chalouan et al., 2001; Zakir et al., 2004).

Despite several studies concentrating on the External Rif Zone (Maaté, 2017; Maaté et al., 2017, 2018), many problems are still unresolved. These are principally due to the lack of homogeneous data and to intrinsic interpretative difficulties such as problems concerning the pre-deformational position of many of the structural units. However, there is an increasing consensus on the arrangement of the External Rif Zone (e.g., Frizon de Lamotte et al., 2017) and that the Intrarif units consist of Upper Jurassic to Miocene sediments that accumulated in a deep basin on oceanic or thin continental crust (Michard et al., 1992, 2007).

Hydrocarbon exploration in Morocco (Kuhnt et al., 2001; Morabet et al., 1998; Kolonic et al., 2002; Coward and Ries, 2003; Lüning et al., 2004; Sachse et al., 2011; Groune et al., 2013a, 2013b; Oukassou et al., 2013, and references therein) was initiated during the 1960s and focused on five areas (Figs. 1 and 2): (1) Anti Atlas and Saharan domain (Paleozoic reservoir targets), (2) Western Meseta domain (Paleozoic to Jurassic reservoir targets), (3) Atlasic domain (Triassic and Jurassic reservoir targets), (4) Atlantic passive margin offshore (Jurassic to Cenozoic reservoir targets), and (5) Rif domain (Mesozoic to Cenozoic reservoir targets). In particular, Morocco is believed to rank seventh in the world for shale oil reserves, and the External Rif Zone is one of the three major shale oil deposits in the country (Groune et al., 2013a, 2013b, 2014). Moreover, the External Rif Zone from the Rif Domain is one of the major oil research areas in Morocco (Groune et al., 2013a, 2013b, 2014). In fact, research in the External Rif Zone has focused on the characterization of organic matter of Upper Cretaceous bituminous marls and shales of Melloussa-Massylienne Nappe, Internal Ketama Units, and External Tanger Nappe (Tanger-Tetouan-Bab Taza area) as possible source rocks (Lüning et al., 2004; Groune et al., 2013a, 2013b, 2014). However, a more detailed understanding of the stratigraphic architecture of the associated units is required to advance the hydrocarbon implications, with specific reference to the distribution of reservoirs and cap rock (reservoir seals). Further studies are required to improve our understanding of the hydrocarbon systems in the external zones of the Rif. This paper contributes to the understanding of these petroleum systems by providing more detailed knowledge of the stratigraphic architecture of the External Rif Zone.

METHODS

The methods used in this research consist of: (1) field analyses to characterize the lithostratigraphic successions (measured meter to meter) and to sample specific stratigraphic levels; (2) laboratory analysis, biostratigraphy, petrography of sandstones (arenites), and clay mineralogy, which is also used to improve the sequence stratigraphy interpretation; and (3) correlation of the main geological events in the corresponding segments of the Maghrebian Chain.

For this work, the terminology of sedimentary rocks for outcrop description followed McBride (1963), Dunham (1962), and Pettijohn (1975) for sandstones, limestones, and mixed siliciclastic-carbonate (mainly marl) rocks, respectively.

The terminology of textural maturity of sedimentary rocks proposed by Folk (1951, 1980) is considered. Classification of carbonate rocks according to depositional texture by Dunham (1962) and Embry and Klovan (1971) is followed, while Folk classification schemes were used to classify terrigenous sandstones (Folk, 1980). For hybrid limestone-sandstone, the scheme of Zuffa (1980, 1985) is considered. For mixed siliciclastic-carbonate rocks (mainly marl), the classification of Pettijohn (1975) is used.

The lithofacies, defined on the basis of field observations, consist of one or more rock type association that is clearly distinguishable in the geological column for discrete intervals and shows a certain lithologic homogeneity (Fig. 3; Table 1). The present paper also is mainly a stratigraphic work; the interpretation of depositional environments (also relative deepening or shallowing trends of facies) results from field observations of: (1) lithological changes; (2) internal and external structures of beds; (3) sedimentary breaks; (4) vertical

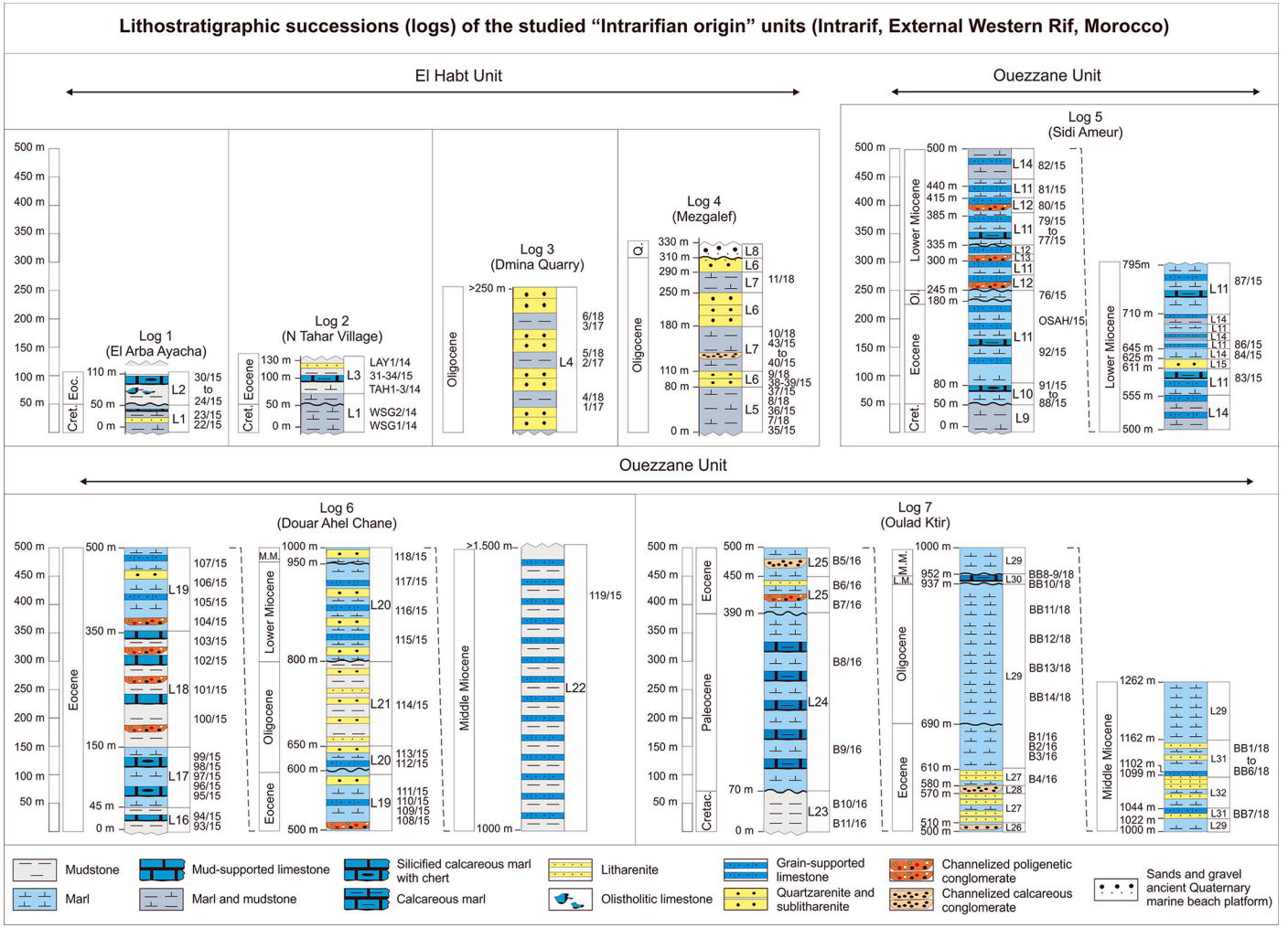

Figure 3. Lithostratigraphic successions studied are shown with the defined lithofacies analyzed and positions of samples (see numbers to the right of lithofacies corresponding with Table 1). The locations of the stratigraphic successions measured are shown in Figure 2.

TABLE 1. MAIN FIELD DATA (LOGS, LOCALITIES, UTM COORDINATES, LITHOFACIES CLASSIFICATION AND DESCRIPTION, THICKNESS, SAMPLES, AND MAIN BOUNDARY TYPES), CHRONOSTRATIGRAPHIC DATA, SEDIMENTARY REALM INTERPRETATION, AND STACKING PATTERN AND/OR TREND OF FACIES OF THE LITHOSTRATIGRAPHIC SUCCESSIONS

Lithofacies	Main Lithology	Chronostratigraphy	Sedimentary realm interpretation	Stacking pattern and/or trend of facies	Samples*	Thickness
EL HABT UNIT (External Intrarif Subdomain)						
Log 1, El Arba Ayacha Village - UTM Coordinates: 30 S/238150 E / 3920100 N, Thickness 110m						
L2	calcareous mudstone, silicified calcareous mudstone, olistolitic limestone, chaotic marl, and limestone	lower Lutetian + Ypresian	Slope/Basin	Shallowing trend	27/15, 28A/15, 29/15, 30/15	60
		Major Unconformity				
L1	mudstone, calcareous mudstone, muddy litharenite, limestones (mudstone/wackestone)	uppermost Cretaceous p.p. near to the K/T boundary	Basin	---	22/15, 23/15, 24/15, 24/15P, 25/15, 26/15	50
Log 2, N Tahar Village - UTM Coordinates: 30 S/237475 E / 3918521 N, thickness 130 m						
L3	mudstone (claystone, siltstone), marl, calcareous marl, litharenite	lower-middle Lutetian	Basin	Shallowing trend	TAH3/14, LAY1/14	55
		Transitional stratigraphic boundary (conformity)				15
L1	Mudstones, (claystone,-siltstone), marl	upper-middle Ypresian	Basin	---	31/15, 32/15, 33/15, 34/15, TAH1/14, TAH2/14	25
		Major Unconformity				
L1	mudstone, (claystone,-siltstone), marl	uppermost Cretaceous p.p., (near to the K/T boundary)	Basin	---	WSG1/14, WSG2/14	50
Log 3, Dmina Quarry - UTM Coordinates: 30 S/221832 E / 3920761 N, thickness >250 m						
L4	Quartzose litharenite, mudstone, calcareous marl	upper-middle Rupelian	Slope/channel	Accretionary stacking	F1/17, EL18-4, F2/17, EL18-5, F3/17, EL18-6, F3/17P	>250
Log 4, Mezgalef - UTM Coordinates: 30 S/219397 E / 3908369 N, thickness >330 m						
L8	sand, gravel	Quaternary	Paleobeach	---	---	>20
Unconformity						
L6	litharenite limestone (grainstone)	Chattian-upper-middle Rupelian	Slope/Channel	Shallowing trend	---	20
L7	mudstone, litharenite, and/or quartzarenite and sublitharenite, calcareous mudstone				EL18-11	40
L6	litharenite limestone (grainstone)	middle Rupelian			---	70
L7	mudstone, marl, litharenite and/or quartzarenite and sublitharenite, microconglomerate				40/15, 41/15, 42/15, 43/15, EL18-10	70
L6	litharenite, limestone (grainstone)	lower-middle Rupelian			38/15P + 39/15P, EL18-9	30
L5	mudstone, marl with nodules of Fe-Mn and chert				35/15, 36/15, 37/15, EL18-7, EL18-8	80
OUEZZANE NAPPE (External Intrarif Subdomain)						
Log 5, Sidi Ameur El Hadi - UTM Coordinates: 30 S/239114 E / 33853312 N, Thickness 795 m						
L11	marl, calcareous marl, limestone (grainstone)	upper Burdigalian	Slope/Basin	Shallowing trend	87/15, 87A/15, 87/15P	85
L14	limestone (grainstone), marly mudstone	upper-middle Burdigalian			---	05
L11	marl, calcareous marl, limestone (grainstone)				---	15
L14	limestone (grainstone), marly mudstone				---	10
L11	marl, calcareous marl, limestone (grainstone)	middle Burdigalian			86/15, 86A/15	15
L14	limestone (grainstone), marly mudstone	middle-lower Burdigalian			85A/15	20
L11	marl, calcareous marl, limestone (grainstone)		Slope/Basin		---	20
L15	litharenite				84/15P	10
L11	marl, calcareous marl, limestone (grainstone)				83/15, 83A/15, OSAH-2A/15	60
L14	limestone (grainstone), marly mudstone	lower Burdigalian			82/15, 82A/15	115
L11	marl, calcareous marl, limestone (grainstone)				81A/15	25
L12	limestone (grainstone), polygenic conglomerate, limestone, litharenite				80/15	30
L11	marl, calcareous marls limestone (grainstone)				77A/15, 78A/15, 79/15, 79A/15	50
Minor Unconformity						
L12	limestone (grainstone), polygenic conglomerate, limestone, litharenite	Chattian probably	Sloppe Channel	Shallowing trend	---	10
L13	polygenic conglomerate				---	25
L11	marl, calcareous marl, limestone (grainstone)				---	25
L12	limestone (grainstone), polygenic conglomerate, limestone, litharenite				---	30
Not evaluated interruption (?)						
L11	marl, calcareous marl, limestone (grainstones)	lower Chattian-upper Rupelian	Slope/Basin		76/15, 76A/15	65
Major Unconformity						

(*Continued*)

TABLE 1. MAIN FIELD DATA (LOGS, LOCALITIES, UTM COORDINATES, LITHOFACIES CLASSIFICATION AND DESCRIPTION, THICKNESS, SAMPLES, AND MAIN BOUNDARY TYPES), CHRONOSTRATIGRAPHIC DATA, SEDIMENTARY REALM INTERPRETATION, AND STACKING PATTERN AND/OR TREND OF FACIES OF THE LITHOSTRATIGRAPHIC SUCCESSIONS (*Continued*)

Lithofacies	Main Lithology	Chronostratigraphy	Sedimentary realm interpretation	Stacking pattern and/or trend of facies	Samples*	Thickness
L11	Marl, calcareous marl, limestone (grainstone)	lower Bartonian	Slope/Basin	Shallowing trend	OSAH/15, OSAH-A/15	100
L10	marl, marly limestones, silicified mudstone, chert lenses	lower Lutetian and upper Ypresian	Basin		88/15, 88A/15, 89/15, 89A/15, 90/15, 90A/15, 91/15, 91A/15, 92/15, 92A/15	30
Major Unconformity						
L9	mudstones, (mainly siltstone), marl with limonite nodules	Upper Cretaceous p.p.	Basin	---	---	50
Log 6, Douar Ahel Chane - UTM Coordinates: 30 S/263677 E / 3863451 N, thickness >1500 m						
L22	mudstone, marly mudstone, limestone (grainstone)	Langhian-Serravallian transition	External Platform	Shallowing trend	119, 119A	>500
L20	quartzarenite and sublitharenite, limestone (grainstone), calcareous-marl	Langhian			---	50
L20	quartzarenite and sublitharenite, limestone (grainstone), calcareous-marl	lower Langhian to lower Burdigalian	Slope		115, 115A, 116A, 117, 117A, 118, 118A	150
Minor Unconformity						
L21	mudstone, marly mudstone, litharenite, quartzarenite and sublitharenite	Chattian-upper Rupelian	Slope Channel	Mainly aggradational	114A	150
L20	quartzarenite and sublitharenite, limestone (grainstone), calcareous-marl	middle Rupelian			112, 112A, 112-15P, 113, 113A	50
Major Unconformity						
L19	marl, calcareous marl, limestone (grainstone), quartzarenite and sublitharenite	lowermost Bartonian and upper Lutetian	Slope Channel/Basin	Progradational (offlap) Shallowing trend	105, 105A, 105-15P, 106A, 106, 107, 107A, 108A, 109, 109A, 110A, 111, 111A	250
L18	mudstone, calcareous-marl, polygenic conglomerate	upper Lutetian to upper Ypresian			100, 100A, 101, 101A, 102, 02A, 103,103A,104, 104A	200
L17	marly limestone, marly beds, silicified mudstone beds, chert lenses	middle-lower Ypresian	Basin		95, 95A, 96, 96A, 97, 97A, 98, 98A, 99, 99A	105
L16	mudstone, limestones (mudstone/wackestone)				93, 93A, 94, 94A	45
Log 7, Oulad Ktir - UTM Coordinates: 30 S/273351 E / 3827972 N, thickness > 1262m						
L29	marl	upper Langhian	External Platform	Progradational (offlap) Shallowing trend	---	>100
L31	marl, limestone (grainstone), litharenite				BB1/18, BB2/18, BB3/18, BB4/18, BB5/18, BB6/18	63
L32	litharenite, marl	uppermost part of the lower Langhian			---	55
L31	marl, limestone (grainstone), litharenite				BB7/18	22
L29	marl				---	70
Minor Unconformity						
L30	calcareous marl, marly limestone	lower Burdigalian	Slope	--	BB8/18, BB9/18, BB10	15
Minor Unconformity						
L29	marl	upper Chattian to middle Rupelian	Slope	--	BB11/18, BB12/18, BB13/18, BB14/18	247
Major Unconformity						
L29	marl	lower Bartonian and upper Lutetian	Slope	Progradational (offlap) Shallowing trend	B1/16, B2/16, B3/16	80
L 27	litharenite (litharenite)	---	Slope/Channel		B4/16	30
L 28	polygenic conglomerate	---			---	10
L 27	litharenite (litharenite)	---			---	60
L26	marl, conglomerate	middle-lower Lutetian			B5/16	60
L25	marl, litharenite, conglomerate with polygenic and chert clasts), calcareous marl	lower Lutetian and upper Ypresian			B6/16, B7/16	60
L24	marl, calcareous marl	lower Ypresian	Basin		B8/16	160
Major Unconformity						
L24	marl, calcareous marl	lower Paleocene	Basin	Retrogradational (onlap) Deepening trend	B9/16	160
		possible unconformity				
L23	mudstone	upper Maastrichtian	Basin	---	B10/16	>70
		middle-Upper Maastrichtian			B11/16	

*A—mineralogy; P—petrography.

and lateral organization of geological bodies (stacking patterns, onlap, offlap, etc.); (5) markers of different depositional environments (carbonate platform, shelf, slope, basin); (6) sedimentary structures (cross lamination and plane lamination, slumps, Bouma intervals); and (7) basinward/landward shifts of depositional units. The recognition of unconformities both in the field and through biostratigraphic analyses allowed subdivision of the sedimentary record into units of sedimentary lithosomes, and their boundaries are not defined in terms of traditional sequence stratigraphy interpretations.

The chronology of sediment accumulation was established through biostratigraphic analysis of the planktonic foraminifera found in 71 beds of marl-clay. The samples were subjected to the traditional methodology of washing and fractionation by sieving at 150 μm (main studied fraction) and 125 μm. Reworked organic components are considered as a part of the detrital fraction and are not considered as part of the autochthonous microfossil assemblage. If necessary, reworked components mark a limit of the oldest age.

For the Paleogene interval, tropical to subtropical biozonations were used following Berggren et al. (1995), Olsson et al. (1999), and Berggren and Pearson (2005, 2006) and revised by Wade et al. (2011). For Miocene strata, the standard zonation of Blow (1969) was used, and the more significant planktonic foraminiferal bio-events in the Mediterranean area were considered (Iaccarino, 1985; Serrano, 1992; Di Stefano et al., 2008) as well as the Global Standard Chronostratigraphic Scale (Lourens et al., 2004). In addition, four samples of Oligocene calcareous clay were analyzed to determine the calcareous nannoplankton observed in samples diluted on a slide. To apply the biostratigraphic and chronostratigraphic correlation to Cenozoic strata, the zonation standard of Martini (1971) was used.

Four samples from the El Habt Tectonic Unit and eight samples from the Ouezzane Tectonic Unit were examined in thin section with a polarized light optical microscope for petrography. The nomenclature and classification schemes of Folk (1980), Dunham (1962), and Zuffa (1980) were used for petrographic (thin section) descriptions. Quantification of mineralogy was achieved by counting 400–500 points per thin section using the Gazzi–Dickinson method (Gazzi, 1966; Dickinson, 1970; Ingersoll et al., 1984). Framework components (sand grains) were divided into the four petrographic groups defined by Zuffa (1980, 1985): non-carbonate extrabasinal (NCE), carbonate extrabasinal (CE), non-carbonate intrabasinal (NCI), and carbonate intrabasinal (CI). Carbonate grains were classified as extraclasts or intraclasts on the basis of criteria proposed by Zuffa (1980, 1985, and 1987) and Fontana et al. (1989). To minimize dependence of the rock composition on grain size, coarse-grained lithic fragments (single crystals larger than 0.0625 mm in size) were separated from fine-grained lithic fragments (single crystals smaller than 0.0625 mm in size) (Dickinson, 1970, Zuffa, 1980; Ingersoll et al., 1984). A Q-F-L* ternary plot was used to classify the different types of sandstones with L* representing fine-grained rock fragments (including carbonate extraclasts [CE]).

Mineralogical assemblages of the whole-rock and <2 μm grain-size fraction (clay fraction hereafter) of 42 selected samples (15 from Log 5 and 27 from Log 6; location in Fig. 3) were examined. Powders obtained after grinding the samples were analyzed by X-ray diffraction (XRD) using a PANalyticalX'Pert Pro diffractometer (Cu-Kα radiation, 45 kV, 40mA) equipped with an X'Celerator solid-state lineal detector located in the laboratory of the Mineralogy and Petrography Department of the Granada University, Spain. The diffraction patterns were obtained by a continuous scan from 3° 2θ to 60° 2θ with a 0.01° 2θ resolution. The XPOWDER ® program (Martín-Ramos et al., 2012) was used to evaluate the semiquantitative mineral composition of the whole-rock and clay-fraction samples.

For the non-calcareous clay fraction, four oriented mounts on glass slides per sample were prepared following these steps: air-drying, ethylene-glycol and dimethyl-sulfoxide solvation for 24 h, and heating at 550ºC for 2 h for expandable clay-mineral identification (Holtzapffel, 1985; Moore and Reynolds, 1997). The reflections and reflecting powers of Biscaye (1965) and Holtzapffel (1985) were used to identify and quantify the mineral phases. On the basis of the XRD technique, the semiquantitative evaluation of each mineral phase (in weight percent [wt%] normalized to 100%) has an accuracy of ~5%. Replicate analyses of a few selected samples gave a precision of ± 3% (2σ).

The following XRD parameters were examined: (1) the ratio of the intensities of the Qtz(001):Qtz(101) peak areas of quartz (Qtz(001):Qtz(101) ratio hereafter) in the whole-rock XRD diffractograms to discern authigenic quartz from secondary quartz in the absence of a volcanic component (Eslinger et al., 1973); (2) the ratio of the intensities of the Sme(003):Sme(002) peak areas of smectite (Sme(003):Sme(002) ratio hereafter) from ethylene-glycol solvated clay-fraction XRD diffractograms to differentiate dioctahedral and trioctahedral smectites (Drits et al., 1997; Moore and Reynolds, 1997); and (3) the ratio of the intensities of the Ill(002):Ill(001) peak areas of illite (Ill(002):Ill(001) ratio hereafter) from decomposed air-dried clay-fraction XRD diffractogram to discern authigenic from mature illite (Esquevin, 1969: Hunziker, 1986).

OUTCROP DESCRIPTIONS, BIOSTRATIGRAPHIC, AND PETROLOGICAL-MINERALOGICAL DATA

Four stratigraphic sections were measured in the El Habt Tectonic Unit (Logs 1–4) for a stratigraphic thickness of over 820 m, and three stratigraphic sections were measured in the Ouezzane Tectonic Unit (Logs 5–7) for a stratigraphic thickness of over 3557 m. According to Suter (1980a, 1980b), both tectonic units have a paleogeographic origin from the Intrarif (Fig. 2).

The field study, integrated by mineralogical and petrographic analyses, consisted of compiling the inventory of the recognized litho-petrofacies according to criteria explained in the "Methods" section. The main features of the 32 recognized lithofacies are described below, and these descriptions are also summarized in Figure 3 and Table 1, where the log thicknesses and sample locations are also shown. The biostratigraphic (Fig. 4 and Tables 2–4), petrological (Figs. 5–6 and Table 5), and mineralogical (Fig. 7 and Table 6) results are also presented in this section of the manuscript.

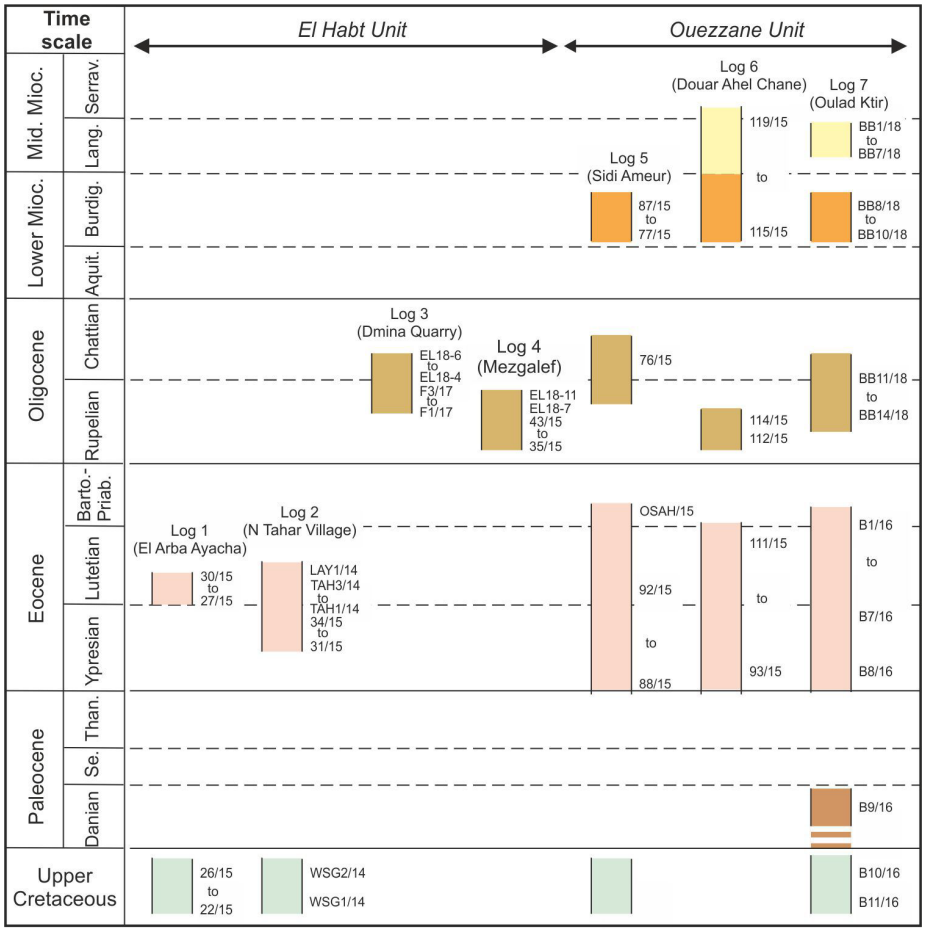

Figure 4. Chronostratigraphic range and synthetic chronology of the successions studied with the locations of samples analyzed (see numbers alongside logs) are shown. The logs are colored according to the ages of sediments.

El Habt Tectonic Unit

The El Habt Tectonic Unit (External Intrarif) shows a duplex structure with westward thrusting (Suter, 1980a, 1980b). Four logs were measured from El Arba Ayacha, North Tahar Village, Dmina Quarry, and Mezgalef. The first two logs describe outcrops on the NE side of the tectonic unit at the footwall both of the Mellouse Flysch Nappe and the External Tanger Tectonic Unit northward. Moreover, the El Habt Tectonic Unit overrides the Internal Prerif in the NW sector, where the Dmina Quarry and Mezgalef Logs were described. In the four logs of the El Habt Tectonic Unit, the lithofacies L1–L8 described below were recognized (Table 1 and Fig. 3).

Log 1 (El Arba Ayacha Village; Total Thickness 110 m)

This log is located at 30S 238006 E 3920389 N. The log is from a NW-SE–trending syncline. Log 1 (Fig. 3) is composed of Lithofacies 1 and 2.

Lithofacies 1 (L1). This lithofacies is 50 m thick and consists of greyish and in some places green and red homogeneous mudstone and calcareous mudstone with interbedded centimeter-long beds of muddy sandstone and mud-supported limestones without obvious sedimentary structures (arenite with mudstone/arenite ratio = 40/60; 70/30). The microfauna from these strata is made up of calcareous and agglutinated foraminifera. The planktonic assemblage with *Globotruncana* ssp., *Globotruncanita* ssp.,

TABLE 2. MOST SIGNIFICANT SPECIES MAKING UP THE ASSEMBLAGES OF PLANKTONIC FORAMINIFERA OF THE PALEOCENE-EOCENE STRATA IN THE INTRARIFIAN SEQUENCES

AREAS	LOGS	SAMPLES	PLANKTONIC FORAMINIFERA																																		PALEOCENE-EOCENE ZONES*	AGE
			Parasubbotina pseudobulloides (Plummer)	*Parasubbotina inaequispira* (Subbotina)	*Praemurica inconstans* (Subbotina)	*Praemurica uncinata* (Bolli)	*Acarinina soldadoensis* (Brönniman)	*Acarinina angulosa* (Bolli)	*Acarinina quetra* (Bolli)	*Acarinina pentacamerata* (Subbotina)	*Acarinina bullbrooki* (Bolli)	*Acarinina cunelcamerata* (Blow)	*Acarinina praetopilensis* (Blow)	*Acarinina topilensis* (Cushman)	*Igorina broedermanni* (Cushm.& Berm.)	*Morozovella praeangulata* (Blow)	*Morozovella acuta* (Toulmin)	*Morozovella aequa* (Cushman & Renz)	*Morozovella occlusa* (Loeblich & Tappan)	*Morozovella velascoensis* (Cushman)	*Morozovella subbotinae* (Morozova)	*Morozovella edgari* (Premoli Silva & Bolli)	*Morozovella aragonensis* (Nuttall)	*Morozovella caucasica* (Glaessner)	*Morozovelloides crassatus* (Cushman)	*Globanomalina compressa* (Plummer)	*Globanomalina chapmani* (Parr)	*Pseudohastigerina micra* (Cole)	*Hantkenina dumblei* Wienzierl & Applin	*Hantkenina lehneri Cushman & Jarvis*	*Hantkenina liebusi* Shokhina	*Globigerinatheka subconglobata* (Shutskaya)	*Globigerinatheka barri* Brönnimann	*Globigerinatheka index* (Finlay)	*Turborotalia possagnoensis* (Tourm.&Bolli)	*Turborotalia pomeroli* Tourm.&Bolli	*Turborotalia cerroazulensis* Cole	*Subbotina linaperta* (Finlay)	*Subbotina senni* (Beckman)	*Globigerina eocaena* Gümbel	*Globigerina corpulenta* (Subbotina)		
OUEZZANE UNIT	LOG 7 Oulad Ktir	B1/16																													O		O	O			O	O	E12–E13	early Bartonian
		B2/16									O		O										O						O	O	O	O			O	O	upper E11	
		B3/16									O		O	O									O				O								O	O	E10–E11	late Lutetian
		B5/16		O						O	O	O	O		O							O		O										O		O	O	E8–E9	early-middle Lutetian
		B6/16		O						O	O	O			O							O		O										O		O	O	E8	early Lutetian
		B7/16		O			O	O		O												O												O	O			E5–E6	late Ypresian
		B8/16					O	O									O			O					O													E3	early Ypresian
		B9/16	O		O	O																			O													P2	latest early Paleocene
		B10-11/16	UPPER CRETACEOUS ROCK-STRATA																																			
	LOG 6 Douar Qahel Chane	109/15																						O						O					O	O	E11	Lutetian-Bartonian transition
		107/15																																O		O			
		105/15									O	O	O											O		O							O	O	O	O	lower E11–E10	late Lutetian
		104/15									O	O	O	O										O		O	O			O			O	O	O	O		
		103/15									O	O	O	O										O		O				O			O	O	O	O	E10	
		102/15									O	O	O											O		O				O			O	O	O	O	E9–E10	middle-late Lutetian
		101/15									O	O	O									O				O							O		O	O	E7–E8	latest Ypresian-early Lutetian
		100/15		O							O	O	O									O											O	O			E6–E7	late Ypresian
		99/15					O	O												O														O				E4	middle Ypresian
		96/15					O	O									O			O														O					
		95/15																																O					
		93/15					O	O	O								O			O																			
	LOG 5 Sidi Ameur	OSAH/15																									O				O	O	O	O		O	O	E12–E13	early Bartonian
		92/15		O							O	O	O										O						O					O		O	O	E8–E9	early Lutetian
		91/15		O							O	O	O																O					O		O	O	E8–E9	early Lutetian
		90/15		O							O	O	O		O							O	O						O					O	O	O	O	E8–E9	early Lutetian
		89/15		O						O	O	O	O		O							O												O	O	O		E7	late Ypresian
		88/15									O				O																			O		O		E7	late Ypresian
EL HABT UNIT	LOG 2 N Tahar Village	LAY1/14		O						O	O	O			O												O				cf			O	O			E8–E9	early-middle Lutetian
		TAH3/14	Agglutinated foraminifera and radiolarian; significant carbonate dissolution																																		E5–E8	late Ypresian-early Lutetian
		34/15																																				
		33/15																																				
		32/15		O			O	O		O																												E4–E5	middle-late Ypresian
		31/15		O			O	O		O										O		cf												O				
		TAH2/14								O																								O					
		TAH1/14		O			O			O										O		cf												O				
		WSG1-2/14	UPPER CRETACEOUS ROCK-STRATA																																			
	LOG 1 El Arba Ayacha	30/15																																	O	O	E8–E9	early Lutetian
		29/15		O																		O													O	O		
		28/15	Microfauna made up mainly by radiolarian; no planktonic foraminifera identified																																			
		27/15	Agglutinated foraminifera; no planktonic foraminifera identified																																			
		22-26/15	UPPER CRETACEOUS ROCK STRATA																																			

*References: Olsson et al. (1999), and Pearson et al. (2006).

TABLE 3. MOST SIGNIFICANT SPECIES MAKING UP THE ASSEMBLAGES OF PLANKTONIC FORAMINIFERA OF THE OLIGOCENE-MIOCENE STRATA IN THE INTRARIFIAN SEQUENCES

AREAS	LOGS	SAMPLES	PLANKTONIC FORAMINIFERA																															OLIGOCENE–MIOCENE ZONES*	AGE
			Globigerina ampliapertura Bolli	*Globigerina increbescens* Bandy	*Globigerina eocaena* Gumbel	*Globigerina corpulenta* (Subbotina)	*Globigerina venezuelana* Hedberg	*Globigerina praebulloides* Blow	*Globigerina angulisuturalis* Bolli	*Globoturborotalita woodi* (Jenkins)	*Paragloborotalia opima* (Bolli)	*Neogloboquadrina siakensis* (LeRoy)	*Neogloboquadrina acrostoma* (Wezel)	*Neogloboquadrina continuosa* (Blow)	*Globigerinoides primordius* Blow & Banner	*Globigerinoides altiaperturus* Bolli	*Globigerinoides subquadratus* (Brönnimann)	*Globigerinoides trilobus* (Reuss)	*Globigerinoides bisphaericus* Todd	*Praeorbulina sicanus* (De Stefani)	*Praeorbulina glomerosa* (Blow)	*Orbulina suturalis* Brönnimann	*Orbulina universa* d'Orbigny	*Globigerinella obesa* (Bolli)	*Globorotalia kugleri* (Bolli)	*Globorotalia peripheroronda* Blow & Banner	*Globorotalia praescitula* Blow	*Globorotalia praemenardii* Cushman & Stainforth	*Globigerinita glutinata* (Egger)	*Turborotalita quinqueloba* (Natland)	*Globoquadrina baroemoenensis* (LeRoy)	*Globoquadrina globosa* Bolli	*Globoquadrina altispira* (Cushman Jarvis)	*Globoquadrina langhiana* (Cita & Gelati)	*Globoquadrina dehiscens* (Chapman, Parr & Collins)	*Globorotaloides suteri* Bolli	*Catapsydrax dissimilis* Cushman & Bermúdez		
OUEZZANE NAPPE	LOG 7 Oulad Ktir	BB1/18										O						O				O	O	O		O				O					
		BB2/18						O				O						O			O	O		O		O				O				N9	late Langhian
		BB4/18						O				O					O	O	O	O	cf							O			O	O			
		BB6/18						O				O					O	O	O	O			O		O		O		O	O	O	O			upper N8	latest early Langhian
		BB7/18						O				O					O	O	O	O			O	O	O		O		O		O				
		BB8/18					O	O		O		O	O	O		O	cf	O					O	O								O	O		
		BB9/18					O	O		O		O		O		O		O					O	O								O	O	middle N5	early Burdigalian
		BB10/18					O	O		O		O				O		cf					O				O		O			O	O		
		BB11/18			O	O	O	O	O			O			cf								O										O	O	O6	late Chattian
		BB12/18			O	O	O	O	O		O	O											O										O	O	O4–O5	latest Rupelian-early Chattian
		BB13/18			O	O	O	O			O																						O	O	O3	late Rupelian
		BB14/18	O	O	O	O	O	O																									O	O	O2	middle Rupelian
	LOG 6 Douar Qahel Chane	119/15						O		O		O		O				O				O		O	O	cf	O		O			O			N10–N11	Langhian-Serravallian transition
		118/15						O		O		O	O	O		O	O	O	O				O	O	O		O		O	O		O			N8	early Langhian
		117/15						O		O		O	O	O		O	O	O					O	O	O		O		O	O	O	O	O		N6–N7	late Burdigalian
		115/15					O	O		O		O		O	O	O		O					O	O			O		O	O		O	O	O	N5	early Burdigalian
		113/15	O	O	O	O	O	O			O	O											O										O	O	O2	middle Rupelian
		112/15	O	O	O	O	O	O															O										O	O		
	LOG 5 Sidi Ameur	87/15						O		O		O	O	O		O	O	O	O				O					O		O	O		O	O	N6–N7	late Burdigalian
		86/15					O	O		O		O		O		O	O	O					O	O					O	O		O	O		O	upper N5	middle Burdigalian
		82/15					O	O		O		O		O		O		O					O		O		O		O	O		O	O		O		
		79/15					O	O		O		O	O	O		O		O					O				O	O	O	O	O			O	O	lower N5	early Burdigalian
		76/15			O	O	O	O	O		O																							O	O	O4–O5	latest Rupelian-early Chattian
EL HABT UNIT	LOG 4 Mezgalef	43/15	O	O	O	O	O	O			O																							O	O	upper O2	middle Rupelian
		42/15			O		O																											O	O		
		41/15	O	O	O	O	O	O																										O	O	O2	
		40/17		O	O	O	O	O																										O	O		
		37/15	No planktonic foraminifera. Microfauna made up mainly by radiolarians																																		
		36/15	Microfauna made up by agglutinated foraminifera																																		
		35/15	Barren in microfauna																																		
	LOG 3 Dmina Quarry	S3/17			O	O	O	O																										O	O	O3	late Rupelian
		S2/17			O	O	O	O			O	O											O											O	O		
		S1/17	O	O	O	O	O	O			O																							O	O	upper O2	middle Rupelian

*Oligocene zones by Berggren and Pearson (2005), and Neogene zones by Blow (1969).

TABLE 4. MOST SIGNIFICANT SPECIES MAKING UP THE ASSEMBLAGES OF CALCAREOUS NANNOPLANKTON OF THE OLIGOCENE STRATA IN THE INTRARIFIAN SEQUENCES

EL HABT UNIT	SAMPLES	CALCAREOUS NANNOPLANKTON: *Coccolithus eopelagicus* (Bramlette & Riedel) Bramlette & Sullivan, 1961	*Cyclicargolithus abisectus* (Müller) Wisse, 1973	*Cyclicargolithus floridanus* (Roth & Hay) Bukry, 1971	*Zygrablithus bijugatus* (Deflandre) Deflandre, 1959	*Sphenolithus predistentus* Bramlette & Wilcoxon, 1967	*Sphenolithus distentus* Bramlette & Wilcoxon, 1967	*Sphenolithus ciperoensis* Bramlette & Wilcoxon, 1967	*Sphenolithus moriformis* Bramlette & Wilcoxon, 1967	*Discoaster deflandrei* Bramlette & Riedel, 1954	*Discoaster tanii nodifer* Bramlette & Riedel, 1954	*Reticulofenestra umbilica* Martini & Ritzkowski, 1968	*Reticulofenestra bisecta* Roth, 1970	*Reticulofenestra gartneri* Hay et al., 1967	*Helicosphaera euphratis* Haq, 1966	*Helicosphaera perchnielseniae Jafar & Martini, 1975*	*Ericsonia formosa (Kamptner) Haq, 1971*	BIOSTRATIGRAPHIC ZONES	CHRONOSTRATIGRAPHY
Log 3	6/18		O	O				cf.					O					NP 24/25	Chattian
Dmina Quarry	4/18	O	O	O	O	O			O	O			O	O	O	O		NP23	middle Rupelian
Log 4	10/18	O	O	O		O	O		O	O	O		O	O				NP-23	middle Rupelian
Mezgalef	9/18	O	O	O	O	cf.		O		O	O	O	O	O			O	NP 21/22	early Rupelian

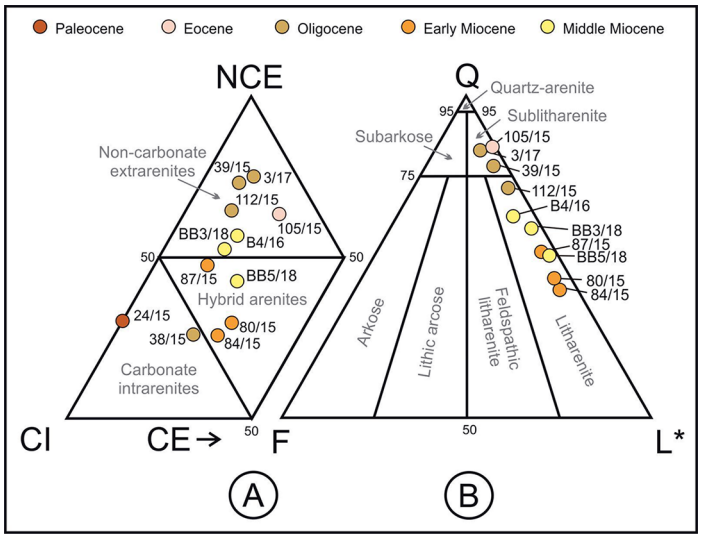

Archaeoglobigerina ssp., and *Heterohelix* ssp. belongs to the Late Cretaceous period (Campanian–Maastrichtian) (Fig. 4). This lithofacies (Uppermost Cretaceous *p.p.* near the K/T boundary) is topped by a major unconformity. In this lithofacies sample, 24/15 is classified in the NCE-CI-CE diagram (Zuffa, 1980) as carbonate intrarenite (Fig. 5; Table 5). This rock is a finely laminated planktic foraminiferal (globigerinid) wackestone (Dunham, 1962) with abundant fine-grained monocrystalline quartz grains (20–60mm, variably rounded). Glauconitic grains (>50 mm) are also present. Bioclasts are filled with polycrystalline calcite and/or ferruginous cement. Matrix shows a variable amount of clay minerals and Fe-oxides. The laminae vary in thickness (millimeter to

Figure 5. Ternary plots describe the composition of El Habt and Ouezzane Sandstones (arenites). (A) First-order compositional plot. NCE—non-carbonate extrabasinal grains; CE—carbonate extrabasinal; CI—carbonate intrabasinal. The rocks are classified as non-carbonate arenites, carbonate intrarenites, and hybrid arenites using the criteria proposed by Zuffa (1980, 1985). (B) Quartz-feldspar-lithic fragments including carbonate rocks (Q-F-L*) diagram shows the main clastic petrographic compositional features of the arenite samples (after Folk, 1980).

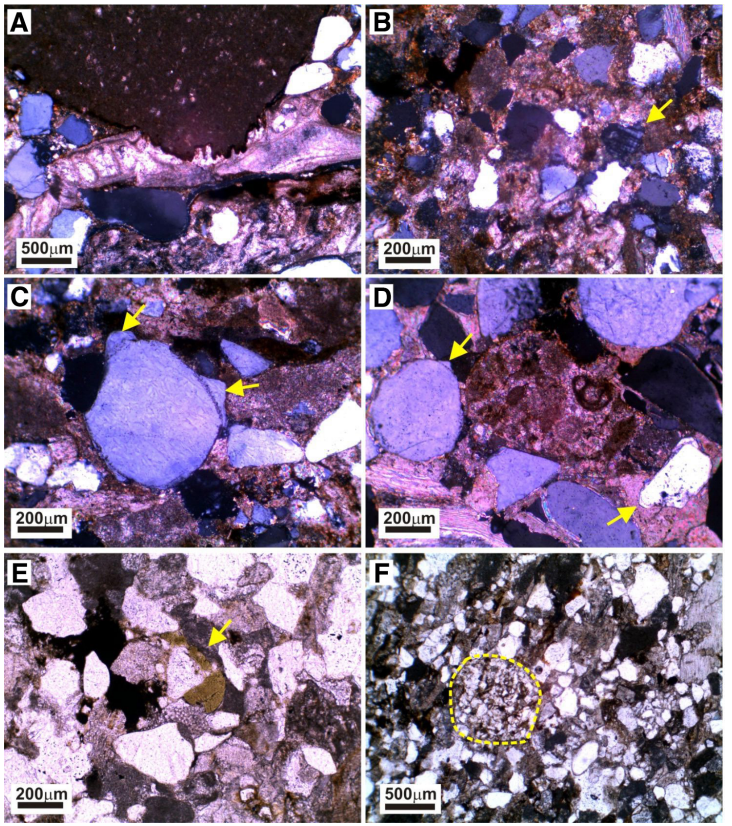

Figure 6. Micrographs of the main petrofacies studied in thin section are shown with (A–D) in cross-polarized light and (E–F) in plane-polarized light. Petrographic classification scheme is from Folk (1980), and the nomenclature of Zuffa (1980) is used for petrographic description and classification of siliciclastic rocks. (A) Sample 38–15 (carbonate intrarenite, Log 4, El Habt Tectonic Unit). Detail of pressure-dissolution features between wackestone extraclast (CE) and bioclast (Cl) is shown. This sample is classified as quartz-rich packstone (Dunham, 1962). (B) Sample BB3 (litharenite, Log 7, Ouezzane Tectonic Unit). Corroded monocrystalline quartz and K-feldspar (arrow) grains. (C) Sample BB5 (hybrid arenite, Log 7, Ouezzane Tectonic Unit). Coarse, well-rounded, second-cycle quartz grains (arrows: inherited syntaxial cement). (D) Sample 39–15 (sub-litharenite, Log 4, El Habt Tectonic Unit). Detail of recycled quartz and carbonate (packstone) extrabasinal grains is shown (arrow). (E) Sample 87–15 (hybrid arenite, Log 5, Ouezzane Tectonic Unit). General view of hybrid arenite with evidence of mechanical compaction (arrow: broken and deformed glauconite grain). (F) Sample BB5 (hybrid arenite, Log 7, Ouezzane Tectonic Unit). General view of hybrid arenite with fine-grained siliciclastic fragment (dashed line).

sub-millimeter) and are defined by the relative content of terrigenous grains, bioclasts, and Fe content in matrix. Small veins parallel to lamination and filled with calcite cement are also present.

Lithofacies 2 (L2). This lithofacies is 60 m thick and consists of greyish calcareous mudstone, silicified calcareous mudstone, and 2–4-m-thick olistolithic limestone. Lenticular bodies of chaotic marl and limestone deposits containing silicified deformed bands and corresponding to a large slump are present. In Log 1, the lower deposits belong to lithofacies 2, which rests above the Cretaceous strata of Campanian–Maastrichtian age, and it contains only rare agglutinated foraminifera (sample 27/15) or small radiolarians (sample 28/15). Above, deposits with similar lithofacies (sample 29/15) contain planktonic foraminifera, among which *S. senni, G. eocaena, P. inaequispira,* and *M. aragonensis* (formal names in Table 2) were identified. This assemblage suggests that the deposits belong to the E8–E9 interval of the zonation by Berggren and Pearson (2006), which corresponds to the Eocene Epoch (lower Lutetian Stage) (Fig. 4).

Log 1 (Fig. 3, Table 1) consists of the following stratigraphic units (from top to base):

(2) a 60-m-thick unit of marl, calcareous marl, and olistolithic limestones (Lithofacies L2).

(1) a 50-m-thick unit of mudstone, marly mudstone, and micritic limestone (Lithofacies L1) that is capped by an unconformity.

Log 2 (North Tahar Village, Total Thickness 130 m)

This log is located at 30S 237104 E 3919083 N. The log is from a monoclinal structure with E-dipping beds. Lithofacies L1 and L3 were recognized.

Lithofacies 1 (L1). This lithofacies is 75 m thick and consists of homogeneous gray-green mudstone (claystone and siltstone) and marls. The occurrence in the succession of the same unconformity recognized in Log 1 divides the lithofacies into an Upper Cretaceous portion (below the unconformity) and a Cenozoic *p.p.* portion (above the unconformity). Similar to lithofacies 1 of Log 1, the lower part of these sediments contains typical Late Cretaceous (Senonian) planktonic foraminifera.

Lithofacies 3 (L3). This lithofacies is 55 m thick and consists of alternating beds of homogeneous, varicolored mudstone (claystone and siltstone) and yellow-white marl and marlstone with the occurrence of centimeter-thick beds of sandstone (arenite) in the upper portion of the log. The lower 15 m of this lithofacies consists of alternating 10–30-cm-thick beds of varicolored mudstone. The strata above the lower 15 m of varicolored mudstone are beds of marl and marlstone. These beds of marl and calcareous marl strata (Tahar 1–2/14 and 31–32/15) show signs of carbonate dissolution and contain microfaunal assemblage of agglutinated foraminifera and radiolarians, although rare planktonic foraminifers are also present. The presence of *A. soldadoensis* and *M. subbotinae*, as well as morphotypes close to *M. aragonensis* (cf. *M. lensiformis* (Subbotina), suggest that these strata are of Eocene age and

TABLE 5. RESULTS OF THE MODAL POINT COUNT OF THE SANDSTONES STUDIED (ARENITES) USING THE GAZZI (1966) AND DICKINSON (1970) METHOD

		El Habt Unit				Ouezzane Unit							
		Log 1	Log 3	Log 4		Log 5		Log 6				Log 7	
		24/15	3/17	38/15	39/15	80/15	84/15	87/15	105/15	112/15	B4/16	BB3/18	BB5/18
NCE	Qmr	11,90	36,64	11,78	32,55	9,44	5,69	18,61	29,40	28,30	32,00	17,09	13,09
	Qmo	13,07	27,27	5,74	18,50	2,78	2,51	13,40	16,87	18,41	9,23	11,18	8,99
	Qp2-3	–	–	0,60	0,47	0,28	–	1,24	0,48	2,75	–	0,64	0,26
	Qp>3c	1,10	0,28	2,42	5,15	1,94	0,91	0,74	0,24	0,55	–	–	–
	Qp>3f	2,85	4,96	2,11	–	1,94	0,46	3,72	9,64	9,34	4,31	8,63	5,13
	Qfrm	–	–	–	0,23	–	–	–	–	–	2,15	–	0,64
	Qfrg	–	–	–	–	–	–	1,24	0,48	0,82	–	0,32	–
	Qfrs	–	–	3,02	0,47	6,67	9,34	2,98	–	–	–	2,24	1,67
	Cq	0,95	–	–	12,18	–	0,68	–	2,41	–	–	6,23	4,88
	Ks	–	1,10	–	1,64	–	0,91	0,99	–	–	2,15	0,16	0,13
	Kfi	–	–	–	–	2,50	0,68	0,74	–	0,55	0,92	0,16	–
	Ps	–	1,38	–	0,47	0,56	–	0,50	0,24	1,10	1,23	0,80	0,90
	Pfi	–	–	–	–	0,56	–	–	–	0,27	–	0,32	0,26
	Ch	–	–	0,60	0,70	0,83	0,46	–	–	0,27	0,62	1,12	0,64
	Lm	–	–	–	–	0,28	2,51	–	–	–	–	0,32	4,11
	Ms	–	–	–	–	–	0,68	0,50	–	–	–	–	–
	HM	1,10	0,83	–	–	0,28	0,46	0,50	0,48	0,82	2,15	0,64	0,13
CE	*Mi*	–	7,44	6,65	12,65	11,11	15,95	14,89	7,71	18,41	19,38	18,37	18,61
	Sc	–	3,58	15,11	2,58	16,39	10,48	12,41	–	3,30	4,62	11,02	13,22
	Fo	–	0,55	–	0,70	–	–	9,93	2,89	0,55	–	–	–
NCI	*Gl*	–	0,83	–	0,70	4,17	2,96	2,48	1,45	1,10	1,23	0,48	0,67
	OM	–	1,93	0,30	0,23	1,94	0,91	0,74	1,93	1,37	1,85	1,92	1,54
	Ph	–	–	–	–	0,28	–	–	–	–	–	–	–
CI	In	–	–	1,81	–	2,22	0,68	–	–	–	–	0,13	–
	Bi	54,10	4,13	38,67	4,45	27,78	34,17	6,45	18,80	7,14	2,46	8,79	18,61
	Cm	5,10	7,71	5,44	5,85	5,83	7,52	6,70	6,02	3,02	14,15	6,39	5,13
	Ma	9,83	1,38	5,44	0,47	2,22	2,05	1,24	0,96	1,92	1,54	1,76	1,28
		100	100	100	100	100	100	100	100	100	100	100	100
	NCE	30,97	72,45	26,59	72,37	28,06	25,28	45,16	60,24	63,19	54,77	50,00	40,82
	CE	–	11,57	21,75	15,93	27,50	26,42	37,22	10,60	22,25	24,00	30,51	31,84
	NCI	–	2,75	0,30	0,94	6,39	3,87	3,23	3,37	2,47	3,08	2,40	2,31
	CI	69,03	13,22	51,36	10,77	38,06	44,42	14,39	25,78	12,09	18,15	17,09	25,03
		100	100	100	100	100	100	100	100	100	100	100	100
	Q	–	83,11	–	79,41	43,46	40,76	51,21	84,59	71,57	62,75	59,18	50,75
	F	–	2,98	–	2,41	4,71	4,27	3,33	0,34	1,96	5,67	2,86	2,63
	L*	–	13,91	–	18,18	51,83	54,97	45,46	15,07	26,47	31,58	37,96	46,62
		–	100	–	100	100	100	100	100	100	100	100	100

Note: Abbreviations used for parameters of the modal analysis: NCE—on–carbonate extrabasinal clasts, Qmr—monocrystalline quartz with low undulosity<5°, Qmo—monocrystalline quartz with high undulosity>5°, Qp2-3—polycrystalline quartz: 2–3 subgrains, Qp>3c—polycrystalline quartz: > 3 subgrains; > 0,062 μm, Qp>3f—polycrystalline quartz: > 3 subgrains; 0,030 -0,062 μm, Qfrm—quartz in low/medium-grade metamorphic rock fragment, Qfrg—quartz in granite/gneiss rock fragment, Qfrs—quartz in sedimentary rock fragment, Cq—quartz grain replaced/corroded by carbonates, Ks—K-feldspar, Kfi—K-feldspar grain replaced by clay minerals, Ps—plagioclase, Pfi—plagioclase grain replaced by clay minerals, Ch—chert: >3 subgrains <0.030 μm, Lm—fine-grained sedimentary fragments, Ms—mica group minerals: mainly muscovite, HM—heavy minerals: mainly zircon, CE—carbonate extrabasinal clasts, Ml—fine-grained carbonate fragments, Sc—coarse-grained carbonate fragments, Fo—fossils, NCI—non-carbonate intrabasinal clasts, Gl—glauconite grains, OM—opaque minerals, Ph—phosphate minerals, CI—carbonate intrabasinal clasts, In—mudstone-wackestone clasts, Bi—bioclasts, Cm—cement: mainly carbonatic, Ma—matrix, Q—total quartz, F—total feldspars, L*—fine-grained rock fragments, including carbonate clasts.

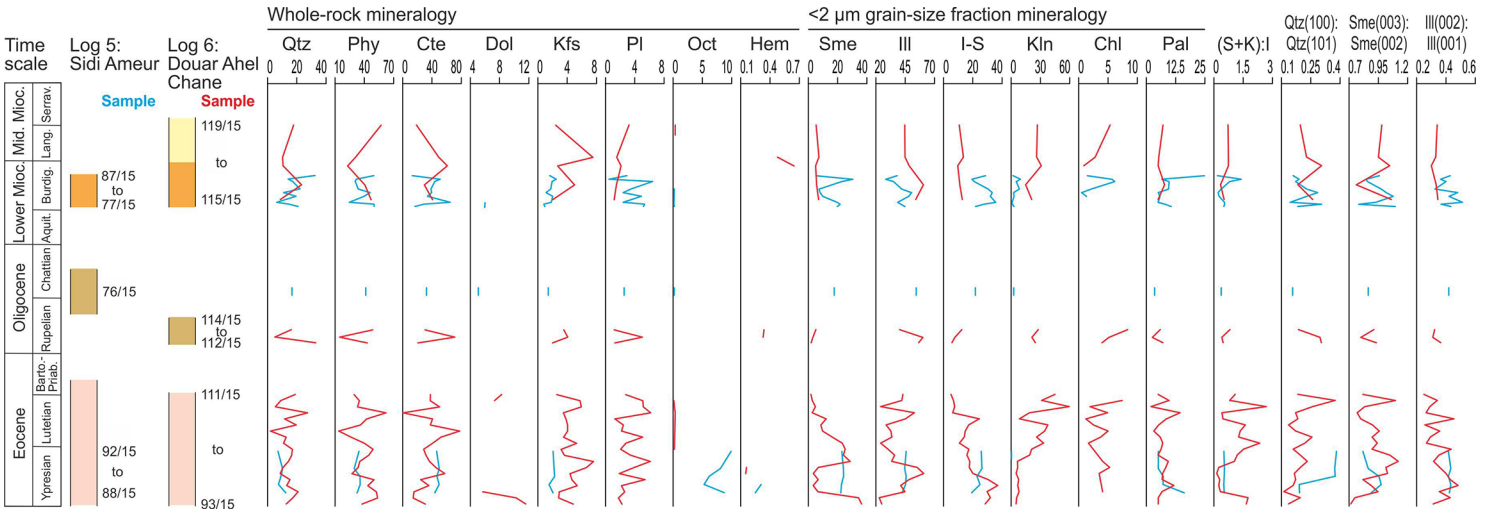

Figure 7. Mineralogical results of Logs 5 (Sidi Ameur succession, blue lines) and 6 (Douar Ahel Chane succession, red lines) are shown for the whole rock and the <2 µm grain-size fraction (in wt%), and the dimensionless (smectite+kaolinite):illite ((S+K):I) ratio. Values of the intensities ratio of the Qtz(001):Qtz(101) peak areas of quartz, and Sme(003):Sme(002) peak areas of smectite, and Ill(002):Ill(001) peak areas of illite under ethylene glycol solvation are included; sample number is as in Table 6 (Qtz—quartz; Phy—phyllosilicates; Cte—calcite; Dol—dolomite; Kfs—K-feldspar; Pl—plagioclase; Oct—opal CT; Hem—hematite; Sme—smectite; Ill—illite; I-S—mixed layer illite–smectite; Kln—kaolinite; Chl—chlorite; Pal—palygorskite).

specifically limited to the E4–E5 interval of the middle–upper Ypresian Stage (Table 2). Upward, similar lithofacies show a complete absence of planktonic foraminifera, and they reappear only in the higher part of the unit (sample LAY1/14) in an assemblage characterized by *A. bullbrooki, A. cuneicamerata, I. broedermanni, P. micra*, and forms similar to *T. possagnoensis* (Table 2). This association characterizes an E8–E9 zonal range of the lower–middle Lutetian.

Log 2 (Fig. 3) consists of the following units (from top to base):

(3) a 55-m-thick unit of mudstone, marl, and calcareous marl and a few beds of sandstone near the top of this unit (Lithofacies L3).

(2) a 25-m-thick unit of mudstone and marly mudstone (Lithofacies L1).

(1) a 50-m-thick unit of mudstone and marly mudstone (Lithofacies L1) that is capped by an unconformity.

Log 3 (Dmina Quarry, Total Thickness >250 m)

This log is located at 29S 766675 E 3920696 N. The log is from a monoclinal structure with moderately eastward-dipping beds, and the strata have been thrust westward over the Internal Prerif. This log (Fig. 3, Table 1) consists of a single lithofacies L4.

Lithofacies 4 (L4). This lithofacies is at least 250 m thick (it characterizes the whole log) and consists of brownish channel shape quartzarenite (graded and laminated; T_a and T_{a-b} Bouma intervals) with thin beds of brown (sometimes green) homogeneous mudstone and at some locations calcareous marls. In this lithofacies (Fig. 4), sample 1/17 contains planktonic foraminifera of the *G. ampliapertura* group, *G. eocaena* group, and *P. opima* (see Table 3 for the formal taxonomic names), which is a characteristic assemblage of the Oligocene zone O2, specifically the middle Rupelian Stage. In the upper part of the Log 3 (2–3/17 samples), the non-observance of morphotypes of *G. ampliapertura* group and *G. angulisuturalis* in the assemblages bearing the couple *G. eocaena–P. opima* suggests that these beds belong to the Oligocene O3 zone of the late Rupelian Stage. Complementary biostratigraphic studies of calcareous nanoplankton confirm these ages. Sample 4/18 (= 1/17) contains *S. praedistentus*, *H. perchnielseniae*, and *H. euphratis* (Table 4 includes formal names), whereas *I. recurvus*, *R. umbilica*, and *S. distentus* are absent. This combination characterizes the Oligocene NP 23 zone (Martini, 1971) of the middle Rupelian Stage. In sample 6/19 (= 3/17), the presence of *S. ciperoensis* suggests that it belongs to the Oligocene NP24–25 zonal interval that ranges between the late Rupelian Stage and the Chattian Stage (Fig. 4). In this lithofacies sample, 3/17 is represented in the NCE-Cl-CE diagram (Zuffa, 1980) as sandstone, while according to the Q-F-L diagram, it is non-carbonate extrarenite (sandstone) (Zuffa, 1980) and sublitharenite (Folk, 1980) (Fig. 5; Table 5). This submature fine-grained, sub-litharenite is mainly composed of monocrystalline quartz grains (100–400 mm) and carbonate rock fragments

TABLE 6. AVERAGE WHOLE-ROCK AND <2 µm GRAIN-SIZE FRACTION MINERALOGY (IN wt%) OF SAMPLES FROM LOG 5: SIDI AMEUR SUCCESSION AND LOG 6: DOUAR AHEL CHANE SUCCESSION

Log	Age	Sample*	Lithology	Whole rock									<2 µm grain-size fraction							Qtz(100): Qtz(101)	Sme(003): Sme(002)	Ill(002): Ill(001)
				Qtz	Phy	Cte	Dol	Kfs	Pl	Oct	Cpt	Hem	Sme	Ill	I-S	Kln	Chl	Pal	(S+K):I			
5	Burdigalian	87/15	marl	32	50	13		<5	<5			tr	5	38	29	<5	<5	25	0.19	0.20	0.96	0.43
		86/15	marl	14	32	51		<5	tr			tr	30	28	19	9	6	7	1.40	0.23	0.85	0.36
		85/15	marly mudstone	17	31	44		<5	6				23	35	21	5	6	10	0.80	0.21	0.86	0.40
		83/15	marl	22	34	39		<5	<5	tr			7	42	31	8	<5	9	0.38	0.26	0.98	0.33
		82/15	marly mudstone	11	46	40		<5	<5				8	50	33	<5	tr	5	0.21	0.30	1.02	0.48
		81/15	marl	19	40	34		<5	5				10	48	32	<5	<5	6	0.27	0.26	1.08	0.42
		79/15	calcareous marl	6	25	65		<5	<5				20	39	36	<5		5	0.54	0.19	0.93	0.51
		78/15	marl	15	50	29		<5	5	tr			22	41	28	<5		8	0.55	0.32	0.78	0.37
		77/15	marl	21	50	17	6	<5	5	tr			20	45	22	<5		11	0.51	0.22	1.09	0.43
	Chattian	76/15	marl	17	41	33	5	<5	5	tr			18	54	22	<5		<5	0.38	0.20	0.86	0.42
	Lutetian	92/15	calcareous marl	7	34	46		<5		10			23	46	26	tr		5	0.51	0.38	0.82	0.42
	Ypresian	91/15	silicified marl	10	30	50		<5		8			24	45	26			5	0.54	0.38	0.86	0.43
		90/15	silicified marl	9	36	47		<5		6			24	46	23			7	0.53	0.38	0.96	0.42
		89/15	silicified marl	7	36	50		<5		5	tr		23	45	25			7	0.50	0.23	0.97	0.43
		88/15	silicified marl	12	33	44		<5		9	tr		22	42	19			16	0.52	0.23	0.89	0.42
6	Langhian	119/15	mudstone	18	57	19		<5	5	tr		tr	5	45	11	27	5	7	0.72	0.23	0.98	0.34
	Burdigalian	118/15	calcareous marl	10	31	49		8	<5		tr		7	45	14	26	<5	5	0.75	0.26	0.95	0.33
		117/15	calcareous marl	11	23	61		<5	<5		<5		5	48	10	31	<5	5	0.74	0.32	1.05	0.30
		116/15	calcareous marl	23	41	30		5	<5				6	61	11	15		8	0.34	0.22	0.76	0.33
		115/15	calcareous marl	9	47	41		<5	<5		tr		7	54	13	21		5	0.52	0.28	1.06	0.34
	Rupelian	114/15	marly mudstone	16	48	31		<5	<5				5	40	13	28	8	6	0.82	0.22	0.91	0.32
		113/15	calcareous marl	5	15	71		<5	5				<5	60	8	21	5	<5	0.41	0.31	0.80	0.31
		112/15	calcareous marl	33	43	21		<5	<5				<5	57	6	25	<5	7	0.47	0.32	0.93	0.36
	Lutetian	111/15	calcareous marl	19	30	38	8	<5	<5				<5	43	5	45		5	1.09	0.22	0.82	0.25
		110/15	calcareous marl	9	35	38	7	6	5	tr			<5	42	7	31	7	10	0.81	0.38	1.10	0.34
		109/15	calcareous marl	5	33	50		6	5				5	24	8	60	<5	<5	2.68	0.28	0.83	0.29
		108/15	calcareous marl	27	62	<5		<5	6	tr			<5	53	6	19	5	14	0.41	0.21	0.77	0.26
		107/15	calcareous marl	12	42	41		<5	<5				12	45	24	9	<5	9	0.46	0.22	0.80	0.45
		106/15	calcareous marl	20	36	38		<5	<5				9	29	17	38	<5	5	1.61	0.18	0.90	0.26
		105/15	calcareous marl	<5	14	78		<5	<5				10	33	15	34	5	<5	1.35	0.21	0.96	0.36
		104/15	marly limestone	13	26	52		<5	5				16	34	14	26	<5	6	1.27	0.28	0.90	0.29
	Ypresian	103/15	marly limestone	11	40	41		5	<5				23	24	11	33	<5	7	2.34	0.25	0.94	0.27
		102/15	marly limestone	17	49	29		<5	<5	tr			25	30	17	21		6	1.52	0.20	0.90	0.44
		101/15	marly limestone	17	45	32		<5	<5				24	36	16	19		5	1.19	0.23	1.05	0.35
		100/15	marly limestone	14	35	37		8	6				29	33	18	7	<5	9	1.05	0.26	1.12	0.32
		99/15	marl	11	34	45		7	<5				7	55	18	7	5	8	0.24	0.23	1.02	0.36
		98/15	marl	9	27	58		<5	<5		tr		<5	61	20	5	<5	7	0.14	0.21	1.03	0.40
		97/15	marl	15	50	25		5	5				7	48	30	8		7	0.30	0.21	0.82	0.43
		96/15	marl	13	44	36		5	<5				<5	41	37	7		12	0.24	0.20	0.89	0.48
		95/15	marl	21	52	15	6	<5	<5				7	45	30	8	<5	7	0.33	0.16	0.95	0.35
		94/15	mudstone	17	54	14	10	<5	<5				34	23	32	6		5	1.75	0.23	0.75	0.43
		93/15	mudstone	13	38	31	12	5	<5				36	25	28	5		5	1.66	0.18	0.71	0.31

Note: tr—traces; Qtz—quartz; Phy—phyllosilicates; Cte—calcite; Dol—dolomite; Kfs—K-feldspar; Pl—plagioclase; Oct—opal CT; Cpt—clinoptilolite; Hem—hematite; Sme—smectite; Ill—illite; I-S—mixed layer illite-smectite; Kln—kaolinite; Chl—chlorite; Pal—palygorskite); and the dimensionless (smectite+kaolinite):illite ((S+K):I) ratio. Intensities ratio of the Qtz(001):Qtz(101) peak areas of quartz, Sme(003):Sme(002) peak areas of smectite, and Ill(002):Ill(001) peak areas of illite under ethylene glycol solvation are included.
*Location of samples in Figure 3.

(wackestone and grainstone). Micro- and crypto-crystalline quartz, feldspars, bioclasts (bivalves, echinoderms, and forams), glauconite, and opaque and heavy minerals (zircon) are also present with sizes ranging from 50 mm to 150 mm. Recycled or second-cycle quartz grains (well-rounded and/or with syntaxial overgrowths) are recognized. Carbonate and glauconite grains are usually deformed by pressure. Long and concave-convex boundaries between quartz grains are present. The scant interstitial material is made up of calcite sparite cement (mosaic, locally poikilotopic) and less often by matrix that is often oxidized.

Log 3 (Fig. 3) consists of a >250-m-thick unit of channelized sandstone beds and a few beds of mudstone and (or) calcareous mudstone (Lithofacies L4). No unconformities were documented in this log.

Log 4 (Mezgalef, Total Thickness >330 m)

This log is located at 29S 764825 E 3908105 N. The log is from a monoclinal structure with gently northeastward-dipping beds that, in turn, override the Internal Prerif westward. This log shows four lithofacies (L5 to L8):

Lithofacies 5 (L5). This lithofacies is 80 m thick and consists of homogeneous brown (tobacco) mudstone and marl with Fe-Mn nodules and chert. The strata show significant carbonate dissolution, such that some beds are barren in microfauna, whereas other beds contain mainly agglutinated foraminifera or radiolarians.

Lithofacies 6 (L6). This lithofacies is 20–70 m thick (and extends laterally ~500 m), and it consists of several beds (up to 2 m thick) of brown amalgamated, lenticular, and channelized sandstone beds (quartzarenitic Numidian Formation-like). Occasional limestone (grainstone) is recognizable. In this lithofacies in the NCE-CI-CE diagram (Zuffa, 1980), sample 38/15 (Fig. 6A) is classified as carbonate intrarenite. Sample 38/15 is a poorly sorted, quartz-rich lithoclastic packstone/grainstone (Dunham, 1962) where bioclasts (mainly fragments of benthic foraminifers and bivalves) are relatively large in size (>1 mm) and quartz grains (50–500 mm), both mono- and polycrystalline, are subrounded to subangular. Some quartz grains contain anhydrite inclusions. Recycled or second-cycle quartz grains (with syntaxial overgrowths) are recognized. Glauconitic grains (50–100 mm) are also present. Lithoclasts mainly consist of sedimentary rock fragments (mudstone, arenite, and siltstone). Matrix (mud) is relatively scarce. Calcite cement is microsparitic. Grain-coating and pore-filling cements of Fe oxides/hydroxides are also present. On the other hand, sample 39/15 (Fig. 6D) is classified as non-carbonate extrarenite (sandstone) in the NCE-CI-CE diagram (Zuffa, 1980), while according to the Q-F-L diagram (Folk, 1980) it is sublitharenite (Fig. 5; Table 5). This mature fine- to medium-grained sublitharenite is mainly made up of monocrystalline quartz grains and carbonate rock fragments (mudstone, wackestone, and packstone). Monocrystalline quartz (50 mm–2 mm) is the main constituent (>50%), with coarser grains (200 mm–2 mm) showing a higher degree of sphericity. Polycrystalline quartz, feldspars, bioclasts (bivalves and echinoderms), glauconite, and opaque minerals are also present with sizes ranging from 50 mm to 150 mm. Recycled, or second-cycle quartz grains (with syntaxial overgrowths) are recognized. Grains are commonly fractured and corroded (replaced by carbonates). Fine-grained carbonate (mudstone) grains are usually deformed by pressure. Calcite sparite cement (mosaic, locally poikilotopic) and matrix, often oxidized, are relatively scarce.

Lithofacies 7 (L7). This lithofacies is 40–70 m thick and consists of brown mudstone and marl with intercalations of sandstone (arenite with mudstone/sandstone ratio = 90/10) and/or quartzarenite. A few occasional 10–30-cm-thick microconglomerate beds are present. The calcareous mudstone (samples 40–43/15) contains planktonic foraminifera of the *G. ampliapertura* group, *G. eocaena* group, and *P. opima* (Table 3), which is a characteristic assemblage of the Oligocene middle Rupelian (zone O2). The combination of the presence of calcareous nannoplankton (Table 3) *R. umbilica* and *S. predistentus* and the absence of *I. recurves* (sample 9/18 = 40/17) as well as the presence of *S. distentus* and the absence of *R. umbilica* (sample 10/18 = 42/17) indicate Oligocene (early–middle Rupelian) ages.

Lithofacies 8 (L8). This lithofacies is >20 m thick, and it consists of greyish, large-scale cross-bedding sands and gravel. This level lies immediately above an unconformity of Quaternary age over Lithofacies L7.

Log 4 (Fig. 3) consists of the following stratigraphic units (from top to base):

(7) a 20-m-thick unit of sands and gravel.
(6) a 20-m-thick unit consisting of several beds of channelized sandstone (Lithofacies L6) capped by an unconformity.
(5) a 40-m-thick unit of mudstone, marly mudstone, and sandstone beds (Lithofacies L7).
(4) a 70-m-thick unit consisting of several beds of channelized sandstone (Lithofacies L6).
(3) a 70-m-thick unit of mudstone, marly mudstone, and sandstone beds (Lithofacies L7).
(2) a 30-m-thick unit consisting of several beds of channelized sandstone (Lithofacies L6).
(1) an 80-m-thick unit of mudstone and marly mudstone (Lithofacies L5).

Ouezzane Tectonic Unit

The sedimentary stacking in the Ouezzane Tectonic Unit (External Intrarif) results from different lithofacies associations (L9 to L32) forming three main successions (logs 5, 6, and 7) of Paleogene and Neogene age (Table 1 and Fig. 3). In addition, there are Neogene strata of Miocene (Aquitanian through Langhian) age. The abundance and better preservation of planktonic foraminifera in strata of the Ouezzane Tectonic Unit allow for a more refined chronological resolution. From the structural point of view (Suter, 1980a, 1980b), the Ouezzane Tectonic Unit is a nappe that overrides the Internal Prerif (Douar Ahel Chane and Oulad Ktir logs) and the External Prerif (Sidi Ameur log).

Log 5 (Sidi Ameur, Total Thickness 795 m)

This log is located at 30S 238853 E 3853859 N. The log is situated in a NW-SE–trending syncline. It is characterized by seven lithofacies (L9 to L15).

Lithofacies 9 (L9). This lithofacies is 50 m thick and consists of homogeneous greyish mudstone (mainly siltstone) and marl with limonite nodules. This lithofacies, which is Upper Cretaceous in age, is similar to the previously described L1 but slightly more siltitic. A major unconformity is present at the top of this lithofacies.

Lithofacies 10 (L10). This lithofacies is 30 m thick and consists of poorly stratified white marl, marly limestones, silicified mudstone and limestone, and chert lenses. Bedding is present in the more calcareous units. The basal deposits of this lithofacies (sample 88/15) contain an assemblage of planktonic foraminifera characterized by the presence of *A. bullbrooki, I. broedermanni*, and *G. eocaena.* This combination has coexisted since the late Ypresian Stage (E7 zone) of the Eocene epoch. However, *G. subconglobata* and *G. corpulenta*, which are typical components of early Lutetian age, were noted only in sample 90/15. In this lithofacies (samples 88/15–91/15), the bulk mineralogy of mudstone includes quartz (7–12%), phyllosilicates (30–36%), calcite (44–50%), opal CT (5–9%), and minor amounts of K-feldspar and clinoptilolite, while the clay fraction includes smectite (22–24%), illite (42–46%), random mixed layer illite-smectite (mixed layer I-S hereafter) (19–26%), and palygorskite (5–16%), which characterizes the Ill+(I-S) ± Sme clay-mineral association (Fig. 7 and Table 6).

Lithofacies 11 (L11). This lithofacies, which is repeated several times in the log, is between 15 m and 100 m thick and consists of poorly stratified yellow-gray marls and calcareous marls with occasional limestone (grainstone) intercalations. The sampled beds in the lowermost interval (sample OSAH/15) contain *T. cerroazulensis* and other planktonic foraminifera (Table 2), which thus indicate that these strata began to accumulate during the early Bartonian Stage of the Eocene epoch. In the lower part of the log, an unconformity marking the Eocene/Oligocene boundary is present within the lithofacies. Thus, ~25 m above the unconformity that caps the Eocene strata, the sampled bed of marly limestones (76/15) contains planktonic foraminifer assemblages (Table 3) with *P. opima* and large globigerinids of the *G. eocaena* group (including *G. corpulenta* and *G. gortani*). However, typical late Eocene species, such as *Hantkenina* ssp. and the *Turborotalia cerrozulensis* group, were not identified, which thus indicates that these strata are of lower Oligocene (Rupelian) age. In addition, the absence of both *P. micra* and specimens of the *G. ampliapertura–G. increbescens* group suggests that the strata belong to the Oligocene zonal interval O4–O5 (Berggren and Pearson, 2005), which is of latest Rupelian–early Chattian age. This age assessment reveals that a stratigraphic gap exists whose maximum range embraces the upper part of the Eocene epoch (upper Bartonian and Priabonian Stages) and most of the Rupelian. In this lithofacies, sample 87/15 (Fig. 6E) is represented in the NCE-Cl-CE diagram (Zuffa, 1980) as fine- to medium-grained hybrid arenite (NCE-Cl-CE diagram, Fig. 5) or litharenite (QFL diagram, Fig. 5B). Its main framework constituents are monocrystalline quartz, sedimentary rock fragments (mudstone, wackestone, fine-grained arenite, and siltstone), and bioclasts (benthic forams, bivalves, and red algae) (Fig. 6E). Bioclasts usually show total to partial silicification. Subrounded monocrystalline quartz (50–500 mm) is the main terrigenous grain type. Recycled or second-cycle quartz grains (with syntaxial overgrowths) are also recognized. Glauconite grains (50–250 mm) are usually deformed by pressure (Fig. 6E) as well as some limestone (mudstone/wackestone). Polycrystalline quartz, feldspars, mica flakes, and opaque minerals are also present with sizes ranging from 50 mm to 150 mm. Cement is scarce and is mainly made up of calcite microsparitic mosaics. In this lithofacies (sample 92/15), the bulk mineralogy of mudstone includes quartz (7%), phyllosilicates (34%), calcite (46%), opal CT (10%), and minor amounts of K-feldspar, while the clay fraction includes smectite (23%), illite (46%), random mixed layer illite-smectite (mixed layer I-S hereafter) (26%), palygorskite (5%), and traces of kaolinite, which characterizes the Ill+(I-S) ± Sme clay-mineral association (Fig. 7 and Table 6). In sample 76/15, the bulk mineralogy of mudstone includes quartz (13%), phyllosilicates (41%), calcite (33%), dolomite (5%), and minor amounts of K-feldspar, plagioclase, and opal CT, while the clay fraction includes smectite (18%), illite (54%), random mixed layer I-S (22%), and minor amounts of kaolinite and palygorskite, which characterizes the Ill+(I-S) ± Sme clay-mineral association (Fig. 7 and Table 6). In samples 77/15–79/15, 83/15, and 85/15–87/15 the bulk mineralogy of mudstone is made up of quartz (6–32%), phyllosilicates (25–50%), calcite (13–65%), plagioclase (<5–6%), and minor amounts of K-feldspar in all samples and dolomite (6%) in sample 77/15, opal CT, and magnetite, while the clay fraction includes smectite (5–30%), illite (28–50%), random mixed layer I-S (19–36%), kaolinite (<5–9%), chlorite (<5–6%), and palygorskite (5–25%), which characterizes the Ill+(I-S) ± Sme+Kln+Chl clay-mineral association (Fig. 7 and Table 6).

Lithofacies 12 (L12). This lithofacies is ~30 m thick and consists of lenticular cream, grain-supported limestone (grainstone) with polygenic conglomerate (average diameter of pebbles: 5–20 cm) and a few beds of limestone, sandstone, and chert. In this lithofacies sample, 80/15 is represented in the NCE-Cl-CE diagram (Zuffa, 1980) as hybrid arenite, while according to the Q-F-L diagram (Zuffa, 1980) it is litharenite (Fig. 5 and Table 5). This rock is a poorly sorted, quartz-rich, lithoclastic grainstone/rudstone (hybrid arenite) with relatively large (>1 mm) bioclasts that mainly consist of fragments of benthic foraminifers, bivalves, and bryozoans. Quartz grains (50–200 mm), both mono- and polycrystalline, show little rounding and variable size. Recycled or second-cycle quartz (with syntaxial overgrowths) are recognized. Glauconitic grains (50–100 mm) are also present. Lithoclasts mainly consist of sedimentary rock fragments (mudstone-wackestone, arenite, and dolosparite). Microsparitic calcite cement is the main interstitial material. Locally, grain-coating ferruginous cement and pore-filling glauconite cements are present.

Lithofacies 13 (L13). This lithofacies is 25 m thick and consists of cream polygenetic conglomerates with up to 22 cm-sized, poorly cemented pebbles. The assemblage of Lithofacies 11, 12, and 13 in the lower part of Log 5 is of Oligocene age. The conglomerates of lithofacies 12 and 13 are capped by an

unconformity, above which lies Lithofacies 14. Sample 79/15, which is from an intercalated marl bed, yielded a Neogene microfauna (Table 3) characterized by *Globigerinoides* (v.g. *G. trilobus* and *G. altiaperturus*), *C. dissimilis*, and *G. suteri.* These microfauna restrict the age of these strata to the Miocene epoch and specifically the lower Burdigalian Stage (lower part of zone N5). In the absence, or at least scarcity, of *G. kugleri,* the first appearance of *G. altiaperturus* is the best and closest biostratigraphic reference to mark the Aquitanian–Burdigalian boundary in the peri-Mediterranean realm (González Donoso et al., 1982) and the persistence of *C. dissimilis* extends to the middle part of the Burdigalian Stage. Throughout the upper part of Log 5, there are beds with consecutive appearances of: (1) *G. praescitula* (sample 82/15); (2) *G. subquadratus* and *G. peripheroronda*, still with persistence of *C. dissimilis* (sample 86/15; upper part of the zone N5, middle Burdigalian Stage); and, finally, (3) (sample 87/15) the presence of *G. bisphaericus* and disappearance of *C. dissimilis*, which marks the top of the N5. This last combination, in which *Praeorbulina* is absent, characterizes the N6–N7 zonal interval of the upper Burdigalian Stage of the Miocene epoch.

Lithofacies 14 (L14). This lithofacies is ~115 m thick and consists of alternating beds of cream sparitic limestone (grainstone) and marly-mudstone (marly-mudstone/grainstone ratio = 70/30).

Lithofacies 15 (L15). This lithofacies is 10 m thick and consists of amalgamated beds of cream-brown, homogeneous sandstone (Numidian Formation-like). In this lithofacies, sample 84/15 is represented in the NCE-Cl-CE diagram (Zuffa, 1980) as hybrid arenite, while according to the Q-F-L diagram (Zuffa, 1980) it is a litharenite (Fig. 5 and Table 5). It is a poorly sorted, quartz-rich lithoclastic grainstone/rudstone (hybrid arenite) with relatively large (>1 mm) bioclasts that mainly consist of fragments of benthic foraminifers, bivalves, and bryozoans. Quartz grains (50–200 mm), both mono- and polycrystalline, show little rounding and variable size. Recycled or second-cycle quartz (with syntaxial overgrowths) are recognized. Glauconitic grains (50–100 mm) are also present. Lithoclasts are abundant and variable (fine-grained arenites, siltstones, laminated shales, and green sands). Microsparitic calcite cement is the main interstitial material. Locally, fractures (200–400 mm wide) filled with drusy calcite cement, grain-coating ferruginous cements, and pore-filling glauconite cements are present.

Log 5 is characterized by some main unconformities separating different lithofacies assemblages characterized by peculiar stacking patterns. The upper part of the Eocene strata shows an increase in detritic sediments, which indicates a negative, coarsening-upward sequence. The Oligocene strata, which also contain a minor unconformity, end with coarse-grained detrital sediments related to a coarsening-upward stacking pattern. Finally, the Miocene strata consist of a mostly homogeneous succession showing a coarsening-upward trend.

Log 5 (Fig. 3) consists of the following 21 stratigraphic units (from top to base):

(21) an 85-m-thick unit of marl and calcareous marl with a few grain-supported limestone beds (Lithofacies L11).
(20) a 5-m-thick unit of alternating beds of grain-supported limestone (grainstone) and marly mudstone (Lithofacies L14).
(19) a 15-m-thick unit of marl and calcareous marl with a few grain-supported limestone beds (Lithofacies L11).
(18) a 10-m-thick unit of alternating beds of grain-supported limestone (grainstone) and marly mudstone (Lithofacies L14).
(17) a 15-m-thick unit of marl and calcareous marl with a few grain-supported limestone beds (Lithofacies L11).
(16) a 20-m-thick unit of alternating beds of grain-supported limestone (grainstone) and marly mudstone (Lithofacies L14).
(15) a 20-m-thick unit of marl and calcareous marl with a few grain-supported limestone beds (Lithofacies L11).
(14) a 10-m-thick unit of amalgamated beds of sandstone with erosive base (Lithofacies L15).
(13) a 60-m-thick unit of marl and calcareous marl with a few grain-supported limestone beds (Lithofacies L11).
(12) a 115-m-thick unit of alternating beds of grain-supported limestone (grainstone) and marly mudstone (Lithofacies L14).
(11) a 25-m-thick unit of marl and calcareous marl with a few grain-supported limestone beds (Lithofacies L11).
(10) a 30-m-thick unit of lenticular, grain-supported limestone and channelized polygenetic conglomerate (Lithofacies L12).
(9) a 50-m-thick unit of marl and calcareous marl with a few grain-supported limestone beds (Lithofacies L11).
(8) a 10-m-thick unit of lenticular, grain-supported limestone and channelized polygenetic conglomerate (Lithofacies L12) that is capped by an unconformity.
(7) a 25-m-thick unit of channelized polygenetic conglomerate (Lithofacies L13).
(6) a 25-m-thick unit of marl and calcareous marl with a few grain-supported limestone beds (Lithofacies L11).
(5) a 30-m-thick unit of lenticular, grain-supported limestone and channelized polygenetic conglomerate (Lithofacies L12).
(4) a 65-m-thick unit of marl and calcareous marl with a few grain-supported limestone beds (Lithofacies L11) that is capped by an unconformity.
(3) a 100-m-thick unit of marl and calcareous marl with a few grain-supported limestone beds (Lithofacies L11) that is capped by an unconformity.
(2) a 30-m-thick unit of marl, marly limestone, mudstone, and chert beds (Lithofacies L10).
(1) a 50-m-thick unit of mudstone and marly mudstone (Lithofacies L9), which is capped by an unconformity.

Log 6 (Douar Ahel Chane, Total Thickness >1500 m)

This log is located at 30S 263256 E 3863415 N. This log is from a N-S–trending syncline. It is made by seven lithofacies (L16 to L22):

Lithofacies 16 (L16). This lithofacies, which is the oldest interval of the log, is 45 m thick and consists of homogeneous greyish mudstone with thin beds of gray-white, mud-supported (mudstone-wackestone) limestones. This lithofacies (sample 93/15) yielded planktonic foraminifera with *A. soldadoensis* group (including *A. angulosa*) and *M. subbotinae* group (including *M. aequa)*, whereas more modern forms of these genres (e.g., groups of *A. bulbrooki* and *M. aragonensis*) were absent (Table 2). This combination suggests that the strata are of Eocene age and specifically from the zonal interval E3–E4 of the lower–middle Ypresian. In this lithofacies (samples 93/15 and 94/15), the bulk mineralogy of mudstone includes quartz (13–17%), phyllosilicates (38–54%), calcite (14–31%), dolomite (10–12%), and minor amounts of K-feldspar and plagioclase, while the clay fraction includes smectite (34–36%), illite (23–25%), random mixed layer I-S (28–32%), kaolinite (5–6%), and palygorskite (5%), which characterizes the Ill+(I-S) ± Sme+Kln clay-mineral associations (Fig. 7 and Table 6).

Lithofacies 17 (L17). This lithofacies is 105 m thick and consists of stratified, gray-white marly limestone, occasional marly beds, and silicified mudstone and limestone beds with blue chert lenses. The assemblages of planktonic foraminifera in this lithofacies are similar to those of lithofacies 16 (Table 2) and therefore are from the Eocene (lower–middle Ypresian). In this lithofacies (samples 95/15–100/15), the bulk mineralogy of mudstone includes quartz (9–21%), phyllosilicates (27–52%), calcite (15–58%), dolomite (6%) in sample 95/15, K-feldspar (<5–8%), and plagioclase (<5–6%), while the clay fraction includes smectite (<5–29%), illite (33–55%), random mixed layer I-S (18–37%), kaolinite (5–8%), chloride (<5–5%) in some samples, and palygorskite (7–12%), which characterizes the Ill+(I-S) ± Sme+Kln clay-mineral associations (Fig. 7 and Table 6).

Lithofacies 18 (L18). This lithofacies is 200 m thick and consists of stratified gray-white mudstone with intercalations of yellowish calcareous marl and occasional thin beds of channelized conglomerate. Some polygenic conglomerate beds are also present with erosive base. From the lower levels (100/15) of this lithofacies, *A.* gr. *soldadoensis* and *M.* gr. *subbotinae* are absent, and they are substituted by *A.* gr. *bulbrooki* and *M.* gr. *aragonensis*, which thus indicates the Eocene E6–E7 zonal span, which is late Ypresian in age. Upwards, successive foraminiferal assemblages indicate that the strata are of middle Eocene (Lutetian and early Bartonian) age (Table 2). Thus, (1) sample 101/15 yielded *G. eocaena–G. corpulenta* and *P. micra*, which indicates a Ypresian-Lutetian age; (2) sample 102/15 yielded *M. crassatus* and *G. subconglobata*, whereas *M.* gr. *aragonensis* was not recorded (Table 2), which suggests that this interval corresponds to the E9–E10 zonal span of middle–late Lutetian age; (3) sample 103/15 yielded *A. topilensis* and *T. possagnoensis*, which characterizes the zone E10 of late Lutetian age; and (4) sample 104/15 yielded *H. lehneri, H. liebusi*, and *T. pomeroli* (Table 2), which indicates an E10–E11 zonal range of late Lutetian age. In this lithofacies (samples 101/15–103/15), the bulk mineralogy of mudstone includes quartz (11–17%), phyllosilicates (40–49%), calcite (29–41%), and minor amounts of K-feldspar and plagioclase in all samples, while the clay fraction includes smectite (23–25%), illite (24–36%), random mixed layer I-S (11–17%), kaolinite (19–33%), palygorskite (5–7%), and minor amounts of chloride in sample 103/15, which characterizes the Ill+(I-S) ± Sme+Kln clay-mineral associations (Fig. 7 and Table 6).

Lithofacies 19 (L19). This lithofacies is 250 m thick and consists of greyish marls and calcareous marls with intercalations of medium to thick beds of grain-supported limestone (grainstone) and thicker, quartz-rich (sublitharenite) sandstone beds, both of which have turbiditic features (bed thickness up to 2–5 m). This interval has chaotic structures with many blocks of the previous lithofacies. The top of this lithofacies is marked by an unconformity. The samples of this lithofacies (107–109/15) contain rare planktonic foraminifera, but no age-diagnostic foraminifera were identified (Table 2). In this lithofacies, sample 105/15 is represented in the NCE-Cl-CE diagram (Zuffa, 1980) as non-carbonate extrarenite (sandstone), while according to the Q-F-L diagram (Folk, 1980) it is fine- to medium-grained sublitharenite (Fig. 5 and Table 5). Their main constituents are monocrystalline quartz, sedimentary rock fragments (mudstone, wackestone, and grainstone), and bioclasts (benthic forams, bivalves, and echinoderms). Subrounded to subangular monocrystalline and polycrystalline quartz grains (100–300 mm) are the main siliciclastic types. Recycled or second-cycle quartz (with syntaxial overgrowths) are recognized. Quartzose grains are commonly corroded (replaced by carbonates). Feldspars (plagioclase) and glauconite are also present with sizes ranging from 50 mm to 250 mm. The scant interstitial material is made up of calcite microsparite mosaics and, locally, siliceous syntaxial overgrowths. In this lithofacies (samples 104/15–111/15), the bulk mineralogy of mudstone includes quartz (<5–27%), phyllosilicates (14–62%), calcite (<5–78%), dolomite (7–8%) in samples 110/15 and 111/15, minor amounts of K-feldspar (<5–6%), and plagioclase (<5–6%) in all samples and traces of opal CT and clinoptilolite in some of them, while the clay fraction consists of the Ill+Kln ± (I-S)+Sme+Chl clay-mineral associations (Fig. 7 and Table 6).

Lithofacies 20 (L20). This lithofacies is 150 m thick and consists of brownish, quartz-rich (quartzarenite and sublitharenite) sandstone (Bouma sequences T_{a-b}, T_{a-b-c}, $T_{a-b-c-d}$, and T_{a-c} intervals are frequent) and limestone (grainstone) with the presence of calcareous marl. This lithofacies (L20) lies immediately above the unconformity surface that caps Lithofacies 19. As at Sidi Ameur, Log 5 also shows an unconformity at the Eocene–Oligocene transition. Sample 112/15 from a marly intercalation of lithofacies 20 contains an Oligocene microfauna characterized by *G. ampliapertura, G. increbescens, G. eocaena* group (including *G. corpulenta*), and *C. dissimilis*, but *P. micra* and typical Eocene species are absent. This assemblage corresponds to the Oligocene Zone O2 (middle Rupelian Stage). A little higher in the section, sample 113/15 made of marl contains *P. opima*, which suggests the proximity of the late Rupelian Stage. Therefore, the unconformity seems to include the upper Eocene (most part of the Bartonian and the Priabonian Stages) and the lowermost Oligocene (lower Rupelian Stage). A major unconformity that has removed upper Oligocene–Aquitanian strata is also present in Log 6 immediately above the sandstone and grainstone with calcareous-marl intercalations. The reappearance of Lithofacies 20 shows a succession of Burdigalian bio-events that is similar to that of

lithofacies 11 in Log 5. However, lithofacies 20 contains more strata of Miocene age, as demonstrated by the presence of *P. sicanus* in the upper units (sample 118/15), which thus characterizes the middle Miocene Zone N8 (lower Langhian). In this lithofacies sample 112/15 is represented in the NCE-Cl-CE diagram (Zuffa, 1980) as non-carbonate extrarenite (sandstone), while according to the Q-F-L diagram (Folk, 1980) it is a fine- to medium-grained litharenite (Fig. 5 and Table 5). Framework is mainly composed of monocrystalline quartz, sedimentary rock fragments (wackestone, packstone), and bioclasts (benthic forams, bivalves, red algae, and echinoderms). Subangular monocrystalline quartz (100–500 mm) and composite fine-grained quartz are the main siliciclastic grain types. Recycled or second-cycle quartz (with syntaxial overgrowths) are recognized. Quartzose grains are commonly corroded (replaced by carbonates). Feldspars (plagioclase), glauconite, and opaque minerals are also present with sizes ranging from 50 mm to 250 mm. The scant interstitial material is made up of calcite cement (mosaic and syntaxial). In this lithofacies (samples 112/15 and 113/15), the bulk mineralogy of mudstone includes quartz (5–33%), phyllosilicates (15–43%), calcite (21–71%), and minor amounts of K-feldspar and plagioclase, while the clay fraction includes smectite (<5%), illite (57–60%), random mixed layer I-S (6–8%), kaolinite (21–25%), chlorite (<5–5%), and palygorskite (<5–7%), which characterizes the Ill+Kln ± (I-S)+Sme+Chl clay-mineral association (Fig. 7 and Table 6). In the samples 115/15–118/15, the bulk mineralogy of mudstone includes quartz (9–23%), phyllosilicates (23–47%), calcite (30–61%), and minor amounts of K-feldspar and plagioclase in all samples and opal CT and clinoptilolite in some, while the clay fraction includes smectite (5–7%), illite (45–61%), random mixed layer I-S (10–14%), kaolinite (15–31%), palygorskite (5–8%), and minor amounts of chlorite, which characterize the Ill+(I-S) ± Sme+Kln+Chl clay-mineral association (Fig. 7 and Table 6).

Lithofacies 21 (L21). This lithofacies is 150 m thick and consists of stratified white-cream mudstone, marly mudstone, litharenite, and quartzarenite (mudstone/sandstone ratio = 75/25); thin 2–25-cm-thick beds of brownish sandstone show internal sedimentary structures (T_{a-b}, T_{a-b-c}, $T_{a-b-c-d}$, and T_{a-c} of Bouma). The top of this lithofacies is marked by an unconformity. In this lithofacies (sample 114/15), the bulk mineralogy of mudstone includes quartz (16%), phyllosilicates (48%), calcite (31%), and minor amounts of K-feldspar and plagioclase, while the clay fraction includes smectite (5%), illite (40%), random mixed layer I-S (13%), kaolinite (28%), chlorite (8%), and palygorskite (6%), which characterize the Ill+Kln ± (I-S)+Sme+Chl clay-mineral association (Fig. 7 and Table 6).

Lithofacies 22 (L22). This lithofacies is >500 m thick and consists of white-cream marly mudstone with a few beds of grain-supported limestone (grainstone). One sample (119/15) for biostratigraphical studies from the upper beds of this lithofacies contained *Orbulina* and intermediate morphotypes between *G. miozea* and *G. praemenardii* (identified as *G.* cf. *praemenardii*), which suggests that the top of Log 6 has an age near the Langhian–Serravallian boundary. In this lithofacies (sample 119/15), the bulk mineralogy of mudstone includes quartz (18%), phyllosilicates (57%), calcite (19%), minor amounts of K-feldspar and plagioclase, and traces of opal CT and hematites, while the clay fraction includes smectite (5%), illite (45%), random mixed layer I-S (11%), kaolinite (27%), chlorite (5%), and palygorskite (7%), and minor amounts of chlorite, which characterize the Ill+(I-S) ± Sme+Kln+Chl clay-mineral association (Fig. 7 and Table 6).

Log 6 (Fig. 3) consists of the following nine stratigraphic units (from top to base):

(9) a >500-m-thick unit of mudstone, marly mudstone, and a few beds of grain-supported limestone (grainstone) (Lithofacies L22).
(8) a 50-m-thick unit of beds of sandstone and beds of grain-supported limestone (grainstone) (Lithofacies L20).
(7) a 150-m-thick unit of beds of sandstone and beds of grain-supported limestone (grainstone) (Lithofacies L20) that is capped by an unconformity.
(6) a 150-m-thick unit of beds of mudstone, marly mudstone, and sandstone (Lithofacies L21) that is capped by an unconformity.
(5) a 50-m-thick unit of beds of sandstone and beds of grain-supported limestone (grainstone) (Lithofacies L20).
(4) a 250-m-thick unit of marl and calcareous marl with thin sandstone beds (Lithofacies L19) that is capped by an unconformity.
(3) a 200-m-thick unit of mudstone and calcareous marl with a few beds of channelized conglomerate (Lithofacies L18).
(2) a 105-m-thick unit of beds of marly limestone and beds of mudstone with chert lenses (Lithofacies L17).
(1) a 45-m-thick unit of mudstone with thin beds of mud-supported limestone (mudstone-wackestone) (Lithofacies L16).

Log 7 (Oulad Ktir, Total Thickness 1.262 m)

This log is located at 30S 273173 E 3828202 N. The log is from a NW-SE–trending syncline. This log is formed by 10 lithofacies (L23 to L32):

Lithofacies 23 (L23). This lithofacies is >70 m thick and consists of homogeneous black mudstone and is capped by an unconformity. The microfauna are predominantly calcareous and agglutinated benthic foraminifera, but there are also some planktonic foraminifera. The presence of *Rosita contusa* in sample B11/16 and of *Racemiguembelina fructicosa* and *Abatomphalus mayaroensis* in sample B10/16 suggest a Cretaceous (middle–late Maastrichtian) age.

Lithofacies 24 (L24). This lithofacies is 320 m thick and consists of yellow-white marls with a few beds of calcareous marls. This lithofacies represents the oldest Cenozoic strata in the Ouezzane Tectonic Unit. The lowest sampled level (B9/16) above the Upper Cretaceous strata (lithofacies 23) contains a rich planktonic assemblage with *P. pseudobulloides, P. uncinata, P. inconstans,* and *G. compressa* (formal names are in Table 2). This assemblage is devoid of the *Acarinina* and *Morozovella* that characterizes the P2 zone of Olsson et al. (1999) and corresponds to the upper part of the lower Paleocene. Nevertheless, the sample is 30 m above the top of the Cretaceous strata, and thus a Paleocene age is possible. In a higher sample from this lithofacies (B8/16 level), the presence of *G. chapmani* associated with *Acarinina* (*A. soldadoensis* and *A. angulosa*) and *Morozovella* (*M. subbotinae* and *M. aequa*) suggests an

Eocene age, specifically the E3 zone of the early Ypresian Stage (Fig. 4). A gap between the Paleocene and Eocene strata is also probable.

Lithofacies 25 (L25). This lithofacies is 60 m thick and consists of yellow-gray marls and thin (thickness from 5 cm to 20 cm), well-stratified, fine-grained cream sandstone beds with occasional 50–60 cm up to 1-m-thick beds of conglomerates with polygenetic and cherty clasts. Calcareous marly (fine-grained carbonate and terrigenous siliciclastic) beds are also present. Showing sedimentary continuity with the underlying lithofacies, the successive appearance of *M. aragonensis* and *S. senni* (sample B7/16), and of *A. bullbrooki, A. cuneicamerata, P. micra*, and the large globigerinids such as *G. eocaena* and *G. corpulenta* (sample B6/16), indicate an Eocene (late Ypresian and early Lutetian) age.

Lithofacies 26 (L26). This lithofacies is 60 m thick and consists of gray marls with a few channelized conglomerate intercalations. Strata of the this lithofacies (sample B5/16) yielded planktonic microfauna in which *M. crassatus* was present, which thus suggests continuity of sediment accumulation during the middle-late Lutetian Stage.

Lithofacies 27 (L27). This lithofacies is a 30–60-m-thick interval and consists of amalgamated beds of fine- to medium-grained cream sandstone (litharenite) with 5–10-cm-thick breccias at the base of each bed and rare, several-meter-thick beds of well-stratified, white-gray marls. In this lithofacies sample, B4 is represented in the NCE-CI-CE diagram (Zuffa, 1980) as non-carbonate extrarenite (sandstone), while according to the Q-F-L diagram (Folk, 1980), it is a fine- to medium-grained litharenite (Fig. 5 and Table 5). Its main constituents are monocrystalline quartz (100–300 mm) and sedimentary rock fragments (mudstone and wackestone) (50–100 mm). Sub-rounded monocrystalline quartz and composite fine-grained quartz are the main terrigenous type. Recycled or second-cycle quartz (with syntaxial overgrowths) are recognized. Quartzose and feldspathic grains are commonly corroded (replaced by carbonates). Bioclasts (benthic forams, bivalves, and echinoderm), feldspars, glauconite, micas, and opaque and heavy minerals (zircon) are also present with sizes ranging from 50 mm to 250 mm. Interstitial material is made up of calcite cement (mosaic, poikilitic, and syntaxial) and more seldomly matrix that is often oxidized. Ferruginous pore-filling cements are also present.

Lithofacies 28 (L28). This lithofacies is 10 m thick and consists of cream-brown, clast-supported, cemented polygenetic conglomerate with rounded sandstone clasts (diameter of 5–10 cm).

Lithofacies 29 (L29). This lithofacies is 70–247 m thick and consists of homogeneous yellow marls. Inside the first interval of occurrence of this lithofacies in the log, an unconformity separates Oligocene strata from overlying Miocene strata. Above the coarse detrital sediments of lithofacies 27 and 28, the lower span of lithofacies 29 (sample B3/16) yielded *A. topilensis, M. crassatus, H. dumblei*, and other microfauna of middle Eocene (late Lutetian Stage) age (Table 2). The lower span of lithofacies 29 (samples B2/16 and B1/16) also yielded *T. cerroazulensis* and *G. index*, which are of middle Eocene (early Bartonian Stage) age. As in Logs 5 and 6, an unconformity that has removed upper Eocene (Bartonian *p.p.*–Priabonian Stages) and lower Oligocene (lower Rupelian Stage) age strata is present in Log 7. Nevertheless, the most comprehensive section of Oligocene strata is present in Log 7. In this lithofacies, the disappearance of *G. ampliapertura* (marker of the O2/O3 zonal boundary), which is used as a reference for the base of the upper Rupelian Stage (Fig. 4), occurs between sample BB14/18 and sample BB13/18 (both of which exist in marl beds). The first appearance of *G. angulisuturalis* (Oligocene O3/O4 zonal boundary; reference for the beginning of the uppermost Rupelian Stage) occurs between sample BB13/18 and sample BB12/18 (both of which exist in marl beds); and the disappearance of *P. opima* (O5/O6 boundary, lower Chattian) occurs between sample BB12/18 and sample BB11/18 (both of which exist in marl beds). Finally, the highest sample (BB11/18), which is from a marly bed, contains large globigerinids of the *G. oecaena* group. This appears in combination with morphotypes close to *G. praebulloides* having supplementary dorsal apertures, which are identified as *G.* cf. *primordius*. This association suggests a limited time-span of upper Oligocene (late Chattian) age (Fig. 4), prior to the appearance of *G. kugleri*, which marks the Oligocene/Miocene boundary.

Lithofacies 30 (L30). This lithofacies is 15 m thick and consists of interbedded, white-yellow calcareous marl and marly limestone. A minor gap (unconformity) seems to be present at the top of this lithofacies, in which strata of Miocene (Burdigalian *p.p.*–lowermost Langhian) age have been removed. Sample BB7/18, which is from a bed of calcareous marl near the base of this lithofacies, contains *G. bisphaericus, P. sicanus*, and *P. glomerosa*. This assemblage is characteristic of the upper part of early Miocene Zone N8 (latest early Langhian) age. Sample BB1–6/18 (calcareous marl) suggests the continuity of sediment accumulation during the Langhian Stage. In sample BB2/18 (calcareous marl), the appearance of *Orbulina* indicates a middle Miocene (late Langhian) age. The major unconformity below this lithofacies has removed lower Miocene (Aquitanian) strata. Beds of this lithofacies (samples BB10/18, BB9/18, and BB8/18) contain assemblages of planktonic foraminifera characterized by *G. altiaperturus, G. trilobus,* and *G. peripheroronda* in combination with *G. suteri* and *C. dissimilis*. The combined presence of these species constrains the age to Miocene Zone N5 (except for the lowermost part) of the standard zonation of Blow (1969). Considering that *G. subquadratus* is not present in the assemblages, these lower deposits of Miocene *p.p.* sequence must be early Burdigalian in age. Approximately 70 m of strata of the upper part of this lithofacies were not sampled for biostratigraphical purposes, and thus the existence of upper Burdigalian strata in this lithofacies cannot be ruled out.

Lithofacies 31 (L31). This lithofacies is 22–63 m thick and consists of homogeneous white-yellow marl with intercalations of grain-supported limestone (grainstone) (up to 50 cm thick) and more rare thin sandstone (arenite) beds. In this lithofacies, samples BB3 (Fig. 6B) and BB5 (Figs. 6C and 6F) are represented in the NCE-CI-CE diagram (Zuffa, 1980) as non-carbonate extrarenite (sandstone), while according to the Q-F-L diagram (Folk, 1980), it is a fine- to medium-grained litharenite (Fig. 5 and Table 5). Its main constituents are monocrystalline quartz (50–250 mm) and sedimentary rock fragments (wackestone) (50–250 mm). Sub-rounded, monocrystalline quartz and composite

fine-grained quartz are the main terrigenous type. Recycled or second-cycle quartz (with syntaxial overgrowths) are recognized. Quartzose and feldspathic grains are commonly corroded (replaced by carbonates). Bioclasts (benthic forams, bivalves, and echinoderms), feldspars, glauconite opaque and heavy minerals (zircon) are also present with sizes ranging from 50 mm to 250 mm. Carbonate and glauconite grains (25–50 mm) are usually deformed by pressure-producing pseudomatrix. Interstitial material is made up of calcite (mosaic, syntaxial), siliceous (syntaxial), and ferruginous (pore-filling) cements. On the other hand, sample BB5/18 is represented in the NCE-CI-CE diagram (Zuffa, 1980) as a fine- to medium-grained hybrid arenite, while according to the Q-F-L diagram (Folk, 1980) it is a litharenite (Fig. 5 and Table 5). Its main framework constituents are monocrystalline quartz, sedimentary rock fragments (mudstone, wackestone, fine-grained arenite, and shale), and bioclasts (benthic forams, bivalves, and red algae). Bioclasts usually show total to partial silicification. Sub-rounded monocrystalline quartz (50–400 mm) is the main terrigenous type. Recycled or second-cycle quartz (with syntaxial overgrowths) are recognized. Glauconite grains (25–50 mm) are usually deformed by pressure as well as by some limestone (wackestone) extraclasts. Polycrystalline quartz, feldspars, mica flakes, and opaque minerals are also present with sizes ranging from 50 mm to 150 mm. Cement is scarce and mainly consists of calcite microsparitic mosaics. Locally, siliceous (syntaxial) and ferruginous (pore-filling) cements are recognized.

Lithofacies 32 (L32). This lithofacies is 55 m thick and consists of amalgamated beds of fine- to medium-grained brown-cream sandstone with 5–10-cm-thick beds of breccias at the base and rare beds of well-stratified, cream-yellow marls.

Log 7 (Fig. 3) consists of the following 16 stratigraphic units (from top to base):

(16) a 100-m-thick unit of marl (Lithofacies L29).
(15) a 60-m-thick unit of marl with some beds of limestone (grainstone) and rare beds of sandstone (Lithofacies L31).
(14) a 3-m-thick unit of grain-supported limestone (grainstone) and sandstone (Lithofacies L31).
(13) a 55-m-thick unit of amalgamated beds of sandstone with rare beds of marl (Lithofacies L32).
(12) a 22-m-thick unit of marl with some beds of grain-supported limestone (grainstone) and rare beds of sandstone (Lithofacies L31).
(11) a 70-m-thick unit of marl (Lithofacies L29).
(10) a 15-m-thick unit of beds of calcareous marl and marly limestone (Lithofacies L30) that is capped by an unconformity.
(9) a 247-m-thick unit of marl (Lithofacies L29) that is capped by an unconformity.
(8) an 80-m-thick unit of marl (Lithofacies L29) that is capped by an unconformity.
(7) a 10-m-thick unit of amalgamated sandstone beds (Lithofacies L27).
(6) a 10-m-thick unit of polygenic conglomerates (Lithofacies L28).
(5) a 60-m-thick unit of amalgamated sandstone beds (Lithofacies L27).
(4) a 60-m-thick unit of marl with a few beds of channelized conglomerate (Lithofacies L26).
(3) a 60-m-thick unit of marl with thin beds of sandstone (Lithofacies L25).
(2) a 320-m-thick unit of marl with a few beds of calcareous marl (Lithofacies L24).
(1) a 70-m-thick unit of mudstone (Lithofacies L23) that is capped by an unconformity.

In summary, the two tectonic units are characterized by different lithofacies associations and vertical sediment distributions. The El Habt Tectonic Unit is prevalently characterized by the widespread presence of thick beds of quartzitic sandstone, mudstone, and marly mudstone (e.g., Log 3). Instead, the Ouezzane Tectonic Unit is characterized by a wider diversity of lithofacies with the presence of immature sandstone (arenites), limestone (grainstone), and polygenic conglomerates and rare quartzitic sandstone. Both successions contain many unconformities and evidence of biostratigraphic gaps of various significance.

INTERPRETATIONS OF DEPOSITIONAL ENVIRONMENTS

Lithofacies L1 to L3 indicate a basin environment (below the calcite compensation depth [CCD] in the case of L2 by the exclusive presence of agglutinated foraminifera and radiolarians), which also agrees with the Upper Cretaceous deposits of other sectors of the Maghrebian Chain (Guerrera and Martín-Martín, 2014). Lithofacies L4 and L5 probably represent a channelized slope area as the lenticular shapes (L4) and internal Bouma structures indicate. Lithofacies L6 consists of amalgamated, lenticular, and channelized sandstone beds that point out a channelized depositional area of a submarine fan. Lithofacies L7 probably represents a base-slope affected by the contribution of occasional coarse-grained supply. Lithofacies L8 clearly represents a Quaternary paleobeach. Lithofacies L9 and L10 are again interpreted as a basin environment while Lithofacies L11 is probably related to a slope/basin realm. Lithofacies L12 and L13 are ascribable to a slope channeled area, while Lithofacies L14 and L15 are related to a slope/basin realm. The widespread silicization of Lithofacies L16 and L17 and the character of the fossil assemblages indicate a basinal area. Lithofacies L18 also includes channelized beds, which probably reflects a more proximal sector of a basinal area. The presence in Lithofacies L19 of thicker turbidite sandstones, slumps, and rare planktonic foraminifera allows a base-slope to be proposed as the sedimentary environment. Lithofacies L20 and L21, characterized by prevalently turbidite sandstones and sometimes channelized, were interpreted to have been deposited in a slope marked by channels. Contrarily, Lithofacies L22 represents a platform area, while the characteristics of Lithofacies L23 clearly can be related to a sedimentary basin environment. Also, Lithofacies L24 is related to a basin area but is affected by a lesser terrigenous supply. The different lithotypes, which are occasionally channelized, seen in Lithofacies L25 to L30 have been interpreted to have been deposited in a slope realm poor in channeling, while Lithofacies L31 and L32 clearly indicate a platform environment.

The Cretaceous succession is visible in Logs 1, 2, 5, and 7, while the Paleocene is only recognized in Log 7. The Paleogene deposits of the Ouezzane Tectonic Unit show features of pelagic sedimentation that is usually above the CCD. Paleocene strata denote the absence of platform sedimentary structures and the presence of pelagic planktonic foraminifera that seem to indicate a deep marine environment. The reduced Paleocene terrigenous supply with respect to the Cretaceous could indicate a relative sea-level rise. The Eocene succession (Logs 1, 2, 5, 6, and 7) points out a general thickening-upward evolution and a progressive occurrence of detritic supply with a shallowing-upward trend in an onlap stacking pattern. The Oligocene strata (Logs 3–7) are arranged in a negative stacking pattern that shows shallowing-upward and coarsening-upward (progradational) evolution. The Miocene strata (Logs 5, 6, and 7) show a new shallowing-upward trend, but an evident stacking pattern is not recognizable.

PETROGRAPHY AND CLAY MINERALOGY

According to petrographic analysis, the siliciclastic grains observed in the sandstone are mainly monocrystalline quartz (28–65% in litharenites, 8–32% in hybrid arenites) (Fig. 6B) and polycrystalline quartz (4–12%, 1–6%, litharenites and hybrid arenites, respectively). Quartz grains (50–500 mm) are well-rounded to very angular in shape (Fig. 6). Occasionally, monocrystalline quartz shows a euhedral shape and anhydrite inclusions (38–15P, El Habt Tectonic Unit, Log 4, Lower Oligocene). Recycled or second-cycle quartz grains (coarse, well-rounded, and/or with syntaxial overgrowths) are present in all samples (Figs. 6C–6D). Detrital K-feldspar and plagioclase (<6%) (Fig. 6B), mica flakes (mainly muscovite) (<1%), and heavy minerals (mainly zircon) (<3%) occur in both arenites and hybrid arenites with sizes ranging from 50 mm to 150 mm. Also, small amounts of non-carbonate intrabasinal clasts, including glauconite grains (0.5–3%) (Fig. 6E) and opaque minerals (<2%), are present in most of samples. Sedimentary lithic fragments (mainly fine-grained and coarse-grained carbonates) dominate the lithic population and constitute up to 25% of total grains. Carbonate extrabasinal clasts (CE) mainly consist of rounded limestone (wackestone and packstone) fragments, biomicrite, and biosparite fragments, and they have a grain size similar to that of other noncarbonated particles (Figs. 6B–6D). Carbonate intra-basinal (CI) grains consist of bioclast (mainly bivalves, echinoderms, benthic foraminifers, and red algae) and minor amounts of fine-grained intraclasts. These particles generally have larger grain sizes and are more angular grains with respect to extrabasinal clasts, especially in the calcarenites and hybrid arenites, where bioclasts are usually coarser than 1 mm. These hybrid arenites also show higher variability in the typology of sedimentary lithics, where the presence of fragments of siliciclastic arenites, shales, siltstones, and green sands is relatively common (Fig. 6F).

Modal analyses of sandstone (mostly litharenite) indicate middle to upper rank metamorphic and sedimentary source terranes for the extrabasinal grains (Fig. 8A). The intrabasinal grains must be derived from erosion of the local limestone substrate and from areas with active benthic carbonate production (platform). During the early to middle Miocene, where hybrid arenites dominate (Ouezzane Tectonic Unit), carbonate sedimentary sources, both coeval and not coeval, are more persistent. All samples fall into the "recycled orogen" (Dickinson et al., 1983) tectonic setting (Fig. 8B). Specifically, the hybrid arenite correspond to the "transitional recycled" sub-type and most of the terrigenous sandstone (arenite) to the "quartzose recycled" sub-type. The presence of features associated with recycling processes, such as the existence of second-cycle or recycled quartz grains and the abundance of sedimentary rock fragments, suggests an origin related to the erosion of older siliciclastic and carbonate formations. The abundance of monocrystalline quartz (with evidence of recycling), the scarce presence of unstable minerals (feldspars and micas), and the presence of ultra-stable heavy minerals (zircon) point to a multicyclic origin of these grains. Several repeated erosion-sedimentation cycles are also inferred for the terrigenous petrofacies (represented by mature sandstone: quartzarenite and sublitharenite *sensu* Folk, 1980) from the Cenozoic succession from the External Tanger-Ketama Tectonic Unit (Maaté et al., 2017). All provenances can be interpreted as being derived from the West African craton, the Pan-African belt, and the Varican Moroccan Mesetas.

The clay-mineral associations that indicate potential External Rifian source areas are relatively well-known: (1) Ill+Chl ± Kln for Upper Jurassic and Lower Cretaceous epicontinental formations affected by low-grade metamorphism

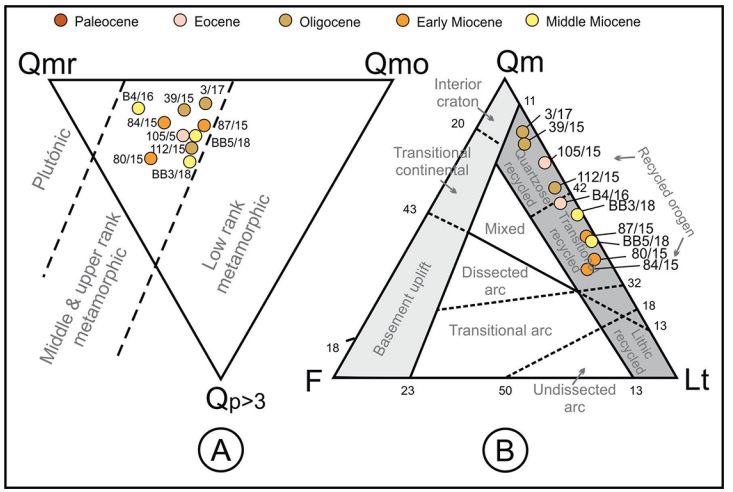

Figure 8. Sandstone provenance diagrams are shown. (A) Qmr/Qmo/Qp ternary diagram (Basu et al., 1975; Tortosa et al., 1991). Qmr—monocrystalline quartz, undulosity <5°; Qmo—monocrystalline quartz, undulosity >5°; Qp—polycrystalline quartz. (B) Qm/F/Lt ternary provenance discrimination diagram (Dickinson et al., 1983). Qm—monocrystalline quartz; F—feldspars (plagioclase and K-feldspars); Lt—lithic fragments (including carbonate extrabasinal clasts [CE]).

(Azdimousa et al., 2003; El Ouahabi et al., 2014); (2) Ill+Kln ± (I-S)+Sme and Ill+(I-S) ± Sme+Kln for Albian-Cenomanian marine formations with remarkable abundance of inherited palygorskite (up to 50% of the clay fraction) and kaolinite (Pletsch et al., 1996; Pletsch, 1997; El Ouahabi et al., 2014); and (3) Ill+(I-S) ± Sme (Maaté et al., 2017) and Ill+Sme ± (I-S)+Kln (Faleh and Sadiki, 2002) from Upper Cretaceous and Paleogene marine formations, respectively. The variable abundances of inherited chlorite from the Upper Jurassic to Lower Cretaceous; mixed layer I-S, kaolinite, and palygorskite from the Albian-Cenomanian; and smectite from the Upper Cretaceous and Paleogene allow us to deduce that there were changes in the supply from different source areas over time. Ternary plots for the main (end-members) whole-rock and clay-fraction mineral phases allow interpretation of how mineral assemblages from Logs 5 and 6 (Fig. 9) as mixtures in varying proportions of mineral assemblages from Jurassic to Paleogene source areas changed in time. So, mixtures varied in proportions of mineral assemblages from Jurassic to Paleogene source areas from top to bottom in the series.

The Ill+(I-S) ± Sme clay-mineral association identified in the Ypresian, Lutetian, and Chattian successions in Log 5 are mostly derived from a mix of Upper Cretaceous to Paleogene terrains. In Log 6, the Ill+(I-S) ± Sme+Kln clay-mineral association identified in the Ypresian succession derives from the mixing of

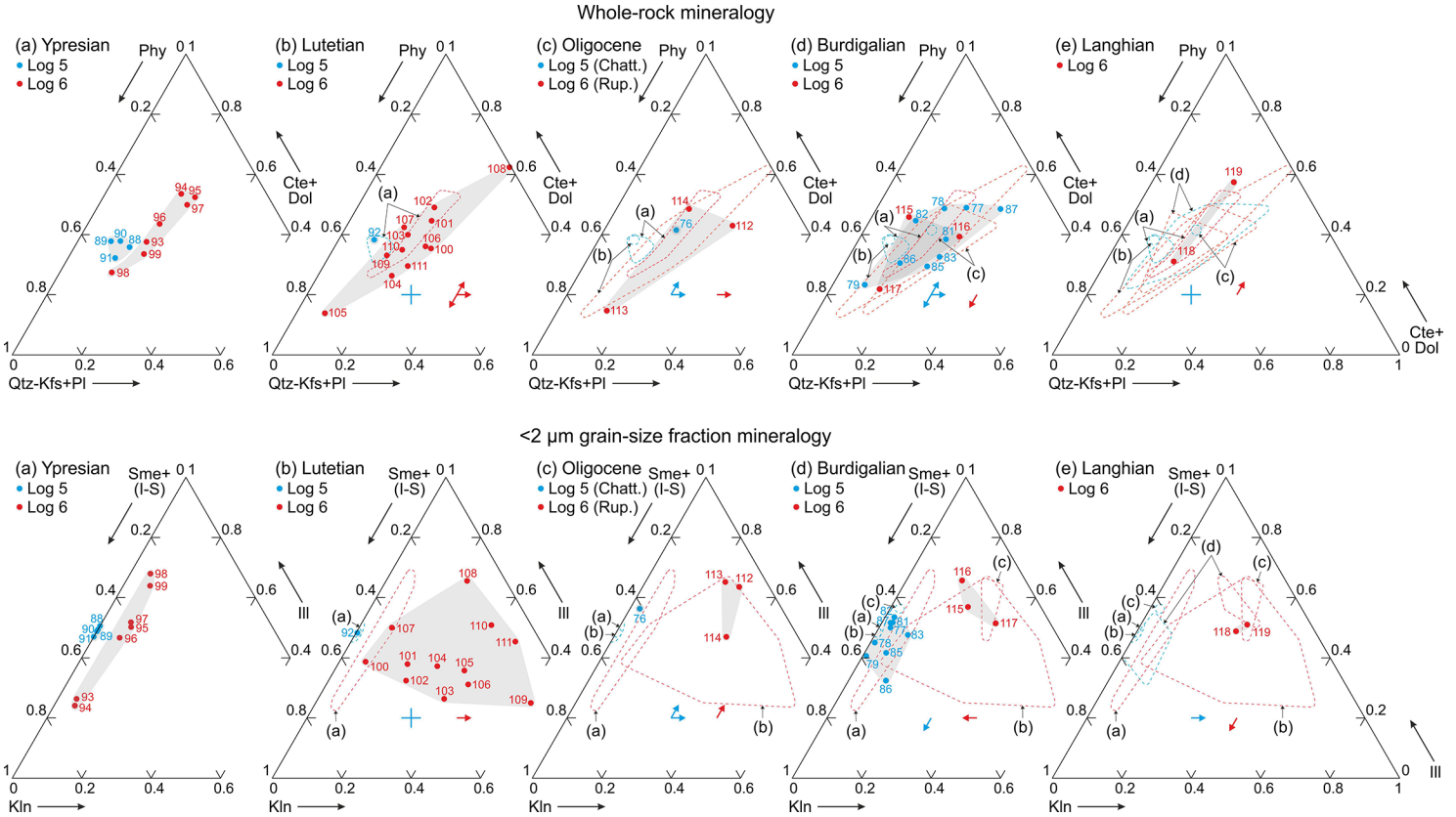

Figure 9. Ternary plots show whole-rock and clay-fraction mineralogical associations from Log 5 (Sidi Ameur [blue points and lines]) and Log 6 (Douar Ahel Chane [red points and lines]). Data are clustered by ages of sequences in each log: (A) Ypresian; (B) Lutetian; (C) Oligocene; (D) Burdigalian; (E) Langhian, as in Figure 7; sample number over data points is as in Table 6 (Qtz—quartz; Phy—phyllosilicates; Cte—calcite; Dol—dolomite; Kfs—K-feldspar; Pl—plagioclase; Sme—smectite; Ill—illite; I-S—mixed layer illite–smectite; Kln—kaolinite). Within plots (B–E), dotted lines show the mineralogical compositional field of former successions in relation to the plotted compositional field, and arrows show the evolution of the mineral assemblage of the plotted succession in relation to the previous plotted successions.

Albian–Cenomanian to Paleocene terrains. The Albian–Cenomanian supply was identified by the presence of mixed layer I-S, kaolinite, smectite, and palygorskite in samples from the Upper Cretaceous to Paleogene. The Ill+(I-S) ± Sme+Kln+Chl clay-mineral association identified in the Burdigalian succession in Logs 5 and 6 is interpreted to be derived from a mix of Upper Jurassic to Paleocene terrains. The source-area history described suggests a complex erosional evolution. Deposits were initially fed by erosion of Paleogene and Upper Cretaceous terrains, then by Albian–Cenomanian, Lower Cretaceous, and Upper Jurassic terrains, and finally by all of them in variable proportions. For Eocene to lower Miocene marine formations, the sediment supply is interpreted as derived from the External Rif. Maaté et al. (2017) and El Mourabet et al. (2018) described a similar Ill+(I-S) ± Sme+Kln clay-mineral association with the occasional presence of chlorite.

INTERPRETATIONS OF DIAGENESIS (POST-DEPOSITIONAL MODIFICATIONS)

In the petrographic samples, post-depositional modification during burial is evidenced by: (1) microsparitic and/or poikilotopic calcite cementation (Fig. 6D); (2) compaction manifested by mechanical deformation of ductile grains (carbonate grains and glauconite), fracturation of grains, and the presence of long and concave-convex boundaries between quartz grains (Figs. 6A and 6E); (3) corrosion (replaced by carbonates) of quartz and feldspar clasts (Fig. 6B); and (4) local clay pore-filling and replacement (epimatrix after feldspar).

In Log 5, the clay mineralogy samples for Cenozoic strata have: (1) dimensionless (S+K):I ratios of 0.50–0.54 (Ypresian), 0.51 (Lutetian), 0.38 (Chattian), and 0.19–1.40 (Burdigalian); (2) Qtz(100):Qtz(101) ratios of 0.23–0.38 (Ypresian), 0.38 (Lutetian), 0.20 (Chattian), and 0.19–0.32 (Burdigalian); (3) Sme(003):Sme(002) ratios of 0.86–0.97 (Ypresian), 0.82 (Lutetian), 0.86 (Chattian), and 0.78–1.09 (Burdigalian); and (4) Ill(002):Ill(001) ratios of 0.42–0.43 (Ypresian), 0.42 (Lutetian), 0.42 (Chattian), and 0.33–0.51 (Burdigalian) (Table 6 and Fig. 7). These values suggest variable amounts of authigenic (late Ypresian and Lutetian) and secondary quartz and dioctahedral and trioctahedral (Burdigalian) smectites. Only inherited illite was detected. In Log 6, the clay mineralogy samples for Cenozoic strata have (1) dimensionless (S+K):I ratios of 0.14–2.34 (Ypresian), 0.41–2.68 (Lutetian), 0.41–0.82 (Rupelian), 0.34–0.75 (Burdigalian), and 0.72 (Langhian); (2) Qtz(100):Qtz(101) ratios of 0.16–0.26 (Ypresian), 0.18–0.38 (Lutetian), 0.22–0.32 (Rupelian), 0.26–0.32 (Burdigalian), and 0.23 (Langhian); (3) Sme(003):Sme(002) ratios of 0.71–1.12 (Ypresian), 0.77–1.10 (Lutetian), 0.80–0.93 (Rupelian), 0.76–1.06 (Burdigalian), and 0.98 (Langhian); and (4) Ill(002):Ill(001) ratios of 0.27–0.48 (Ypresian), 0.25–0.45 (Lutetian), 0.31–0.36 (Rupelian), 0.30–0.34 (Burdigalian), and 0.34 (Langhian). These values suggest variable amounts of authigenic (four samples in Lutetian, Rupelian, and Burdigalian) and secondary quartz, dioctahedral and trioctahedral (seven samples in Ypresian, Lutetian, and Burdigalian) smectites, and inherited and mature (one sample in late Ypresian and five in Lutetian) illite.

In Log 6, the identification of authigenic illite in late Ypresian and Lutetian could suggest incipient low-grade (burial) metamorphism (anchizone) (Nieto et al., 1996). However, the presence of smectite and random mixed layer I-S in all samples in Logs 5 and 6 restrict this range to weak burial diagenesis at most, as suggested in the literature (Nadeau and Bain, 1986; Gingele et al., 1998; Liu et al., 2008; Lanson et al., 2009; Moiroud et al., 2012; Alcalá et al., 2013a, 2013b). The Sme(003):Sme(002) values suggest (Hunziker, 1986; Drits et al., 1997; Moiroud et al., 2012) variable mixing of inherited Mg-rich phases (dioctahedral) like montmorillonite and beidellite (ratios < 1) and Al-rich phases (trioctahedral) like nontronite and saponite (ratios > 1). The Ill(002):Ill(001) ratios below 0.30 are attributed to mature illite under weak burial diagenesis, at most, while values higher than 0.30 identify inherited micas from low-grade metamorphic terrains; the former were identified only in some samples in Log 6. The Qtz(001)/Qtz(101) ratios lower and higher than 0.30 identify secondary and authigenic quartz, respectively (Table 6 and Fig. 7).

DISCUSSION

The data presented above allow an improved understanding of the sequence stratigraphy, depositional environments, and reconstruction of sediments source areas. Moreover, some correlations beyond the study area have been proposed (the Betic External Zones and the Tunisian Tell). This study also provides new insights into the hydrocarbon potential of the area.

Unconformities and Sequence Stratigraphy

Two major unconformities marked by abrupt lithologic changes and biostratigraphic gaps were recognized in all of the logs. The oldest gap (Fig. 10) observed in almost all of the logs extends from latest Cretaceous (Maastrichtian *p.p.*) to earliest Eocene (Ypresian *p.p.*); in Log 7, this gap begins in the early Paleocene *p.p.* The second gap (Fig. 10) extends, also in a variable way, across the Eocene-Oligocene boundary. Minor unconformities and their correlated conformities in some parts of the basin were also recognized. In particular, two minor unconformities (not observed in Log 6 and in the Cenozoic succession from the External Tanger-Ketama Tectonic Unit; Fig. 10) marking the late Oligocene *p.p.*–Burdigalian *p.p.* and across the Burdigalian–Langhian boundary (Fig. 10) were defined. On the basis of the major unconformities, the Cenozoic strata can be subdivided into the following three stratigraphic sequences: (1) lower Paleocene (Danian *p.p.*) strata that are present only in Log 7; (2) Eocene (lower Ypresian–lower Bartonian *p.p.*) strata; (3) Oligocene–Miocene (lower Rupelian–lower Serravallian *p.p.*) strata. The Oligocene–Miocene stratigraphic strata are divided by two minor unconformities that mark gaps extending from upper Oligocene (Chattian *p.p.*) to lower Miocene (Burdigalian *p.p.*) and across the lower–middle Miocene (Burdigalian–Langhian) boundary. These two unconformities separate the following three minor stratigraphic sequences:

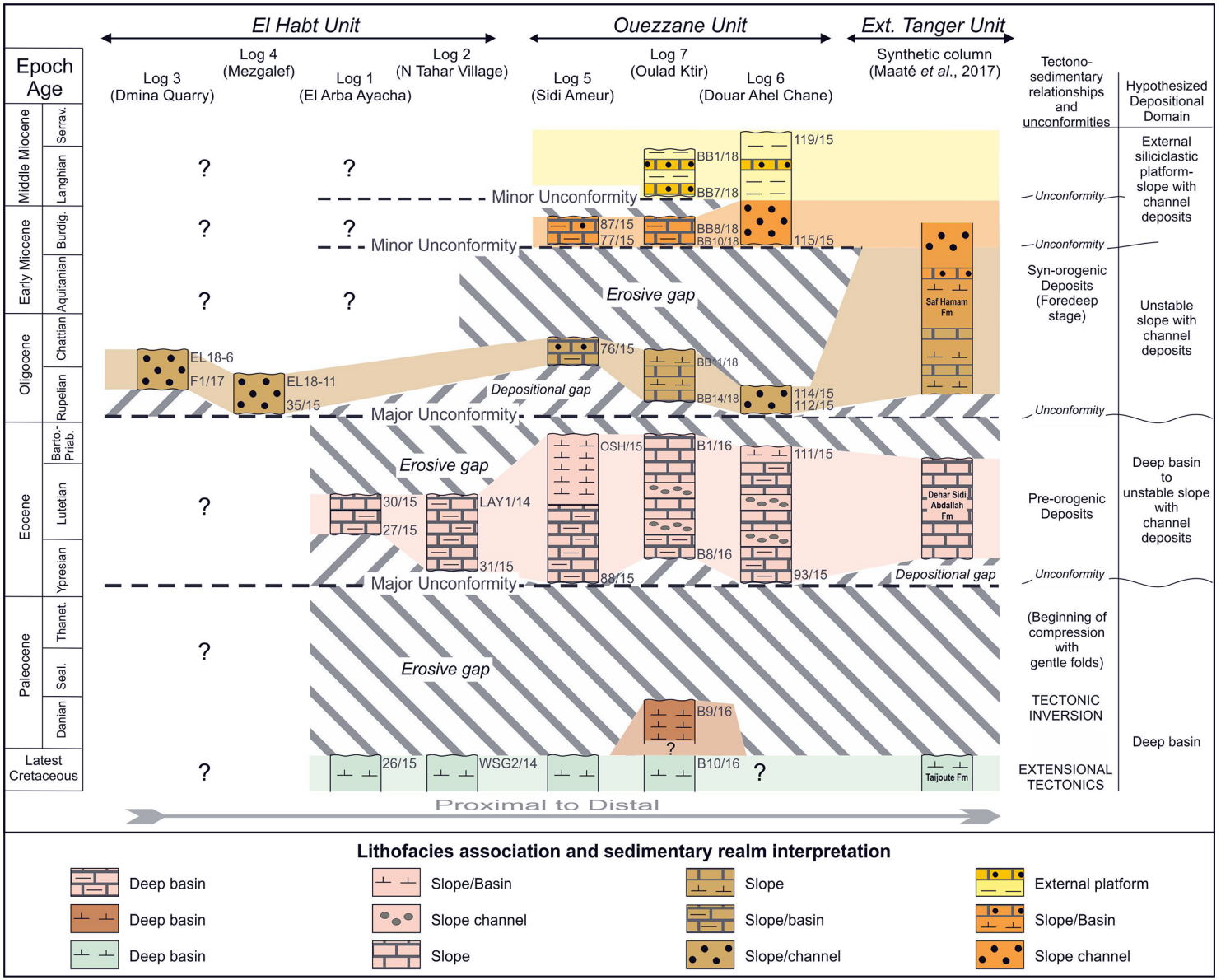

Figure 10. Sequences, vertical and lateral variations, and depositional environments resulting from the stratigraphic architecture are shown. Stratigraphic gaps (unconformities) are interpreted as non-depositional and/or erosive phases. The upward trends of facies are also indicated. External Tanger Unit synthetic column and tectono-sedimentary evolution are based on Maaté et al. (2017).

(3a) Oligocene (lower Rupelian–upper Chattian *p.p.*) strata; (3b) lower Miocene (Burdigalian *p.p.*) strata; (3c) middle Miocene (Langhian–Serravallian *p.p.*) strata.

The unconformities are interpreted (Fig. 10) as having been caused by erosion related to relative sea-level fall or by non-deposition over structural highs (paleo-reliefs) during relative sea-level rise. The origin of these relative sea-level changes is thought to have been controlled primarily by tectonics, although climate cannot be discarded (see below). Works in the Saharan area (Swezey, 2009) and in other African sectors (Carena et al., 2019) studied the hiatus during the Cenozoic in the African continent. In the case of the Cretaceous–Cenozoic boundary, a global warming event (Paleocene–Eocene thermal maximum) is suggested (Carena et al., 2019). This warming should be reflected in sedimentation in a deepening with an absence of unconformities. Nevertheless, we found practically an absence of Paleocene strata that should have been controlled by tectonics. Only an extreme warming such as the Messinian desiccation could provoke an erosive unconformity that is climatically controlled, but this is not the case during the Paleogene. In the case of the Oligocene period, the generalized absence or reduction of strata is also asserted (Swezey, 2009; Carena et al., 2019). This period belongs to a generalized sea-level fall due to global cooling during the build-up of the Antarctica ice sheet (Carena et al., 2019) but also results from an uplifting of part of the African continent caused by rapid seafloor spreading in the South Atlantic that led to the rotation and northward movement of Africa (Carena et al., 2019). In the case of the Miocene, a sea-level rise was probably accompanied by continuous sedimentation (Swezey, 2009). Nevertheless, a main (Burdigalian–Langhian boundary) and a secondary (Aquitanian-Burdigalian boundary) unconformity have been recognized in our study area that are probably related to local tectonics.

The synthetic column of the Cenozoic succession from the External Tanger-Ketama Tectonic Unit and the tectono-sedimentary evolution presented in Figure 10 are based on Maaté et al. (2017). It is accepted in literature that the tectonic inversion from extension to compression in the Alpine domains took place in the latest Cretaceous (Martín-Martín et al., 2020a, 2020b; Guerrera et al., 2021, and references therein). Also, it is accepted that the foredeep stage of the Maghrebian Flysch Basin began with the generalized terrigenous supply from Oligocene time onward. This is the so called neo-Alpine phase (Martín-Martín et al., 2020a, 2020b; Guerrera et al., 2021), when turbidites, slumps, and chaotic intervals are also seen in all of our studied sections. Evidence of Eocene tectonics recorded in the sedimentation is also accepted in the literature (Martín-Martín et al., 2020a, 2020b; Guerrera et al., 2021) and is linked to the neo-Alpine phase that affected mainly the internal zones of the peri-Mediterranean chains (Betic, Rif, Tell, and Apennines), the Pyrenees, or the Alps.

Stratigraphic Correlations Beyond the Immediate Study Area

Figure 11 shows a paleogeographic sketch map that differentiates oceanic and continental domains based on Scheibner and Speijer (2008) and Müller et al. (2018) at the Late Cretaceous period. Some inferences can be made when the Cenozoic stratigraphic record of the units studied (El Habt and Ouezzane Tectonic Units from the Intrarif: Fig 11, Logs 1–7) is compared with the Cenozoic succession from the External Tanger-Ketama Tectonic Unit (Internal Intrarif: Fig 11, Log 8), with the External Betic Zone (SE Spain: Fig 11, Log 9), and with the external portion of the Maghrebian Flysch Basin of the Tunisian Tell (Fig. 11, Log 10), especially because all of these areas have been studied using a similar methodology (Guerrera et al., 2006, 2014; Belayouni et al., 2012, 2013; Maaté et al., 2017; Martín-Martín et al., 2018).

In fact, in the case of the Cenozoic succession from the External Tanger-Ketama Tectonic Unit (Fig 11, Log 8), a Paleocene unconformity is also present in the Intrarif (Maaté et al., 2017). The Eocene stratigraphic sequence is well represented with the same facies (siliceous limestone sometimes), which is thus a good marker in most of the sections of the Intrarif. This widespread Eocene siliceous level, although diagenetic, implies extensive high silica content in the seawater in this period. In contrast, the Oligocene *p.p.*–Miocene *p.p.* strata of the External Tanger Tectonic Unit show continuous sedimentation but with similar lithofacies (marl, marly limestones, and sandstone) described in

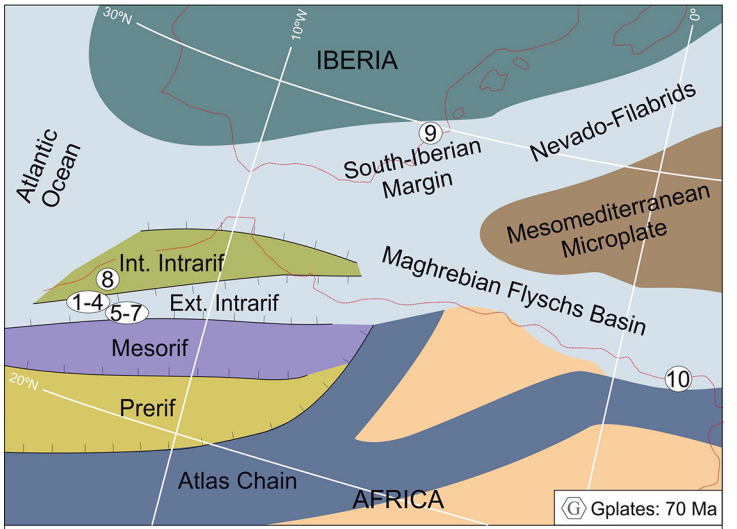

Figure 11. Paleogeographic sketch map of the Late Cretaceous generated with GPlates software (based on Scheibner and Speijer, 2008, and Müller et al., 2018). Locations of Logs 1–7 and the sectors studied are shown. External Tanger Unit (8) is after Maaté et al. (2017); eastern External Betic Zone (9) is after Guerrera et al. (2006, 2014) and Martín-Martín et al. (2018), and the northern Tunisian Tell (10) is after Belayouni et al. (2012, 2013).

Maaté et al. (2017). This latest continuity in the Oligocene–Miocene sedimentation could be related to the original paleogeographic position of the Cenozoic succession from the External Tanger-Ketama Tectonic Unit in a more distal, deep position that was unaffected by this unconformity.

Studies in other Moroccan External Rif (Asebriy, 1984, 1994; Asebriy et al., 2003) and Saharan areas (Swezey, 2009; Adnet et al., 2010) have found evidence of similar sedimentary evolution (carbonate platform development), which allows us to propose middle–late Eocene global warming as the main control on sedimentation. Also, studies in the African continent allow us to propose episodes of climatic and tectonic (continent rising since Eocene times) interference as controls on sedimentary evolution and the development of unconformities (Burke and Wilkinson, 2016; Carena et al., 2019). According to these authors, a tectonic rise took place in the African continent that could have affected sedimentation at the margins.

During the last several years, several studies on the eastern side (Murcia and Alicante Provinces) of the External Betic Zone (S Spain: Fig. 11, Log 9) have been published by Guerrera et al. (2006, 2014, 2021). These studies found an unconformity (hiatus) that affected the Paleocene *p.p.* at the beginning of the Eocene. Moreover, diffused olistostrome deposits were described in the Eocene and Oligocene strata. These unconformities and olistostrome deposits were related to syn-sedimentary tectonics and the break-up and dismantling of lands that emerged (Guerrera et al., 2006, 2014, 2021; Martín-Martín et al., 2018). This tectonic scenario has been related to compressive conditions due to the convergence of Africa, Iberia, and Europe in the westernmost Tethys domain, while at the same time the Iberian Range and Pyrenean Belt formed (Martín-Martín et al., 2001, and references therein).

When comparing the area studied in Morocco with the Tunisian Tell (Fig. 11, Log 10), similar stratigraphic architecture was described by Melki et al. (2011), Belayouni et al. (2012, 2013), Bejaoui et al. (2017), and Messadi et al. (2019). In this case, the main difference corresponds to the absence in Tunisia of unconformities across the Cretaceous/Paleocene and Paleocene/Eocene boundaries, and the sedimentation observations suggest continuous sediment accumulation (Swezey, 2009). Eocene siliceous limestones and Oligocene–Miocene siliciclastic strata are also described in the Tunisian Tell (Swezey, 2009; Belayouni et al., 2012, 2013).

This stratigraphy and sedimentation patterns are recognized not only in the Rif (this work), the Tell, and Betic Cordillera but also at the scale of the entire Tethys realm and continental areas (Jolivet et al., 2016; Gimeno-Vives et al., 2020). The important point is that in the case of the Intrarif, we are not in an intra-continental basin along a margin but in an oceanic domain. It's remarkable to verify that the oceanic domain also recorded the "tectonic events" that are well registered in the fringing continents.

The data in this paper and the other published data (e.g., Swezey, 2009; Adnet et al., 2010; Melki et al., 2011; Burke and Wilkinson, 2016; Bejaoui et al., 2017; Carena et al., 2019) on the External Betic Zone, Tunisian Tell, and other African regions indicate that a paleogeographic reorganization of the external domains in the westernmost Tethys occurred after the Cretaceous. This reorganization would have caused unconformities and lateral variations of lithofacies and strata thicknesses. In some cases, as with the Eocene–Oligocene boundary, these changes could be enhanced by the occurrence of a generalized global sea-level fall due to climatic cooling and the growing of polar ice caps (Salamy and Zachos, 1999; Swezey, 2009). The equivalent effect (unconformities and lateral variations in lithofacies and stratal thicknesses) in other sectors (Betics and Tunisian Tells) have been interpreted as related to pre-nappe tectonics of basement soft folding (Guerrera et al., 2006, 2014; Belayouni et al., 2012, 2013). A possible interpretation is that these features could have been caused by the onset of tectonic inversion (from extensional to compressional), which was probably related to the neo–Alpine phase (Pyrenean) as the first moderate manifestation of the Africa/Europe convergence. The pre-nappe tectonics could be characterized by thick-skinned, basement-controlled folds and blind thrusts that led to the end of pre-orogenic sediment accumulation, which is similar to the hypothesis proposed for the Tunisian Tell (Belayouni et al., 2012) for the External Betic Cordillera (Guerrera et al., 2006, 2014) and for the whole Maghrebian Chain (Frizon de Lamotte et al., 2006).

Implications for Petroleum System in Morocco

Although hydrocarbon exploration is very limited in the External Rif Zone, there is significant evidence that the key components of hydrocarbon source, maturation, reservoir presence, and trapping mechanisms are present to enable a successful petroleum system to be instituted. The challenge is that the paleogeographic and tectonic evolution is poorly understood and difficult to model.

The paleogeography of the region, at the juncture of the Atlantic and Tethyian seaways, supports the presence of a widely distributed and extensive high-quality petroleum source rock as a consequence of high sediment accumulation rates and high productivity zones of upwelling (Kuhnt and Wiedmann, 1995). This setting has led to the presence of the Cretaceous (Cenomanian and Turonian) petroleum source rocks in the Rif area (Kuhnt et al., 2001; Kolonic et al., 2002; Groune et al., 2013a, 2013b) and in particular within the Melloussa-Massylienne Nappe, the Internal Tanger, and the External Tanger-Ketama Tectonic Units of the Tanger-Tetouan-Chaouen area (Fig. 2). The widespread presence of this Upper Cretaceous source rock is substantiated by its occurrence further east in the western Tellian Domain of Algeria in the Oujda Basin (Fig. 1) (Arab et al., 2015). More speculative, but potentially of equal importance, are several Cenozoic petroleum source rocks and reservoirs present in northern Algeria (Arab et al., 2015). The difficulty with these intervals is that they are associated with the transition from a relatively predictable and regional depositional system to a more localized compressional margin associated with the Mediterranean Alpine Belts (Chalouan et al., 2008), which results in very variable gross depositional environments with changes occurring at a wavelength controlled by thrust sheet size rather than at the passive margin scale (Chalouan et al., 2008). The local timing of nappe development becomes

critical for determining the onset and distribution of flysch (sandstones and mudstones of deep marine turbidite origin) juxtaposed in close proximity to mudstones of deep marine pelagic origin. This superimposition of petroleum systems is well documented in northern Algeria (Arab et al., 2015) and results in a diverse range of kerogen types (Types II, III, and IV; Lüning et al., 2004; Groune et al., 2013a, 2013b, 2014) and reservoir intervals.

The generation, migration, and trapping mechanism of the petroleum system is also useful to consider in the context of the two phases of basin evolution. Current heat flow variations are variable and increase toward the north (Zarhloule et al., 2010), which reflects both the variations in crustal thickness and the inversion of the passive margin (Michard et al., 2008). This heat flow variability has an impact on regional hydrocarbon maturation, but the presence of individual thrust sheets and the timing of nappe emplacement, to a large extent, controls the maturation of source rocks in a more localized setting, in particular, in the potential sub-thrusts beneath the Melloussa-Massylienne and External Tanger-Ketama Nappes. Such variations may explain the local presence and maturation of bituminous marl and shale (Groune et al., 2013a, 2013b, 2014) but we caution against assuming that this maturation level is uniform across the basin. The impact of faulting on geothermal fluid circulation in the area will enhance maturation in areas of increased faulting (Sabri et al., 2019) and is particularly important where NE-oriented strike-slip faults may be conduits to mantle-derived, CO_2-rich fluids (Tassi et al., 2006).

The occurrence of nappe structures in the External Rif Zone leads to the potential presence of a variety of structural, stratigraphic, and combined hydrocarbon traps throughout the Upper Cretaceous and Cenozoic strata. In the literature, the Cenomanian–Turonian has been proposed as possible source rocks for Moroccan hydrocarbon (Groune et al., 2013a, 2013b, 2014). The architecture of the Intrarif Cenozoic strata described in this study supports a multilayer petroleum system comprised of fractured Eocene siliceous limestone and porous Oligocene–Miocene sandstone (arenite), conglomerate, and grain-supported limestone (grainstone-packstone) beds from the Intrarif. The mudstone and marl of late Eocene and middle Miocene (late Langhian) age could be good seal rocks. In some cases, the unconformity at the Eocene–Oligocene boundary could juxtapose both units across this contact. Moreover, there is a non-tabular stratigraphy with lateral changes in lithofacies, thickness, and diachronous boundaries, which could enhance the likelihood of a petroleum system because it provides the constituent components for such a system (source rocks, reservoir rocks, seal rocks, overburden rocks, trap formation, and generation migration-accumulation timing processes; Magoon and Dow, 1994) within the area.

Many stratigraphic similarities have been pointed out in recent times between the Tunisian Tell and the External Rif Zone (Maaté et al., 2017). In Tunisia (Beavington-Penney et al., 2008; Houatmia et al., 2015; Hezzi et al., 2015; Bédir et al., 2016; Njahi et al., 2017; Nadhem et al., 2017), similar Eocene and Oligocene–Miocene stratigraphic units (Cherahil, El Gueria, Ain Ghrb, Birsa, and Saouaf Formations) have been proposed as hydrocarbon reservoirs, and their source hydrocarbon rock is the Cretaceous strata (Hezzi et al., 2015). The Eocene Cherahil and El Gueria Formations are hydrocarbon systems composed of fractured limestone and porous nummulitic limestone, respectively. The Oligocene–Miocene Ain Ghrb, Birsa, and Saouaf Formations consist of deltaic porous sandstone and conglomerate. The Cherahil Formation (Njahi et al., 2017) consists of a multilayer calcareous system separated by marly, shaly, clay beds in which the unconformable Oligocene strata are considered the stratigraphic trap. The hydrocarbon system related to the El Gueria Formation (Beavington-Penney et al., 2008; Hezzi et al., 2015; Nadhem et al., 2017) is stratigraphically trapped by the marly-shaly Souar Formation. The Oligocene–Miocene Ain Ghrb, Birsa, and Saouaf Formations also consist of a multilayer detritic system separated by marly, shaly, clay beds. Structural traps (Hezzi et al., 2015) were also formed in this region during the Atlasic compression and folding phases during the Miocene (Chalouan et al., 2008). The impact of sediment recycling will further modify the quality of reservoirs. Some of these hydrocarbon traps and reservoir intervals have been tested and proven in the northern Algeria hydrocarbon reservoirs (Arab et al., 2015). Any such analysis of the petroleum system should also focus on establishing a critical events chart that would account for the timing of the formation of hydrocarbon source rocks and reservoir rocks but also incorporate the relative timing of maturation, trap formation, and unroofing events. These unroofing events may impact source rock maturation by increasing the maximum burial depth of source rock intervals and by modifying trap efficiency and integrity. These elements could only be accounted for by combining petroleum system modeling with structural restorations and unroofing/erosion estimates (e.g., from vitrinite reflectance and fission track analysis), which are beyond the scope of this study. Nevertheless, this paper concludes that there is the potential for a hydrocarbon system in the study area.

CONCLUSIONS

This study makes a new contribution to our understanding of the Cenozoic evolution of the Intrarif of the External Rif Zone. The main results can be summarized as follows:

(1) The stratigraphic record of the El Habt and Ouezzane Tectonic Units belonging to the Intrarif (Rif, Morocco) was documented. An Upper Cretaceous to Miocene succession (dated with planktonic foraminifera and calcareous nannoplankton) of marine strata was deposited in basinal, slope, and upper slope environments.

(2) The biostratigraphic analysis provided evidence of two major unconformities marked by significant biostratigraphic gaps. The oldest extends from Maastrichtian *p.p.* (or from the Danian *p.p.*) to Ypresian *p.p.* A reduced lower Paleocene (Danian *p.p.)* interval resting on Cretaceous strata is observed only in the case of the Oulad Ktir area (Log 7). Our data indicate that a reduced gap across the K/T boundary is not negligible (Fig. 10). The second main unconformity extends across the Eocene–Oligocene boundary. Two minor unconformities were also

detected that mark the time span from late Oligocene *p.p.* to Burdigalian *p.p.* and are located across the Burdigalian–Langhian boundary, respectively.

(3) On the basis of the recognized major unconformities, the following main stratigraphic sequences were proposed: (1) lower Paleocene (Danian *p.p.*), which was detected only in Log 7; (2) Eocene (lower Ypresian–lower Bartonian *p.p.*); and (3) lower Rupelian–lower Serravallian *p.p.* This last sequence is characterized by three minor stratigraphic sequences due to the recognition of two second-order unconformities: (3a) lower Rupelian–upper Chattian *p.p.*; (3b) Burdigalian *p.p.*; and (3c) Langhian-Serravallian *p.p.*

(4) On the basis of lithofacies associations, sedimentary structures, stacking patterns, shifting of realms, fossil associations, and mineral distribution, the following interpretations concerning reconstruction of the paleoenvironments were deduced: (1) the Upper Cretaceous–lower Paleocene strata accumulated in a deep basin; (2) the lower Eocene p.p.–upper Eocene p.p. strata accumulated in a deep basin to slope realm with channelized areas; (3) the Oligocene *p.p.* strata may have accumulated on an unstable slope, furrowed by channels, that evolved into an external siliciclastic platform; and (4) the lower–middle Miocene (Burdigalian *p.p.*-Langhian) strata (divided by a minor unconformity into two minor stratigraphic sequences) probably accumulated in a deep basin and slope (with channels) that evolved into a platform realm.

(5) The Cenozoic strata are arranged into shallowing-upward intervals; meanwhile, the gaps (unconformities) are interpreted as having formed by erosion due to relative sea-level falls. The entire Cenozoic strata shows a major shallowing-upward trend.

(6) The petrofacies of the source terrains identified belong to middle-upper rank metamorphic and sedimentary rocks derived from "recycled orogen" (transitional recycled and quartzose recycled sub-types). The clay-mineral associations indicate a complex erosional evolution with a Paleogene and Upper Cretaceous terrain initial source area, followed by Albian–Cenomanian, Lower Cretaceous, and Upper Jurassic terrains, and finally a terrain with all of them in variable amounts.

(7) Our data and published data on the External Betic Zone and Tunisian Tell indicate a paleogeographic reorganization after the Cretaceous of the external domains in the westernmost Tethys with the diversification of facies, evidence of syn-sedimentary tectonics, and the appearance of hiatus in the sedimentation. A possible interpretation could be the onset of the tectonic inversion (from extensional to compressional), which is probably related to the neo-Alpine phase (Pyrenean) as the first moderate manifestation of the Africa/Europe convergence.

(8) The Cenozoic tectono-sedimentary evolution reconstructed in the External Rif Chain can be correlated with other sectors of the African (Tunisian-Algerian Tell) and Iberian (Betic Cordillera) Plates.

(9) The existence of Cretaceous oil source rocks in the area examined is well documented in the literature. Our results suggest that fractured Eocene strata (limestone and siliceous limestone) and porous Oligocene–Miocene strata (grain-supported limestone, sandstone, and conglomerate) may be possible hydrocarbon reservoirs.

ACKNOWLEDGMENTS

This research was supported by Urbino University grants DiSPeA Ricerca Scientifica 2020 (to M. Tramontana), CGL2016–75679-P and PID2020–114381GB-I00, by the Spanish Ministry of Education (to M. Martín-Martín) and Science and Research Groups, and by the Generalitat Valenciana of Alicante University (CTMA-IGA). Valuable comments and suggestions from three anonymous reviewers and Frizon de Lamotte are greatly appreciated.

REFERENCES CITED

Adnet, S., Cappetta, H., and Tabuce, R., 2010, A middle–late Eocene vertebrate fauna (marine fish and mammals) from southwestern Morocco; preliminary report: Age and palaeobiogeographical implications: Geological Magazine, v. 147, no. 6, p. 860–870, https://doi.org/10.1017/S0016756810000348.

Alcalá, F.J., Guerrera, F., Martín-Martín, M., Raffaelli, G., and Serrano, F., 2013a, Geodynamic implications derived from Numidian-like distal turbidites deposited along the Internal-External Domain Boundary of the Betic Cordillera (S. Spain): Terra Nova, v. 25, p. 119–129, https://doi.org/10.1111/ter.12014.

Alcalá, F.J., López-Galindo, A., and Martín-Martín, M., 2013b, Clay mineralogy as a tool for integrated sequence stratigraphic and palaeogeographic reconstructions: Late Oligocene-Early Aquitanian Western Internal South Iberian Margin, Spain: Geological Journal, v. 48, p. 363–375, https://doi.org/10.1002/gj.2451.

Arab, M., Bracène, R., Roure, F., Samy-Zazoun, R., Mahdhoub, Y., and Badji, R., 2015, Source rocks and related petroleum system of Chelif Basin (Western Tellian Domain, Algeria): Marine and Petroleum Geology, v. 64, p. 363–385, https://doi.org/10.1016/j.marpetgeo.2015.03.017.

Asebriy, L., 1984, Etude géologique de la zone subrifaine: Nouvelle interprétation paléogéographique et structurale du Rif externe; exemple du Moyen Ouerrha, Maroc [Ph.D. thesis]: Rabat, Morocco, University of Rabat, 187 p.

Asebriy, L., 1994, Evolution tectonique et métamorphique du Rif central (Maroc): Définition du domaine Subrifain [Ph.D. thesis]: Rabat, Morocco, University of Rabat, 248 p.

Asebriy, L., and Cherkaoui, T.E., 1995, Tectonique cassante et sismotectonique dans le Rif et son avant-pays (Maroc): Africa Geoscience Review, v. 2, no. 1, p. 141–149.

Asebriy, L., de Luca, P., Bourgois, J., and Chotin, P., 1987, Resédimentation d'âge sénonien dans le Rif central (Maroc): Conséquences sur les divisions paléogéographiques et structurales de la chaîne: Journal of African Earth Sciences, v. 6, p. 917.

Asebriy, L., Azdimousa, A., and Bourgois, J., 2003, Structure du Rif externe sur la transversale du Massif de Ketama: Rabat, Morocco, Travaux de l'Institut Scientifique, v. 21, p. 27–46.

Azdimousa, A., Bourgois, J., Poupeau, G., and Montigny, R., 1998, Histoire thermique du massif de Kétama (Maroc): sa place en Afrique du Nord et dans les Cordillères bétiques: Comptes Rendus de l'Académie des Sciences, v. 326, p. 847–853, https://doi.org/10.1016/S1251-8050(98)80023-2.

Azdimousa, A., Bourgois, J., Asebriy, L., Poupeau, G., and Montigny, R., 2003, Histoire thermique et surrection du Rif externe et des nappes de flyschs associées (Nord Maroc): Rabat, Morocco, Travaux Institute Scientifique Rabat, v. 21, p. 15–26.

Azdimousa, A., Jabaloy, A., Asebriy, L., Booth-Rea, G., González-Lodeiro, F., and Bourgois, J., 2007, Lithostratigraphy and structure of the Temsamane Unit (Eastern External Rif, Morocco): Revista de la Sociedad Geológica de España, v. 20, no. 3–4, p. 119–132.

Bargach, K., Ruano, P., Chabli, A., Galindo-Zaldivar, J., Chalouan, A., Jabaloy, A., Akil, M., Ahmamou, M., Sanz de Galdeano, C., and Benmakhlouf, M., 2004, Recent tectonic deformations and stresses in the frontal part of the Rif Cordillera and the Saïss Basin (Fes and Rabat regions, Morocco): Pure and Applied Geophysics, v. 161, no. 3, p. 521–540, https://doi.org/10.1007/s00024-003-2461-6.

Basu, A., Young, S.W., Suttner, L.J., James, W.C., and Mack, G.H., 1975, Re-evaluation of the use of undulatory extinction and polycrystallinity in detrital quartz for provenance interpretation: Journal of Sedimentary Petrology, v. 45, p. 873–882.

Beavington-Penney, S.J., Nadin, P., Wright, V.P., Clarke, E., McQuilken, J., and Bailey, H.W., 2008, Reservoir quality variation on an Eocene carbonate ramp, El Garia Formation, offshore

Tunisia: Structural control of burial corrosion and dolomitisation: Sedimentary Geology, v. 209, p. 42–57, https://doi.org/10.1016/j.sedgeo.2008.06.006.
Bédir, M., Arbi, A., Khomsi, S., Houatmia, F., and Naceur-Aissaoui, M., 2016, Seismic tectono-stratigraphy of fluvio-deltaic to deep marine Miocene silicoclastic hydrocarbon reservoir systems in the Gulf of Hammamet, northeastern Tunisia: Arabian Journal of Geosciences, v. 9, p. 726, https://doi.org/10.1007/s12517-016-2745-7.
Bejaoui, H., Aïfa, T., Melki, F., and Zargouni, F., 2017, Structural evolution of Cenozoic basins in northeastern Tunisia, in response to sinistral strike-slip movement on the El Alia-Teboursouk Fault: Journal of African Earth Sciences, v. 134, p. 174–197, https://doi.org/10.1016/j.jafrearsci.2017.06.021.
Belayouni, H., Guerrera, F., Martín-Martín, M., and Serrano, F., 2012, Stratigraphic update of the Cenozoic Sub-Numidian formations of the Tunisian Tell (North Africa): Tectonic/sedimentary evolution and correlations along the Maghrebian Chain: Journal of African Earth Sciences, v. 64, p. 48–64, https://doi.org/10.1016/j.jafrearsci.2011.11.010.
Belayouni, H., Guerrera, F., Martín-Martín, M., and Serrano, F., 2013, Paleogeographic and geodynamic Miocene evolution of the Tunisian Tell (Numidian and Post-Numidian Successions): Bearing with the Maghrebian Chain: International Journal of Earth Sciences, v. 102, p. 831–855, https://doi.org/10.1007/s00531-012-0824-x.
Ben Yaïch, A., Hervouet, Y., and Duée, G., 1991, Les turbidites calcaires du passage jurassique-crétacé du Rif externe occidental (Maroc): Processsus et contrôle de dépôt: Bulletin de la Société Géologique de France, v. 162, p. 841–850, https://doi.org/10.2113/gssgfbull.162.5.841.
Berggren, W.A., and Pearson, P.P., 2005, A revised tropical to subtropical planktonic foraminiferal zonation of the Eocene and Oligocene: Journal of Foraminiferal Research, v. 35, p. 279–298, https://doi.org/10.2113/35.4.279.
Berggren, W.A., and Pearson, P.N., 2006, Tropical and subtropical planktonic foraminiferal zonation of the Eocene and Oligocene, *in* Pearson, P.N., Olsson, R.K., Huber, B.T., Hemleben, C., and Berggren, W.A., eds., Atlas of Eocene Planktonic Foraminifera: Cushman Foundation Special Publication, v. 41, p. 29–40.
Berggren, W.A., Kent, D.V., Swisher, C.C., and Aubry, M.-P., 1995, A revised Cenozoic geochronology and chronostratigraphy, *in* Berggren, W.A., et al., eds., Geochronology, Time-scales, and Global Stratigraphic Correlation: SEPM (Society for Sedimentary Geology) Special Publication 54, p. 129–212, https://doi.org/10.2110/pec.95.04.0129.
Biscaye, P.E., 1965, Mineralogy and sedimentation of recent deep sea clay in the Atlantic Ocean and adjacent seas and oceans: Geological Society of America Bulletin, v. 76, p. 803–832, https://doi.org/10.1130/0016-7606(1965)76[803:MASORD]2.0.CO;2.
Blow, W.H., 1969, Late middle Eocene to Recent planktonic foraminiferal biostratigraphy: Proceedings of the 1st International Conference on Planktonic Microfossils, Geneva, Switzerland, 1967, v. 1, p. 199–422.
Burke, K., and Wilkinson, M.J., 2016, Landscape evolution in Africa during the Cenozoic and Quaternary—The legacy and limitations of Lester C. King: Canadian Journal of Earth Sciences, v. 53, p. 1089–1102, https://doi.org/10.1139/cjes-2016-0099.
Carena, S., Bunge, H.-P., and Friedrich, A.M., 2019, Analysis of geological hiatus surfaces across Africa in the Cenozoic and implications for the timescales of convectively-maintained topography: Canadian Journal of Earth Sciences, v. 56, p. 1333–1346, https://doi.org/10.1139/cjes-2018-0329.
Cazzola, C., and Critelli, S., 1986, Litostratigrafia e petrografia delle quarzareniti torbiditiche oligomioceniche di Asilah (catena del Rif, Marocco Nord-Occidentale): Mineralogia Petrografia Acta, v. 30, p. 203–226.
Chalouan, A., and Michard, A., 2004, The Alpine rif belt (Morocco): A case of mountain building in a subduction-subduction-transform fault triple junction: Pure and Applied Geophysics, v. 161, p. 489–519, https://doi.org/10.1007/s00024-003-2460-7.
Chalouan, A., Michard, A., Feinberg, H., Montigny, R., and Saddiqi, O., 2001, The Rif Mountain building (Morocco): A new tectonic scenario: Bulletin de la Société Géologique de France, v. 172, p. 603–616, https://doi.org/10.2113/172.5.603.
Chalouan, A., Michard, A., El Kadiri, K.H., Frizon de Lamotte, D., Soto, J.I., and Saddiqi, O., 2008, Continental Evolution: The Geology of Morocco: Berlin Heidelberg, Springer-Verlag, Lecture Notes Earth Sciences, v. 116, p. 203–302, https://doi.org/10.1007/978-3-540-77076-3_5.
Coward, M.P., and Ries, A.C., 2003, Tectonic development of North African basins, *in* Arthur, T.J., Macgregor, D.S., and Cameron, N.R., eds., Petroleum Geology of Africa: Geological Society, London, Special Publication 207, p. 61–83.
Critelli, S., 1985/1986, Provenienza delle torbiditi oligo-mioceniche del dominio esterno e della falda Numidica del Rif (Marocco nord-occidentale): Calabria, Italia, Tesi Università della Calabria, 128 p.
Critelli, S., Muto, F., Perri, F., and Tripodi, V., 2017, Interpreting provenance relations from sandstone detrital modes, southern Italy foreland region: Stratigraphic record of the Miocene tectonic evolution: Marine and Petroleum Geology, v. 87, p. 47–59, https://doi.org/10.1016/j.marpetgeo.2017.01.026.
Dickinson, W.R., 1970, Interpreting detrital modes of greywacke and arkose: Journal of Sedimentary Petrology, v. 40, p. 695–707.
Dickinson, W.R., Beard, L.R., Brakenridge, G.R., Erjavec, J.L., Ferguson, R.C., Inman, K.F., Knepp, R.A., Lindberg, F.A., and Ryberg, P.T., 1983, Provenance of North American Phanerozoic sandstones in relation to tectonic setting: Geological Society of America Bulletin, v. 94, p. 222–235, https://doi.org/10.1130/0016-7606(1983)94<222:PONAPS>2.0.CO;2.
Didon, J., and Hoyez, B., 1978, Les séries à faciès mixtes, numidien et gréso-micacé, dans le Rif occidental (Maroc): Comptes Rendus Sommaire de la Societé Géologique de France, v. 6, p. 304–307.
Di Stefano, A., Foresi, L.M., Lirer, F., Iaccarino, S.M., Turco, E., Amore, F.O., Morabito, S., Salvatorini, G., Mazzei, R., and Abdul Aziz, H., 2008, Calcareous plankton high resolution bio-magnetostratigraphy for the Langhian of the Mediterranean area: Rivista Italiana di Paleontologia e Stratigrafia, v. 114, p. 51–76.
Doglioni, C., 1992, Main differences between thrust belts: Terra Nova, v. 4, p. 152–164, https://doi.org/10.1111/j.1365-3121.1992.tb00466.x.
Doglioni, C., Mongelli, F., and Pialli, G., 1998, Boudinage of the Alpine belt in the Apenninic back-arc: Memorie della Societa Geologica Italiana, v. 52, p. 457–468.
Doglioni, C., Fernandez, M., Gueguen, E., and Sabat, F., 1999, On the interference between the early Apennines-Maghrebides back-arc extension and the Alps-Betics orogen in the Neogene geodynamics of the Western Mediterranean: Bollettino della Società Geologica Italiana, v. 118, p. 75–89.
Drits, V.A., Sakharov, B.A., Lindgreen, H., and Salyn, A., 1997, Sequential structure transformation of illite-smectite-vermiculite during diagenesis of Upper Jurassic shales from the North Sea and Denmark: Clay Minerals, v. 32, p. 351–371, https://doi.org/10.1180/claymin.1997.032.3.03.
Dunham, R.J., 1962, Classification of carbonate rocks according to depositional texture, *in* Ham, W.E. ed., Classification of Carbonate Rocks—A Symposium: American Association of Petroleum Geologists Memoir 1, p. 108–121.
Durand Delga, M., 1972, La courbure de Gibraltar, extrémité occidentale des chaînes alpines, unit l'Europe et l'Afrique: Eclogae Geologicae Helvetiae, v. 65, no. 2, p. 267–278.
Durand Delga, M., Rossi, P., Olivier, P., and Puglisi, D., 2000, Situation structurale et nature ophiolitique des roches basiques jurassiques associées aux flysch maghrébins du Rif (Maroc) et de Sicile (Italie): Comptes Rendus de l'Académie des Sciences, v. 331, p. 29–38, https://doi.org/10.1016/S1251-8050(00)01378-1.
El Mourabet, M., Barakat, A., Zaghloul, M.N., and El Baghdadi, M., 2018, Geochemistry of the Miocene Zoumi flysch thrust-top basin (External Rif, Morocco): New constraints on source area weathering, recycling processes, and paleoclimate conditions: Arabian Journal of Geosciences, v. 11, p. 126, https://doi.org/10.1007/s12517-018-3465-y.
El Mrihi, A., Chaluan, A., and Michard, A., 2004, Deformation style and kinematics of Mauretanian flysch-nappe: Northwestern Rif Belt, Morocco: 32nd International Geological Congress, abstract 32, p. 770.
El Ouahabi, M., Daoudi, L., and Fagel, N., 2014, Mineralogical and geotechnical characterization of clays from northern Morocco for their potential use in the ceramic industry: Clay Minerals, v. 49, p. 35–51, https://doi.org/10.1180/claymin.2014.049.1.04.
Embry, A.F., and Klovan, J.E., 1971, A Late Devonian reef tract on Northeastern Banks Island, NWT: Canadian Petroleum Geology Bulletin, v. 19, p. 730–781.
Eslinger, E., Mayer, L., Durst, T., Hower, J., and Savin, S., 1973, A X-ray technique for distinguishing between detrital and secondary quartz in the fine grained fraction of sedimentary rocks: Journal of Sedimentary Petrology, v. 43, p. 540–543.
Esquevin, J., 1969, Influence de la composition chimique des illites sur la cristallinité: Bulletin Centre Recherche. Pau, Société Nationale des Pétroles d'Aquitaine, v. 3, p. 147–154.
Faleh, A., and Sadiki, A., 2002, Glissement rotationnel de Dhar El Harrag: Exemple d'instabilité de terrain dans le Prérif central (Maroc): Bulletin de l'Institut Scientifique Rabat, v. 24, p. 41–48.
Folk, R.L., 1951, A comparison chart for visual percentage estimation: Journal of Sedimentary Petrology, v. 21, no. 1, p. 32–33.
Folk, R.L., 1980, Petrology of Sedimentary Rocks: Austin, Texas, USA, Hemphill Publishing Company, 184 p.
Fontana, D., Zuffa, G.G., and Garzanti, E., 1989, The interaction of eustasy and tectonism from provenance studies of the Eocene Hecho Group turbidite complex (South-Central Pyreneees, Spain): Basin Research, v. 2, p. 223–237, https://doi.org/10.1111/j.1365-2117.1989.tb00037.x.

Frizon de Lamotte, D., Andrieux, J., and Guezou, J.C., 1991, Cinématique des chevauchements néogènes dans l'Arc bético-rifain: Discussion sur les modèles géodynamiques: Bulletin de la Société Géologique de France, v. 162, no. 4, p. 611–626, https://doi.org/10.2113/gssgfbull.162.4.611.

Frizon de Lamotte, D., Michard, A., and Saddiqi, O., 2006, Quelques développements recent sur la géodynamique du Maghreb: Comptes Rendus Geoscience, v. 338, p. 1–10, https://doi.org/10.1016/j.crte.2005.11.006.

Frizon de Lamotte, D., Zaghloul, M.N., Faouziya, H., Mohn, G., Leprêtre, R., Gimeno-Vives, O., Atouabat, A., El Mourabet, M., and Abass, A., 2017, Rif externe: Comment comprendre et expliquer le chaos apparent?: Géologues, v. 194, p. 13–15.

Gazzi, P., 1966, Le arenarie del flysch supracretaceo dell'Appennino modenese; correlazioni con il flysch di Monghidoro: Mineralogia e Petrografia Acta, v. 12, p. 69–97.

Gimeno-Vives, O., Frizon de Lamotte, D., Leprêtre, R., Haissen, F., Atouabat, A., and Mohn, G., 2020, The structure of the Central-Eastern External Rif (Morocco); Poly-phased deformation and role of the under-thrusting of the North-West African paleo-margin: Earth-Science Reviews, v. 205, no. 103198, https://doi.org/10.1016/j.earscirev.2020.103198.

Gingele, F.X., Müller, P.M., and Schneider, R.R., 1998, Orbital forcing of freshwater input in the Zaire Fan area—clay mineral evidence from the last 200 kyr: Palaeogeography, Palaeoclimatology, Palaeoecology, v. 138, p. 17–26, https://doi.org/10.1016/S0031-0182(97)00121-1.

González Donoso, J.M., Linares, D., Molina, E., Serrano, F., and Vera, J.A., 1982, Sobre la edad de la Formación de La Viñuela (Cordilleras Béticas, provincia de Málaga): Boletin de la Real Sociedad Española Historia Natural (Geología), v. 80, p. 255–275.

Groune, K., Halim, M., Benmakhlouf, M., Arsalane, S., Lemée, L., and Amblés, A., 2013a, Organic geochemical and mineralogical characterization of the Moroccan Rif bituminous rocks: Journal of Materials and Environmental Science, v. 4, no. 4, p. 472–481.

Groune, K., Halim, M., and Arsalane, S., 2013b, Thermal and mineralogical studies of Moroccan Rif bituminous rocks: Oil Shale, v. 30, no. 4, p. 536–549, https://doi.org/10.3176/oil.2013.4.06.

Groune, K., Halim, M., Lemée, L., Benmakhlouf, M., and Amblés, A., 2014, Chromatographic study of the organic matter from Moroccan Rif bituminous rocks: Arabian Journal of Chemistry, https://doi.org/10.1016/ j.arabjc.2014.10.019.

Guerrera, F., and Martín-Martín, M., 2014, Geodynamic events reconstructed in the Betic, Maghrebian, and Apennine chains (central-western Tethys): Bulletin de la Société Géologique de France, v. 185, no. 5, p. 329–341, https://doi.org/10.2113/gssgfbull.185.5.329.

Guerrera, F., Martin-Algarra, A., and Perrone, V., 1993, Late Oligocene–Miocene syn- /-late-orogenic successions in Western and Central Mediterranean Chains from the Betic Cordillera to the Southern Apennines: Terra Nova, v. 5, p. 525–544, https://doi.org/10.1111/j.1365-3121.1993.tb00302.x.

Guerrera, F., Martín-Martín, M., Perrone, V., and Tramontana, M., 2005, Tectono-sedimentary evolution of the southern branch of the Western Tethys (Magrebian Flysch Basin and Lucanian Ocean): Terra Nova, v. 17, p. 358–367, https://doi.org/10.1111/j.1365-3121.2005.00621.x.

Guerrera, F., Estévez, A., López-Arcos, M., Martín-Martín, M., Martín-Pérez, J.A., and Serrano, F., 2006, Paleogene tectono-sedimentary evolution of the Alicante trough (external Betic zone, SE Spain) and its bearing in the timing of deformation of the sud-Iberian Margin. Geodinamica Acta, v. 19, no. 2, p. 87–101, https://doi.org/10.3166/ga.19.87-101.

Guerrera, F., Mancheño, M.A., Martín-Martín, M., Raffaelli, G., Rodríguez-Estrella, T., and Serrano, F., 2014, Paleogene evolution of the External Betic Zone and geodynamic implications: Geologica Acta, v. 12, no. 3, p. 171–192.

Guerrera, F., Martín-Martín, M., and Tramontana, M., 2021, Evolutionary geological models of the central-western peri-Mediterranean chains: A review: International Geology Review, v. 63, p. 65–86, https://doi.org/10.1080/00206814.2019.1706056.

Haq, B.U., 1971, Paleogene calcareous nannoflora, Part 4: Paleogenenannoplankton biostratigraphy and evolutionary rates in Cenozoic calcareous nannoplankton: Stockholm Contributions in Geology, v. 25, p. 129–158.

Hezzi, I., Aïfa, T., Khemiri, F., and Ghanmi, M., 2015, Seismic and well log post-Cretaceous reservoir correlations in the Sahel, east Tunisia: Arabian Journal of Geosciences, v. 8, p. 10031–10063, https://doi.org/10.1007/s12517-015-1886-4.

Holtzapffel, T., 1985, Les minéraux argileux: Préparation, analyse diffractométrique et determination: Société Géologique du Nord Publication no. 12, 136 p.

Hottinger, L., and Suter, G., 1962, La structure de la zone prérifaine au Sud du Moyen Ouerrha: Comptes rendus de l'Académie des Sciences, v. 254, série D, p. 140 -142.

Houatmia, F., Khonsi, S., and Bédir, M., 2015, Oligo-Miocene reservoir sequence characterization and structuring in the Sisseb El Alem–Kalaa Kebira regions (Northeastern Tunisia): Journal of African Earth Sciences, v. 111, p. 434–450, https://doi.org/10.1016/j.jafrearsci.2015.08.019.

Hunziker, J.C., 1986, The evolution of illite to muscovite: An example of the behavior of isotopes in low grade metamorphic terrains: Chemical Geology, v. 57, p. 31–40, https://doi.org/10.1016/0009-2541(86)90092-6.

Iaccarino, S., 1985, Mediterranean Miocene and Pliocene planktonic foraminifera, *in* Bolli, H.M., Saunders, J.B., and Perch-Nielsen, K., eds., Plankton Stratigraphy: New York, Cambridge University Press, p. 283–314.

Ingersoll, R.V., Bullard, T.F., Ford, R.L., Grimm, J.P., Pickle, J.D., and Sares, S.W., 1984, The effect of grain size on detrital modes: A test of the Gazzi-Dickinson point-counting method: Journal of Sedimentary Petrology, v. 54, p. 103–116.

Jabaloy-Sánchez, A., Azdimousa, A., Booth-Rea, G., Asebriy, L., Vázquez-Vílchez, M., Martínez-Martínez, J.M., and Gabites, J., 2015, The structure of the Temsamane fold-and-thrust stack (eastern Rif, Morocco): Evolution of a transpressional orogenic wedge: Tectonophysics, v. 663, p. 150–176, https://doi.org/10.1016/j.tecto.2015.02.003.

Jolivet, L., Faccenna, C., Agard, P., Frizon de Lamotte, D., Menant, A., and Sternai, P., 2016, Neo-Tethys geodynamics and mantle convection: From extension to compression in Africa and a conceptual model for obduction: Canadian Journal of Earth Sciences, v. 53, no. 11, p. 1190–1204, https://doi.org/10.1139/cjes-2015-0118.

Kolonic, S., Sinninghé Damsté, J.S., Böttcher, M.E., Kuypers, M.M.M., Kuhnt, W., Beckmann, B., Scheeder, G., and Wagner, T., 2002, Geochemical characterization of Cenomano/Turonian black shales from the Tarfaya Basin (SW Morocco). Relationships between paleoenvironmental conditions and early sulphurization of sedimentary organic matter: Journal of Petroleum Geology, v. 25, p. 325–350, https://doi.org/10.1111/j.1747-5457.2002.tb00012.x.

Kuhnt, W., and Wiedmann, J., 1995, Cenomanian-Turonian source rocks: Paleobiogeographic and paleoenvironmental aspects, *in* Huc, A.Y., ed., Paleogeography, Paleoclimate, and Source Rocks: American Association of Petroleum Geologists, Studies in Geology, v. 40, p. 213–231, https://doi.org/10.1306/St40595C10.

Kuhnt, W., Chellai, H., Holhoum, A., Luderer, F., Thurow, J., Wagner, I., El Albani, A., Beckmann, B., Herbin, J.P., Kawamura, H., Kolonic, S., Nederbragt, S., Street, C., and Ravilinous, K., 2001, Morocco Basins's sedimentary record may provide correlation for Cretaceous paleoceanographic event worldwide: Eos (Transactions, American Geophysical Union), v. 82, p. 361–364, https://doi.org/10.1029/01EO00223.

Lanson, B., Sakharov, B.A., Claret, F., and Drits, V.A., 2009, Diagenetic smectite-to-illite transition in clay-rich sediments: A reappraisal of X-ray diffraction results using the multi-specimen method: American Journal of Science, v. 309, p. 476–516, https://doi.org/10.2475/06.2009.03.

Leprêtre, R., Frizon de Lamotte, D., Combier, V., Gimeno-Vives, O., Mohn, G., and Eschard, R., 2018, The Tell-Rif orogenic system (Morocco, Algeria, Tunisia) and the structural heritage of the southern Tethys margin. Bulletin Société Géologique France Earth Science Bulletin, v. 189, no. 10, https://doi.org/10.1051/bsgf/2018009.

Lespinasse, P., 1977, Les marnes a block de la región de Zoumi. Evolution structural des zones externes du Rif (Maroc): Bulletin de la Société Géologique de France, v. 19, p. 781–787, https://doi.org/10.2113/gssgfbull.S7-XIX.4.781.

Liu, Z., Tuo, S., Colin, C., Liu, J.T., Huang, C.Y., Selvaraj, K., Chen, C.T.A., Zhao, Y., Siringan, F.P., Boulay, S., and Chen, Z., 2008, Detrital fine-grained sediment contribution from Taiwan to the northern South China Sea and its relation to regional ocean circulation: Marine Geology, v. 255, p. 149–155, https://doi.org/10.1016/j.margeo.2008.08.003.

Lourens, L.J., Hilgen, F.J., Laskar, J., Shackleton, N.J., and Wilson, D., 2004, The Neogene Period, *in* Gradstein, F.M., Ogg, J.G., and Smith, A.G, eds., A Geologic Time Scale 2004: New York, Cambridge University Press, p. 409–440.

Lüning, S., Adamson, K., and Craig, J., 2004, Frasnian organic-rich shales in North Africa: Regional distribution and depositional model, *in* Arthur, T.J., Macgregor, D.S., and Cameron, N.R., eds., Petroleum Geology of Africa: New Themes and Developing Technologies: Geological Society, London, Special Publication 207, p. 165–184.

Maaté, S., 2017, Evolution tectono-sédimentaire de la zone intrarifaine occidentale durant le Tertiaire (Marge africaine rifaine, Maroc). Corrélations avec la marge Tellienne tunisienne [Ph.D. thesis]: Tétouan, Maroc, Université Abdelmalek Essâadi, 206 p.

Maaté, S., Alcalá, F.J., Guerrera, F., Hlila, R., Maaté, A., Martín-Martín, M., Raffaelli, G., Serrano, F., and Tramontana, M., 2017, The External Tanger Unit (Intrarif sub-Domain, External Rifian Zones, Morocco): An interdisciplinary study: Arabian Journal of Geosciences, v. 10, p. 556, https://doi.org/10.1007/s12517-017-3347-8.

Maaté, S., Guerrera, F., Hlila, R., Maaté, A., Martín-Martín, M., and Tramontana, M., 2018, New structural data on Tertiary of the External Tanger Unit (Intrarif, Morocco): Geogaceta, v. 63, p. 123–126.

Magoon, L.B., and Dow, W.G., 1994, The petroleum system, *in* Magoon, L.B., and Dow, W.G., eds., The Petroleum System-From Source to Trap: American Association of Petroleum Geologists Memoir 60, p. 3–24, https://doi.org/10.1306/M60585C1.

Martini, E., 1971, Standard Tertiary and Quaternary calcareous nannoplankton zonation, *in* Farinacci, A., ed., Proceedings of the 2nd Planktonic Conference, Rome, 1970: Tecnoscienza, p. 739–785.

Martín-Martín, M., Rey, J., Alcalá, F.J., Tosquella, J., Deramond, J., Lara-Corrona, E., Duranthon, F., and Antoine, P.O., 2001, Tectonic controls on the deposits of a foreland basin: An example from the Eocene Corbières-Minervois basin, France: Basin Research, v. 13, p. 419–433, https://doi.org/10.1046/j.0950-091x.2001.00158.x.

Martín-Martín, M., Guerrera, F., Rodriguez-Estrella, T., Serrano, F., Alcalá, F.J., Raffaelli, G., and Tramontana, M., 2018, Miocene tectono-sedimentary evolution of the eastern external Betic Cordillera (Spain): Geodinamica Acta, v. 30, p. 265–286, https://doi.org/10.1080/09853111.2018.1493879.

Martín-Martín, M., Guerrera, F., and Tramontana, M., 2020a, Geodynamic implications of the latest Chattian-Langhian central-western peri-Mediterranean volcano-sedimentary event: A Review: The Journal of Geology, v. 128, p. 29–43, https://doi.org/10.1086/706262.

Martín-Martín, M., Guerrera, F., Miclaus, C., and Tramontana, M., 2020b, Similar Oligo-Miocene tectono-sedimentary evolution of the Paratethyan branches represented by the Moldavidian Basin and Maghrebian Flysch Basin: Sedimentary Geology, v. 396, no. 105548, https://doi.org/10.1016/j.sedgeo.2019.105548.

Martín-Martín, M., Guerrera, F., and Tramontana, M., 2020c, Tectono-sedimentary evolution of the Cenozoic basins in the Eastern External Betic Zone (SE Spain): Geosciences, v. 10, p. 394, https://doi.org/10.3390/geosciences10100394.

Martín-Ramos, J.D., Díaz-Hernández, J.L., Cambeses, A., Scarrow, J.H., and López-Galindo, A., 2012, Pathways for quantitative analysis by X-ray diffraction, *in* Aydinalp, C., ed., An Introduction to the Study of Mineralogy: Rijeka, Croatia, Cumhur Aydinalp, IntechOpen, p. 73–92, https://doi.org/10.5772/36256.

McBride, E.F., 1963, A classification of common sandstones: Journal of Sedimentary Petrology, v. 33, p. 664–669.

Melki, F., Zouaghi, T., Harrab, S., Casas Sainz, A., Bédir, M., and Zargouni, F., 2011, Structuring and evolution of Neogene transcurrent basins in the Tellian foreland domain, north-eastern Tunisia: Journal of Geodynamics, v. 52, no. 1, p. 57–69, https://doi.org/10.1016/j.jog.2010.11.009.

Messadi, A.M., Mardassi, B., Ouali, J.A., and Touir, J., 2019, Diagenetic process as tool to diagnose paleo-environment conditions, bathymetry and oxygenation during Late Paleocene-Early Eocene in the Gafsa Basin: Carbonates and Evaporites, v. 34, p. 893–908, https://doi.org/10.1007/s13146-018-0424-3.

Michard, A., Feinberg, H., Elazzab, D., Bouybaouene, M., and Saddiqi, O., 1992, A serpentinite ridge in a collisional paleomargin setting: The Beni Malek massif, External Rif, Morocco: Earth and Planetary Science Letters, v. 113, p. 435–442, https://doi.org/10.1016/0012-821X(92)90144-K.

Michard, A., Frizon De Lamotte, D., and Negro, F., 2007, Serpentinite slivers and metamorphism in the External Maghrebides: Arguments for an intracontinental suture in the African paleomargin (Morocco, Algeria): Revista de la Sociedad Geológica de España, v. 20, p. 173–185.

Michard, A., Frizon de Lamotte, D., and Liégeois, J.-P., Saddiqi. O., and Chalouan, A., 2008, Conclusion: Continental Evolution in Western Maghreb, *in* Michard, A., Saddiqi, O., Chalouan, A., and Frizon de Lamotte, D., eds., Lecture Notes in Earth Sciences, v. 116, 404 p.

Michard, A., Saddiqi, O., Missenard, Y., Oukassou, M., and Barbarand, J., 2017, Les grandes regions géologique du Maroc; diversité et soulèvement d'ensemble: Géologues, no. 194, p. 4–12.

Moiroud, A., Martinez, M., Deconinck, J.F., Monna, F., Pellenard, P., Riquier, L., and Company, M., 2012, High-resolution clay mineralogy as a proxy for orbital tuning: Example of the Hauterivian-Barremian transition in the Betic Cordillera (SE Spain): Sedimentary Geology, v. 282, p. 336–346, https://doi.org/10.1016/j.sedgeo.2012.10.004.

Moore, D.M., and Reynolds, R.C., 1997, X-ray Diffraction and the Identification and Analysis of Clay Minerals (2nd edition): New York, Oxford University Press, 378 p.

Morabet, A.M., Bouchta, R., and Jabour, H., 1998, An overview of the petroleum systems of Morocco, *in* MacGregor, D.S., Moody, R.T.J., and Clark-Lowes, D.D., eds., Petroleum Geology of North Africa: Geological Society, London, Special Publication 132, p. 283–296, https://doi.org/10.1144/GSL.SP.1998.132.01.16.

Müller, R.D., Zhirovic, S., Williams, S.E., Cannon, J., Seton, M., Bower, D.J., Tetley, M.G., Heine, C., Le Breton, E., and Liu, S., 2018, A global plate model including lithospheric deformation along major rifts and orogens since the Triassic: Tectonics, v. 38, p. 1884–1907, https://doi.org/10.1029/2018TC005462.

Nadeau, P.H., and Bain, D.C., 1986, Composition of some smectites and diagenetic illitic clays and implications for their origin: Clays and Clay Minerals, v. 34, p. 455–464, https://doi.org/10.1346/CCMN.1986.0340412.

Nadhem, K., Zahra, N., Ménendez, B., Salwa, J., and Jamel, T., 2017, Spatiotemporal sedimentological and petrophysical characterization of El Gueria reservoir (Ypresian) in sFAX and Gulf of Gabes Basins (SE-Tunisia): Journal of African Earth Sciences, v. 130, p. 202–222, https://doi.org/10.1016/j.jafrearsci.2017.03.014.

Nieto, E., Ortega-Huertas, M., Peacor, D.R., and Aróstegui, J., 1996, Evolution of illite/smectite from early diagenesis through incipient metamorphism in sediments of the Basque-Cantabrian basin: Clays and Clay Minerals, v. 44, p. 304–323, https://doi.org/10.1346/CCMN.1996.0440302.

Njahi, Z., Kassabi, N., and Touir, J., 2017, Porosity and reservoir potentiality of the Cherahil Formation limestone (middle–upper Eocene) in the Gulf of Gabes (Tunisia): Journal of African Earth Sciences, v. 131, p. 166–178, https://doi.org/10.1016/j.jafrearsci.2017.04.009.

Olsson, R.K., Hemleben, C., and Berggren, W.A., eds., 1999, Atlas of Paleocene Planktonic Foraminifera: Washington, D.C., Smithsonian Institution, Smithsonian Contributions to Paleobiology, v. 85, p. 1–252.

Oukassou, M., Saddiqi, O., Barbarand, J., Sebti, S., Baidder, L., and Michard, A., 2013, Post-Variscan exhumation of the Central Anti-Atlas (Morocco) constrained by zircon and apatite fission-track thermochronology: Terra Nova, v. 25, p. 151–159, https://doi.org/10.1111/ter.12019.

Pearson, P.N., Olsson, R.K., Huber, B.T., Hemleben, C., and Berggren, W.A., eds., 2006, Atlas of Eocene Planktonic Foraminifera: Cushman Foundation Special Publication, v. 41, 513 p.

Pettijohn, E.J., 1975, Sedimentary Rocks (3rd edition): New York, Harper and Row Publishers, 628 p.

Pletsch, T., 1997, Clay minerals in Cretaceous deep-water formations of the Rif and the Betic Cordillera: Bulletin Société Géologique du Nord, v. 26, p. 1–106.

Pletsch, T., Daoudi, L., Chamley, H., Deconinck, J.F., and Charroud, M., 1996, Palaeogeographic controls on palygorskite occurrence in mid-Cretaceous sediments of Morocco and adjacent basins: Clay Minerals, v. 31, p. 403–416, https://doi.org/10.1180/claymin.1996.031.3.10.

Sabri, K., Marrero-Diaz, R., Ntarmouchant, A., dos Santos, T.B., Ribeiro, M.L., Solá, A.R., Smaili, H., Benslimane, A., Chibout, M., Pérez, N.M., and Padrón, E., 2019, Geology and hydrogeochemistry of the thermo-mineral waters of the South Rif Thrust (Northern Morocco): Geothermics, v. 78, p. 28–49, https://doi.org/10.1016/j.geothermics.2018.11.005.

Sachse, V.F., Kittke, R., Heim, S., Kluth, O., Schober, J., Boutib, L., Jabour, H., Perssen, F., and Sindern, S., 2011, Petroleum source rocks of the Tarfaya Basin and adjacent areas, Morocco: Organic Geochemistry, v. 42, p. 209–227, https://doi.org/10.1016/j.orggeochem.2010.12.004.

Salamy, K.A., and Zachos, J.C., 1999, Latest Eocene–Early Oligocene climate change and Southern Ocean fertility: Inferences from sediment accumulation and stable isotope data: Palaeogeography, Palaeoclimatology, Palaeoecology, v. 145, no. 1–3, p. 61–77, https://doi.org/10.1016/S0031-0182(98)00093-5.

Scheibner, C., and Speijer, R.P., 2008, Decline of coral reefs during late Paleocene to early Eocene global warming: Earth-Science Reviews, v. 3, p. 19–26.

Serrano, F., 1992, Biostratigraphic control of Neogene volcanism in Sierra de Gata (south-east Spain): Geologie & Mijnbouw, v. 71, p. 3–14.

Suter, G., 1980a, Carte géologique du Rif, 1/500000: Notes et Mémoir du Service Géologique du Maroc, 245a.

Suter, G., 1980b, Carte structurale de la chaîne rifaine, 1/500,000: Notes et Mémoires du Service géologique, Maroc, 245b.

Suter, G., and Fiechter, G., 1966, Le Rif meeridional atlantique (Maroc): Aperçu structural sur la reegion Ouezzane-Zourni et le pays du Habt (Larache): Notes et Mémoir du Service Géologique du Maroc, v. 26, no. 188, p. 15–20.

Swezey, C.S., 2009, Cenozoic stratigraphy of the Sahara, northern Africa: Journal of African Earth Sciences, v. 53, p. 89–121, https://doi.org/10.1016/j.jafrearsci.2008.08.001.

Tassi, F., Vaselli, O., Moratti, G., Piccardi, L., Minissale, A., Poreda, R., Huertas, A.D., Bendkik, A., Chenakeb, M., and Tedesco, D., 2006, Fluid geochemistry versus tectonic setting: The case study of Morocco, *in* Moratti, G., and Chalouan, A., eds., Tectonics of the Western Mediterranean and North Africa: Geological Society, London, Special Publication 262, p. 131–145, https://doi.org/10.1144/GSL.SP.2006.262.01.08.

Tejera de Leon, J., and Duée, G., 2003, Relationships between the Neogene foredeep basins of the Western external Rifian belt related to the Arbaoua-Jebha transform fault. Consequences

for the interpretation of the evolution of the Rifian belt (Morocco): Rabat, Morocco, Travaux Institute Scientifique Rabat, série Géologie & Géographie Physique, v. 21, p. 1–19.

Tejera de Leon, J., Boutakiout, M., Ammar, A., AitBrahim, L., and El Hatimi, N., 1995, Les bassins du Rif central (Maroc): Marqueurs de chevauchements hors sequence d'age Miocene terminal au Coeur de la chaîne: Bulletin de la Société Géologique de France, v. 166, p. 751–761.

Tortosa, A., Palomares, M., and Arribas, J., 1991, Quartz grain types in Holocene deposits from the Spanish Central System: Some problems in provenance analysis, *in* Morton, A.C., Todd, S.P., and Haughton, P.D.W., eds., Developments in Sedimentary Provenance Studies: Geological Society, London, Special Publication 57, p. 47–54, https://doi.org/10.1144/GSL.SP.1991.057.01.05.

Vázquez, M., Asebriy, L., Azdimousa, A., Jabaloy, A., Booth-Rea, G., Barbero, L., Mellini, M., and González-Lodeiro, F., 2013, Evidence of extensional metamorphism associated to Cretaceous rifting of the North-Maghrebian passive margin: The Tanger-Ketama unit (external Rif, northern Morocco): Geologica Acta, v. 11, no. 3, p. 277–293.

Wade, B.S., Pearson, P.N., Berggren, W.A., and Pälike, H., 2011, Review and revision of Cenozoic tropical planktonic foraminiferal biostratigraphy and calibration to the geomagnetic polarity and astronomical time scale: Earth-Science Reviews, v. 104, p. 111–142, https://doi.org/10.1016/j.earscirev.2010.09.003.

Zaghloul, M.N., Di Staso, A., Gigliuto, L.G., Maniscalco, R., and Puglisi, D., 2005, Stratigraphy and provenance of Lower and Middle Miocene strata within the External Tanger Unit (Intra-Rif sub-Domain, External Domain; Rif, Morocco): First evidence: Geologica Carpathica, v. 56, p. 517–530.

Zakir, A., Chalouan, A., and Feinberg, H., 2004, Evolution tectono-sédimentaire d'un domaine d'avant-chaîne: Exemple des basin d'El-Habt et de Sidi Mrayt, Rif externe nord-occidental (Maroc); precisions stratigraphiques et modélisation tectonique: Bulletin de la Société Géologique de France, v. 175, p. 383–397, https://doi.org/10.2113/175.4.383.

Zarhloule, Y., Rimi, A., Boughriba, M., Barkaoui, A.E., and Lahrach, A., 2010, The geothermal research in Morocco: History of 40 years, *in* Proceedings, World Geothermal Congress 2010: Bali, Indonesia, International Geothermal Association, p. 1–6.

Zuffa, G.G., 1980, Hybrid arenites: Their composition and classification: Journal of Sedimentary Petrology, v. 50, p. 21–29.

Zuffa, G.G., 1985, Optical analyses of arenites: Influence of methodology on compositional results, *in* Zuffa, G.G., ed., Provenance of Arenites: NATO ASI Series C: Mathematical and Physical Sciences, v. 148, p. 165–189, https://doi.org/10.1007/978-94-017-2809-6_8.

Zuffa, G.G., 1987, Unravelling hinterland and offshore palaeogeography from deep-water arenites, *in* Leggett, J.K., and Zuffa, G.G., eds, Marine Clastic Sedimentology, Models and Case Studies (Volume *in* Memory of C. Tarquin Teatle): London, Graham and Trotman, p. 39–61.